Comparing the Composition of Mesopotamian Iron Oxide Stone Duck Weights, Cylinder Seals and Half-Fabricates, using X-ray Fluorescence and Neutron Radio- and Tomography

Judith J. Mulder

November 23, 2010

Research Project Archaeometry
Course code: 450296
ECTS: 27
Student number: 1473883
Responsible lecturer: Henk Kars
Daily supervisor: Martine de Vries

Abstract

The aim of this project is to find differences and similarities in Mesopotamian iron oxide stone objects in order to establish their provenance.

Therefore, iron oxide stone (duck) weights, cylinder seals and half-fabricates[1] have been analysed using X-ray fluorescence, which measures chemical composition, and neutron radio- and tomography, which measures density throughout the artefact.

Three groups could be identified based on the composition measured by XRF and four groups were distinguished based on the neutron radio- and tomography measurements. The composition and homogeneity do not overlap, since the two sets of groups based on the results of the measurements do not contain the same objects.

XRF analyses indicate that most artefacts measured in this research had a composition more similar to that of Selenkahiye half-fabricates than to that of Tell Bazi raw material. Further research is necessary to be sure about the provenance. After comparing half-fabricates with a known archaeological provenance and raw material with a known geological provenance, it could be concluded that iron oxide objects with the same provenance do not necessarily have the same composition. No significant differences were found between the measured physical and chemical properties of the duck weights and cylinder seals.

In addition, some particularities were discovered during the measurements. For example, calcium was measured as a main element instead of iron at one of the artefacts. In addition, one seal appeared to be made of two different materials which were glued together.

[1]Figure front page: from left to right duck weight A1932/7.138-F (©RMO), cylinder seal APM06370 and half-fabricate APM15888 (taken by the author).

Contents

Chapter 1

Introduction

This thesis presents the composition of a variety of iron oxide artefacts: (duck) weights, cylinder seals and half-fabricates. The compositions are analysed in order to find differences and similarities between the various artefacts and finally to determine their provenance.

At first, this chapter presents the framework of the study and background information, followed by the objectives, aims and research questions. Finally, the acknowledgements and a reading guide of the entire thesis are given.

1.1 Framework

The framework of this research project is provided by the PhD research of Martine de Vries. Her research is about the use of haematite in Mesopotamia in all its aspects. She discusses for example what haematite was used for, what is written about haematite in ancient texts and how haematite was mined, worked and transported. In addition, she writes about the provenance, for example where haematite occurs naturally and she shows the results of analyses of haematite objects, which help to determine the provenance.

1.1.1 Background information

Mesopotamia is the region along the rivers Euphrates and Tigris in present-day Iraq and Syria. Since the area is low on resources, materials such as wood, ore for metals and stone were imported. In order to know more about the people and society of Mesopotamia, we would like to know how the import system works. Studying iron oxide stones is a good choice to know more about the import system, since the stones do not decay easily and they were used in a relative short period, so the influences of political factors can be followed.

Seals, weights and other small artefacts were carved from iron oxide stones in this region mainly during the Old Babylonian Period.

Cylinder seals (fig. 1.1a) were first created in southern Mesopotamia and southwestern Iran in the second half of the fourth millennium B.C.. The seals were for example used to sign clay tablets or to seal doors, jars and other objects by pressing the seals in soft clay. Cylinder seals have not only been made from minerals and rocks, like calcite, carnelian, chalcedony, chlorite, iron oxide, jasper, lapis lazuli, marble and steatite, but also from faïence, glass, baked clay, wood, bone, shell, ivory and metal (Roaf, 1990). Variations in material can be noticed between seals of different regions and periods (Moorey, 1994; Pittman, 1995). In the Old-Babylonian Period (circa 2000-1600 B.C.), up to 70 % of the cylinder seals were made of iron oxides, like haematite, goethite or magnetite, although before and after that period hardly any seals were made from that material (Moorey, 1994).

(a) A cylinder seal (APM06361) at the right with its imprint at the left (Online inventory database of the Allard Pierson museum, ©UvA).

(b) A duck weight (A1932/7.138-F). Photo ©RMO.

Figure 1.1

The earliest weights were produced in the Early Dynastic Period (the middle of the third millennium B.C.). Mesopotamian weights were based on the sexagesimal system, which is counting in sixties. This is easy to calculate with, because 60 can be divided by a lot of numbers. The units shekel, mina and talent were used for weighing. There were 60 shekels in 1 mina and 60 minas in 1 talent. A mina was about 0.5 kg, but differences may have occurred between different cities. For example, in Ugarit, at the Mediterranean Sea, there were 50 shekels in 1 mina and 1 shekel was 9.5 grams.

The weights were often duck- (fig. 1.1b), spherical- or barrel-shaped, and sometimes lion-shaped (Roaf, 1990). From the late third millennium B.C. on, weights were often made from iron oxides. Probably because the stone wears well and therefore it would be immediately noticed if the weight had been modified (Moorey, 1994).

Since goethite and magnetite might look macroscopically similar to haematite, incorrect names are often given to these materials in archaeological studies. These materials had a common name in Mesopotamia, *šadānu*, which means "stone from the mountain".

The geological provenance of the material from which the objects are made is unknown. Since it does not occur naturally in Mesopotamia, it has to be imported. It is generally thought that the materials were imported from Anatolia (Moorey, 1994), but no evidence for that theory is found (Collon, 1986).

Therefore, an important part of the PhD research is the study of geological provenance. I tried to gain a better understanding of the provenance in my Bachelor's thesis and I continued with that in this Research Project.

1.2 Objectives and aims of this study

The composition of iron oxide stone artefacts should be compared with the composition of raw material to find the provenance of the material from which the artefacts are made. In previous research (Mulder, 2008), 148 potential sources of iron oxide stone were found, so it is either very difficult or even impossible to find all these sources, take samples of them and analyse them in order to find their composition. In addition, the current situation of the Near East makes it difficult to obtain raw material from the area around Mesopotamia. Nevertheless, the compositions of the artefacts measured in this research are compared with three half-fabricates with an archaeological and three pieces of raw material with a geological provenance. Apart

from the provenance study I have also looked at the difference in composition of the different artefacts groups, like the duck weights and cylinder seals.

The hypothesis of this thesis is that various groups of artefacts, for example the duck weights and cylinder seals could have a different composition, since they have a different function. The material of both groups of objects should be easy to carve. Symbols have to be carved in great detail in cylinder seals, and weights require material that can easily be carved, because the exact weight has to be obtained by carving off small amounts of material. The weights should have a homogeneous composition, so the size is related to the weight of the object. The weight, so also the homogeneity, does not matter for the seals. Because of this difference, different material could have been chosen for different kinds of objects.

It is hoped that the composition of a sample of raw material is similar to that of an artefact, so it can be concluded that they may originate from the same location and the source of the artefact is known. Unfortunately, there is only a very small chance that this happens, because there is only a very small number of raw material and half-fabricates.

The *research questions* I aim to answer in my research are summarized as follows.

- *What are adequate methods to analyse iron oxide stone artefacts?*
- *What are the compositions of different iron oxide stone artefacts?*
- *What are the differences and similarities of the compositions of duck weights and cylinder seals?*
- *What are the differences and similarities between the objects of raw material or half-fabricates and the other artefacts?*
- *Based on the research achieved above, what can be said about provenance?*

1.3 Acknowledgements

This thesis was done for my Research Project Archaeometry, which is part of the Master's program of Earth Science, specialization Archaeometry, at the VU University Amsterdam.

I would like to thank both Henk Kars and Martine de Vries for supervising me in writing this thesis, and Martine also for helping me to obtain the necessary information and bringing me in contact with other people that helped me with this research.

My project met with a warm welcome at the two museums from which the artefacts were borrowed. The curators of the Allard Pierson Museum (APM) Ron Leenheer, Geralda Jurriaans-Helle and René van Beek, the collection managers of the Dutch National Museum of Antiquities (Rijksmuseum van Oudheden, RMO) Marianne Stauthamer and Robert Ritter and the registrar Heikki Pauts offered their friendly cooperation and enabled me to study and borrow the artefacts. I would like to thank them all for their encouraging support and Ron Leenheer for accompanying me to the ICN!

I am very grateful to Luc Megens of the Instituut Collectie Nederland (ICN) for cooperating on the XRF analyses, explaining a lot about the method and reviewing this report. Ineke Joosten, also of the ICN, is thanked for explaining about iron oxide standards.

It was a great opportunity for me to be able to analyse the radio- and tomography measurements that were done by Dirk Visser. He was a patient tutor and I would like to thank him for his time and input! In addition, the people of the ANTARES department at the Forschungsreaktor München II (FRMII) are thanked for letting us use the computers to analyse the measurements and helping when we had problems with the analyses.

I learned a great deal from the guided tours around ISIS and FRMII, where Winfried Kockelmann and Richard Mole explained how the instruments worked.

Penultimately, thanks to Dave van der Brugge, who recovered most of my work when my computer crashed and who helped me, together with some other friends, understanding the markup language LaTeX in which this thesis is written. I thank him for his never-ending support! At last, I am very grateful to the friends and family, especially my parents, who supported me in writing this thesis.

1.4 Reading guide

In addition to the framework of this report and the objectives and aims outlined in this *introduction*, an overview of previous research done on iron oxide stone artefacts is given in *chapter two*. *Chapter three* presents the objects that have been analysed for this research project, including the archaeological background of the objects. The best methods to analyse the objects are described in *chapter four*. The results of the XRF and the tomo- and radiography analyses are given and described in *chapter five*. The dataset is discussed with regard to the samples in *chapter six*. Differences and similarities between the samples are described and sample groups are compared. *Chapter seven* shows the conclusion and what can be done in further research. This is followed by the *references*. *Appendix one* and *two* show respectively all XRF spectra and the tomographical images made for this research project.

Chapter 2

Previous Research

2.1 Introduction

This chapter presents an overview of previous research about analysing iron oxide stone objects. This comprises investigating which methods are useful for measuring iron oxide stone. The methods which are used in this research are selected in chapter 4 (analytical methods and techniques). Furthermore, the results from the analyses of earlier research are collected, which are compared with the results from the analyses of this research in chapter 6 (the discussion).

So far only a few studies have been performed on iron oxide stone artefacts. Most related research is about iron oxide ochres and iron oxides in sediments and soils. These studies are not useful for this research, because the methods used to analyse these unconsolidated materials are mostly destructive, while a non-destructive method is needed for my research about iron oxide artefacts. In addition, it is not useful to compare the results of these studies with the results of my research. Most materials that have been analysed in previous research are not from the Near East, so they do not come from potential sources of the materials of which the artefacts were made. The materials analysed in previous research that came from the Near East are unconsolidated, so they did not have a similar provenance as the consolidated objects have.

The following paragraphs give an overview of various analyses done on iron oxide stone artefacts. At first, the results of an XRF analysis of some cylinder seals by Cowell (2.2) and a Raman microscopy and XRD analysis of Cypriote seals done by Joyner et al. (2.3) are presented. This is followed by various analyses of seals and raw material, which are related to the PhD project (2.4) and my Bachelor's thesis (2.5).

2.2 XRF analysis on cylinder seals by Cowell

XRF measurements were done on a number of seals from the British Museum which were earlier identified using mineralogy as being made from haematite. The final aim was to find the source of the material of which the cylinder seals are made, but in Cowell's unpublished report 'Report on the analysis of some haematite cylinder seals' (1985-86) only the compositions of the various seals are given and compared with each other. The report is also referred to in Moorey (1994).

In total, 34 seals were analysed with XRF. Cowell states that the raw material from which the seals were made may have originated from either eastern Turkey or from sources local to where the seal was manufactured. Unfortunately, material from Turkey was not available for analysis. In addition to the 34 seals, four specimens of unprocessed haematite were examined, two from Persia, one from the Aegean and one from North Yorkshire.

Besides iron as the main element, calcium (Ca), vanadium (V), manganese (Mn), copper (Cu), lead (Pb), strontium (Sr), zirconium (Zr) and molybdenum (Mo) were generally detected (Cowell, unpublished). The data was converted to approximate concentrations in Cowell's research, although non-destructive XRF is a qualitative method.

Since calcium, copper and lead show wide variations in the duplicate analysis, Cowell considers these unreliable for characterisation (Cowell, 1985-86).

Statistical analysis has been done on the data resulting in the formation of groups. Five of the six Cypriote seals form a coherent group based on low concentrations for most of the elements. Furthermore the Mitannian seals are divided in two groups with one outlier, distinguished by differences in molybdenum, manganese and zirconium. In addition, the compositions of the three Syrio-Cappodocian seals are similar to each other and to the composition of the Cypriotic seals. The other cultural groups do not seem to have a common similarity in composition (Cowell, 1985-86).

The number of samples is, as Cowell also states, too low compared to the number of potential sources and further research is necessary.

2.3 Analyses on Cypriote seals by Joyner et al.

Joyner, Merrillees and Xenophontos describe in their article (2006) the ana-lyses of 86 seals and beads, originating from Cyprus, from the Department of Greek and Roman Antiquities of the British Museum in London. This collection comprises 67 cylinder seals, 16 stamp seals, one triangular seal and two beads. 68 if these 86 objects were excavated in Cyprus, while the other objects have an uncertain archaeological provenance. The excavations on which these objects were found took place in the 1890s, which results in a lower quality of the documentation than current standards.

The goal of their research was to find the geological provenance of the objects. The objects had already been determined macroscopically by Kenna in 1971, but further research was necessary.

Determination by Joyner et al. was done using non-destructive "standard gemmological techniques" and Raman microscopy. In addition, seals which were more difficult to determine were examined by air-path X-ray fluorescence spectroscopy (XRF) and X-ray diffraction (XRD) using Debye-Scherrer cameras. XRD was destructive, although it only required a small sample. The other methods were applied non-destructive.

Twelve of the 68 excavated objects were determined to be made of haematite. Ten of the 18 artefacts with no or an uncertain provenance were made of haematite.

Joyner et al. conclude that haematite was almost certainly imported, because the mineral that occurs naturally in Cyprus is usually porous and brittle and would not have been suitable for making these objects.

The earliest datable haematite cylinder seal at Cyprus is from the Old Babylonian Period. The iconography shows that it originates from the mainland of the Near East, but such seals were later imitated and made from local black material (Joyner et al., 2006).

2.4 Current Research

This paragraph presents the analysis of artefacts from the De Liagre-Böhl (DLB) collection and raw material from Tell Bazi.

The information in this paragraph was obtained not only from an article about this research (De Vries-Melein et al., 2010), but also from the original data of the XRF, neutron diffraction, neutron radio- and tomography and PGAA.

2.4.1 Materials

Thirteen Mesopotamian seals from the De Liagre-Böhl (DLB) collection from The Netherlands Institute for the Near East (NINO) in Leiden (The Netherlands) and 3 pieces of raw material found in the vicinity of the site of Tell Bazi (Syria) have been analysed.

Tell Bazi

Tell Bazi is located on the left bank of the Euphrates River in northern Syria, as fig. 2.1 indicates.

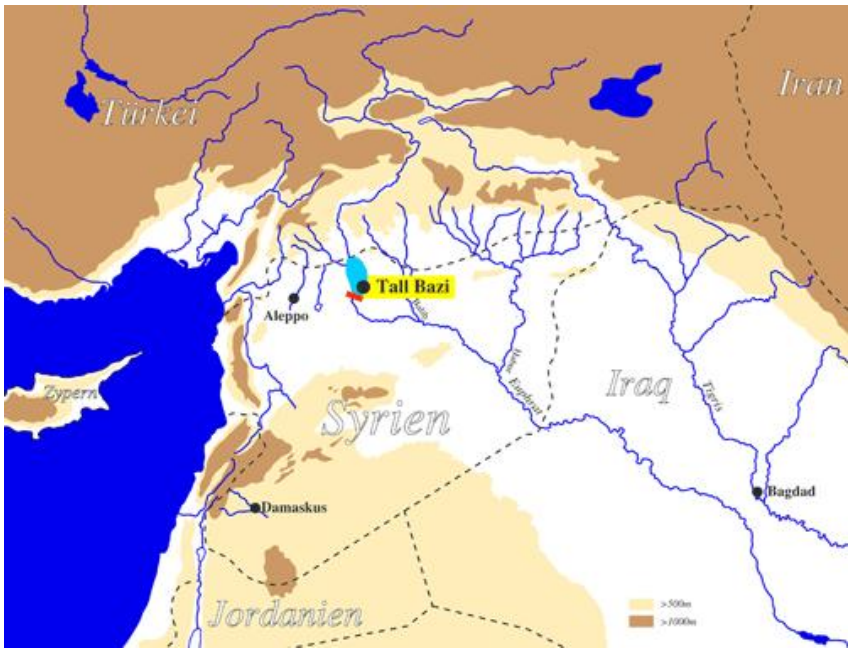

Figure 2.1: Map which shows the location of Tell Bazi (Freunde von Bazi e.V, no date (online)).

The information in this paragraph was obtained from the book "Alltag und Geselschaft zur Spätbronzezeit: eine Fallstudie aus Tall Bazi (Syrien)." by Otto (2006), which is about the excavations in Tell Bazi.

A rescue excavation took place in Tell Bazi from 1993 to 1999, since the area was to be flooded because of the building of a dam at the end of that period. Since only the western suburb was flooded in 1999, the research continued in the other two parts of the town, the citadel and the northern suburb. The citadel, which had fortification walls, probably existed since the Early Bronze Age. The western suburb only existed from 1250-1180 B.C. (Late Bronze Age). It was build as an enlargement of the old city, and it was destroyed by a fire. Because of the sudden abandonment, the western suburb shows a representative image of the daily life.

Many houses in Tell Bazi contained raw haematite and goethite, half-fabricates and finished products. Weights have been found in almost every house in the western suburb, with a total of 150 weights, mostly made of haematite or goethite. Haematite and goethite have also been found in limestone in the mountains around Tell Bazi.

Otto states that one of the important export products from Tell Bazi was haematite as raw material or as a finished product, for example weights for which was a large demand from Western Syria to Babylonia and Anatolia. Trade was done not only with nearby villages and other settlements up- and downstream in the Euphrates valley, but also with the Mediterranean coast in the west and Assyria in the east (Otto, 2006).

The presence of raw material, half-fabricates and finished products of iron oxide in Tell Bazi and the presence of raw material in the area surrounding Tell Bazi indicate that the artefacts found in Tell Bazi were made of material found nearby. To be sure, the composition of the finished products, half-fabricates and raw material should be measured in order to compare these results. When raw material from different locations in the area is measured, it is also known how much material in the same region variates.

2.4.2 Methods

The 13 seals from the DLB collection have been analysed with neutron diffraction, neutron tomography and radiography, PGAA and XRF, while the three objects from Tell Bazi have only been analysed with PGAA and XRF. The qualitative XRF measurements were done with a Bruker Tracer III-V handheld X-ray fluorescence spectrometer with a Rhodium tube operating at a tube voltage of 40 kV and a tube current of 2.2 μA (De Vries-Melein et al., 2010) and were carried out at the Instituut Collectie Nederland (ICN) in Amsterdam (The Netherlands). The neutron diffraction was done at the Rutherford Appleton Laboratory in Didcot (United Kingdom) and the PGAA measurements were performed at the Institute of Isotopes in Budapest (Hungary). Neutron tomography and radiography has been done at FRM II in Garching (Germany), but the results are not available at the moment of writing. The XRF and neutron diffraction analyses of the DLB artefacts are published in an article (De Vries-Melein et al., 2010), while the XRF results of the Tell Bazi artefacts, the PGAA and the neutron tomo- and radiography results are not yet published. An overview of the methods that are applied to the different objects is shown in table 2.1.

Methods Object no.	XRF	PGAA	Neutron diffraction	Neutron radiography and tomography
DLB 45	+	+	+	+
DLB 46	+	+	+	+
DLB 47	+	+	+	+
DLB 55	+	+	+	+
DLB 57	+	+	+	+
DLB 59	+	+	+	+
DLB 61	+	+	+	+
DLB 62	+	+	+	+
DLB 66	+	+	+	+
DLB 67	+	+	+	+
DLB 75	+	+	+	+
DLB 84	+	+	+	+
DLB 118	+	+	+	+
Tell Bazi 1	+	+		
Tell Bazi 2	+	+		
Tell Bazi 3	+	+		

Table 2.1: Overview of measurements done earlier.

2.4.3 Results

The XRF analysis

The 16 objects have been measured with XRF. The spectra are given in the figures 2.2, 2.3 and 2.4 and the results are summarized in table 2.2.

Unlike the other measurements, the third (blue) measurement of DLB 66 is done without a filter, that is why these peaks are relatively high.

The main element in all samples is iron, except in DLB 55 which has calcium (Ca) as main element. In addition, Sr occurs in high quantities in DLB 55, while Fe shows only a small peak.

The elements Mn and V were observed in DLB 45, 46, 47 and 59. The amount in which they occur differs, but the Mn peak is always larger than the V peak. Mn and V also occur in the second Tell Bazi object, but this object also contains other elements.

Furthermore, Mn occurs in DLB 66 and 84. DLB 66 also contains Au according to the article (De Vries-Melein et al., 2010), but Au can not be seen in figure 2.3b, because it is too heavy to fit in the range of the x-axis.

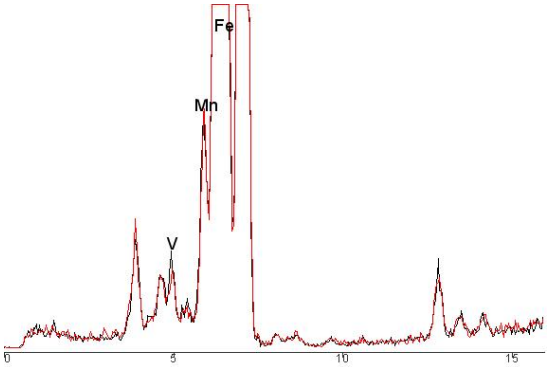

(a) DLB 46, also representing DLB 45, 47 and 59.

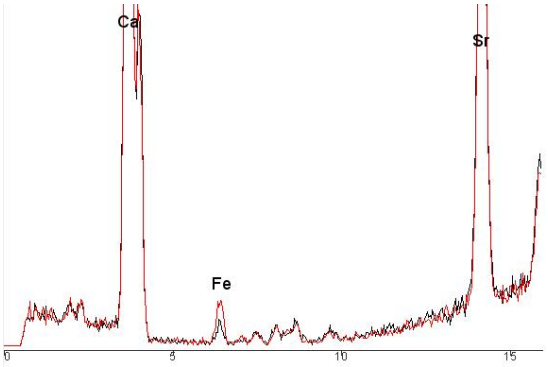

(b) DBL 55

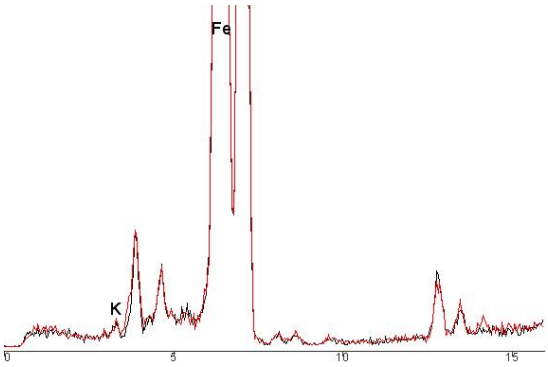

(c) DBL 57

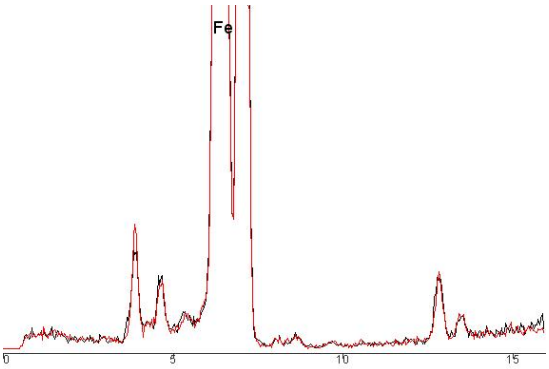

(d) DBL 61

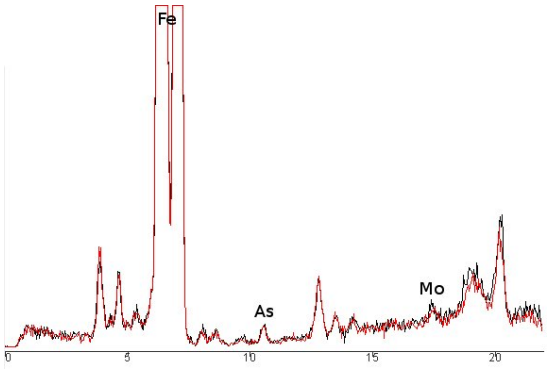

(e) DBL 62

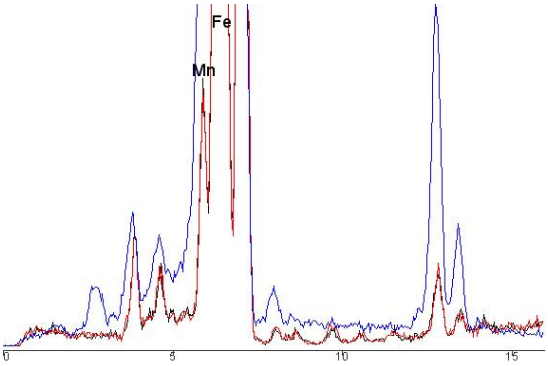

(f) DBL 66

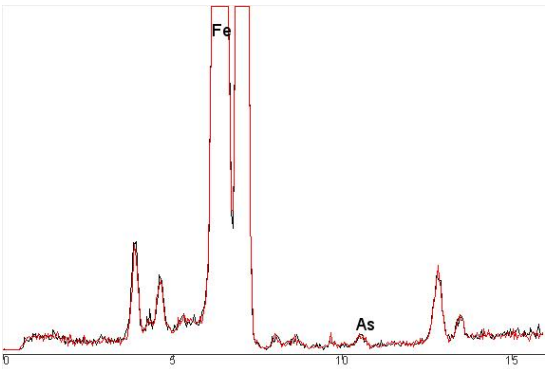

(g) DBL 67

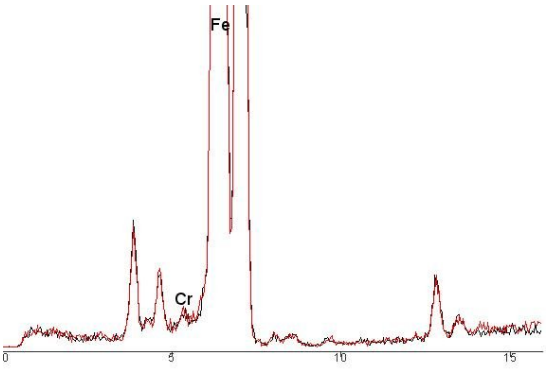

(h) DBL 75

Figure 2.2: XRF spectra from De Liagre-Böhl (DLB).

Both As and Sr are present in DLB 84 and the three Tell Bazi objects, while As is also

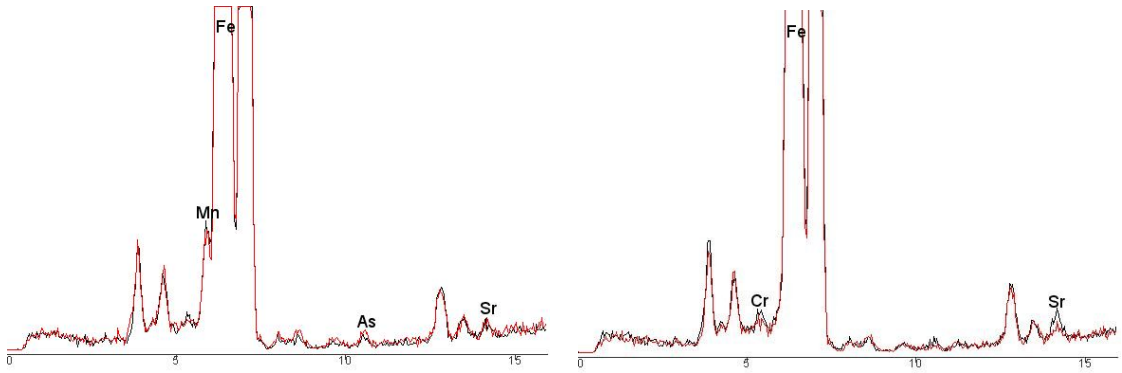

(a) 84 (b) DBL 118

Figure 2.3: XRF spectra from De Liagre-Böhl (DLB).

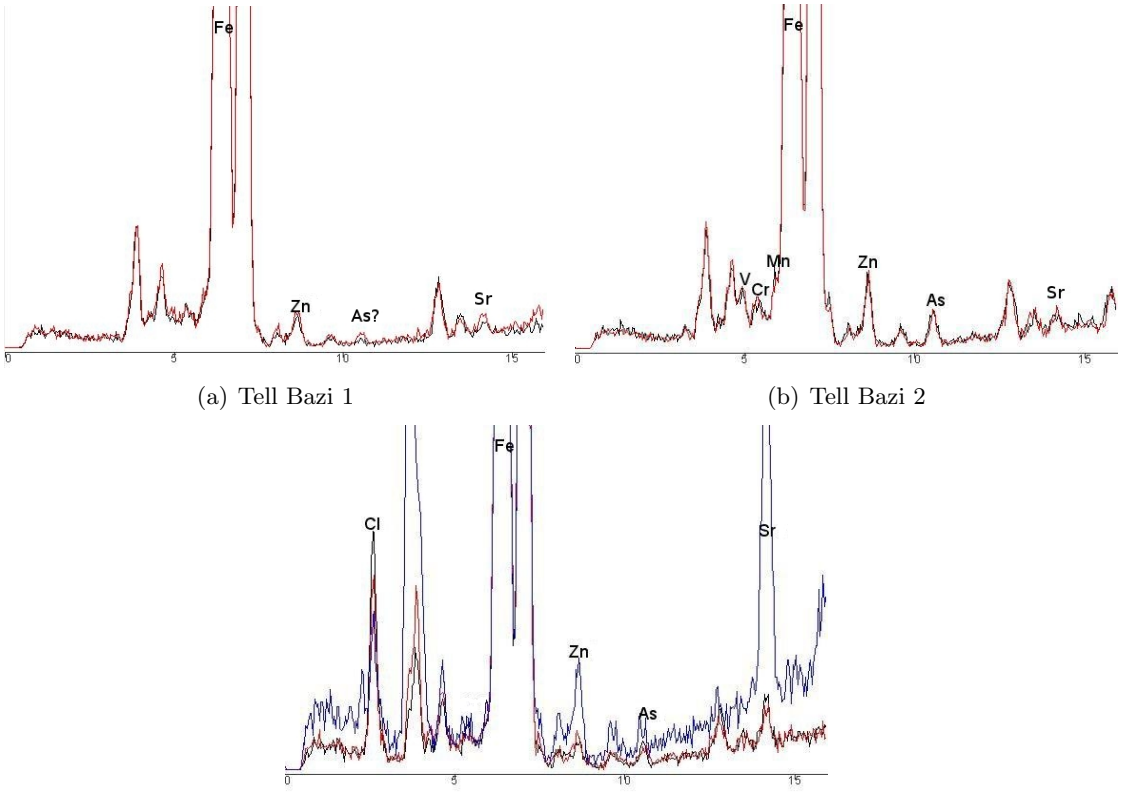

(a) Tell Bazi 1 (b) Tell Bazi 2

(c) Tell Bazi 3

Figure 2.4: XRF spectra of three Tell Bazi artefacts.

present in DLB 62 and 67 and Sr in DLB 118.

In the article (De Vries-Melein et al., 2010) is stated that the objects DLB75 and DLB118 contain Cr, while nothing is said about Cr in the objects DLB47, 59, 61 and 84, which have a similar Cr peak. Since the Cr peaks are small and unclear, it is often difficult to see whether Cr is present. Tell Bazi 2 also contains Cr.

Tell Bazi 2 and 3 contain Zn. K, Mo and Cl are present in only one of the objects. K in DLB 57, Mo in DLB 62 and Cl in Tell Bazi 3.

The peaks of Tell Bazi 3 are higher in the third measurement than in the first and second measurement. The difference between the height of the Sr peaks can be explained by the fact that the instrument is very sensitive for Sr, so the detection of Sr gives a high peak easily.

No.	Main element	Minor and trace elements
DLB 45	Fe	Mn, V
DLB 46	Fe	Mn, V
DLB 55	Ca	Fe, Sr
DLB 57	Fe	K
DLB 59	Fe	Mn, V
DLB 61	Fe	
DLB 62	Fe	As, Mo
DLB 66	Fe	Mn, Au
DLB 67	Fe	As
DLB 118	Fe	Cr, Sr
DLB 47 (not authentic)	Fe	Mn, V
DLB 75 (not authentic)	Fe	Cr
DLB 84 (not authentic)	Fe	Mn, As, Sr
Tell Bazi 1	Fe	Zn, Sr, As$^{?}$
Tell Bazi 2	Fe	V, Cr, Mn, Zn, As, Sr
Tell Bazi 3	Fe	Cl, Zn, As, Sr

Table 2.2: Results of the XRF measurements of both the DLB seals (De Vries-Melein et al., 2010) and the Tell Bazi artefacts.

Neutron diffraction

Neutron diffraction has also been done on the DLB artefacts. The measurements show from which material the objects are made. Nine of the thirteen objects were made of haematite, three were made of goethite, one was made of calcite and the last contained mainly magnetite and partly haematite (table 2.3).

Composition (wt%) Object no.	Haematite	Goethite	Magnetite	Calcite	Quartz	Bornite	Unknown phases
DLB 45	100						
DLB 46	100						+X
DLB 47	100						
DLB 55				97,3	2,7		+X
DLB 57	94,1		5,9				+XX
DLB 59	99,1				0,9		+X
DLB 61		100					
DLB 62	92,5		0,5		7		
DLB 66	100						
DLB 67	37,3		62,7				
DLB 75		100					
DLB 84	100						
DLB 118	3,3	93,2				3,5	

Table 2.3: Overview of the results of neutron diffraction done on the DLB artefacts (De Vries-Melein et al., 2010).

PGAA-measurements

Eighteen measurements have been done with prompt-gamma activation analysis (PGAA) at the Institute of Isotopes in Budapest, Hungary. 13 artefacts from DLB and 3 objects of raw material from Tell Bazi were measured. Two artefacts, DLB 61 and 84, have been measured twice. The analysis of the data is currently being done.

PGAA was performed quantitative, while XRF was only qualitative. In addition, it is more sensitive than XRF. Although the data has not yet been analysed, already can be seen that the elements potassium (K), manganese (Mn) and vanadium (V) are present in more samples according to the PGAA measurements than according the XRF measurements. An

other advantage is that PGAA can measure the whole object, while XRF can not.

Neutron tomography and radiography

Neutron tomography and radiography have been done on the three Tell Bazi artefacts, but the data has not yet been analysed. The DLB data is also not yet available.

2.4.4 Discussion and conclusion

Authenticity

When the objects were analysed, it was not yet known that some of the seals are most likely fake. The cylinder seals DLB 47, 75 and 84 were determined to be not authentic on the base of iconography done by Prof. Dr. Adelheid Otto from the Ludwig-Maximilians-Universität, München. This does not necessarily mean that objects with a similar composition are also fake. When two objects have been produced from the same material, which may have come from the same location, they do not necessarily have to be produced in the same period.

XRF

Since the compositions of DLB 45, 46, 47 and 59 have similarities and DLB 47 is considered not to be authentic, the other three artefacts might also be considered not to be authentic, but this does not necessarily have to be so.

Furthermore, the compositions of the three objects from Tell Bazi are not the same. This is strange, since they were expected to be similar because they all originate from the same area.

The minor and trace elements Mn, V, Cr, Sr, As and K are often associated with occurrence in a mineral iron ore. These elements are most likely connected to small inclusion minerals in the objects. The reason for the occurrence of Au and Y is unknown (De Vries-Melein et al., 2010). A large amount of Cl is present in Tell Bazi 3, which might be contamination.

In addition, equally large peaks of Cr seem to be visible in a number of objects, but Cr is not said to be present in all these objects. Therefore, the presence or absence of Cr in certain objects might be discussed.

Comparison of the results of different methods

Calcite is measured as main element in DLB55 with all methods. Six out of eight objects which were identified as haematite with the neutron diffraction contain Mn according to the XRF, while the objects which were not made of haematite did not.

Since PGAA is more sensitive than XRF, it measures K, Mn and V on more samples than with XRF. K, Mn and V are observed in more samples when measured with PGAA than with XRF. This is not only because PGAA is more sensitive than XRF, but also because it measures the entire object instead of only the surface. If an object contains for example more K at the inside than at the outside, K will be observed in a higher quantity using PGAA than using XRF.

2.5 Potential sources

An inventory of potential sources was made based on a literature study, in my Bachelor thesis (Mulder, 2008, unpublished). After selecting these potential sources on the material quality and logistic factors, 148 locations remained where haematite, goethite, and magnetite could have been mined in the Old Babylonian period.

Figure 2.5 presents an overview map of the potential sources. The information in this map represents not only the locations from the Bachelor's thesis (Mulder, 2008), but also the location

Tell Bazi/Banat (Otto, 2006) was added, because raw iron oxide was found there. An arrow indicates this location. Anatolia is shown as an white area instead of a dot. Mesopotamia is the land along the two rivers in the black oval.

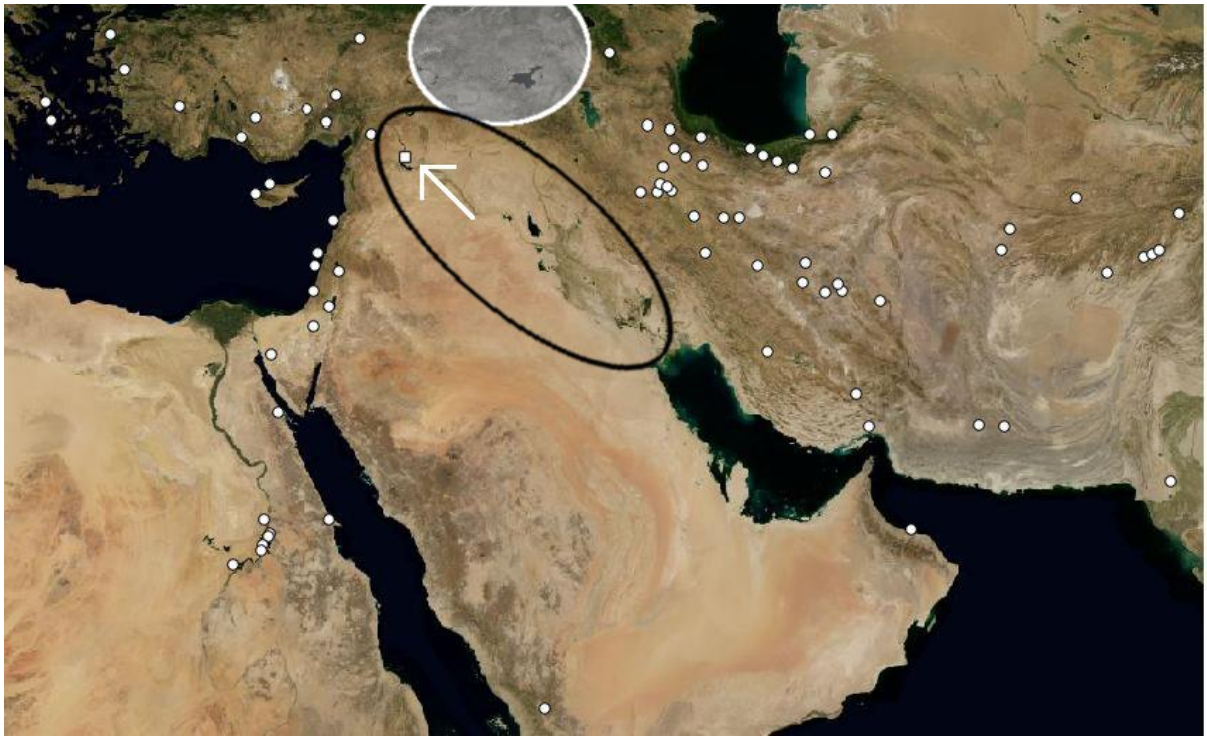

Figure 2.5: Overview map of potential useful iron oxide sources (based on Microsoft Virtual Earth 2009, Mulder 2008 and De Vries-Melein et al. 2010).

The differences in composition per area could not be determined, since little information about the exact composition was found in the literature. Unlike the general idea of Anatolia being the main iron oxide source, the result for the provenance study of my Bachelor's thesis was that iron oxide stone could also be obtained from other sources. The south-east of Anatolia, western Iran and the Levant are the most likely sources of iron oxide stone, since these areas are situated next to Mesopotamia and trade routes existed between these locations. Also evidence is found of trade between Mesopotamia and the rest of Persia and Anatolia, Egypt, the area around the Red Sea, Afghanistan and India, so it is possible that people obtained iron oxide stones from these locations. No evidence is found about trade routes to Sudan, the Caucasus, Turkmenistan, Northern Pakistan and Eastern India and in addition these are too far and too hard to reach.

2.6 Evaluation

The previous studies did not solve the problem of provenancing the artefacts. More raw material and half-fabricates have to be compared with artefacts. Therefore, artefacts and half-fabricates will be measured in this study and compared to raw material. Unfortunately, not much raw material and half-fabricates are available, so the provenance of artefacts may not be determined. However, this research will give more insight in the composition of both artefacts and half-fabricates and the difference between them. In addition, iron oxide stone duck weight will be analysed in this research, which has not been done earlier.

Chapter 3

The Objects

3.1 Introduction

In order to compare various iron oxide stone objects with each other, 38 objects have been analysed in this research. This includes 18 artefacts from the Allard Pierson Museum (APM), of which 7 cylinder seals, 2 duck weights and 9 weights or half-fabricates (3 from Selenkahiye and 6 of unknown source). And 10 cylinder seals and 10 duck weights from the Dutch National Museum of Antiquities (RMO). The photos of the APM objects and all drawings are made by the author, while the photos of the other objects are copyrighted by the RMO.

3.2 Cylinder seals

Descriptions of the 17 cylinder seals can be found in this paragraph. All seals appear to be drilled from both sides, except were this is noted differently. Five seals have text inscribed. Photos of the seals are presented in the figures a, while schematic overviews of the carvings are presented in the figures b. In these schematic overviews, damages are presented as green areas and mineralogical particularities are red. The inscribed texts are hatched because the symbols are notoriously difficult to draw by non-Assyriologists.

A1952/1.3

Size:	25 x 13 mm.
Weight:	13.36 grams.
Material:	Black with rings that were already in the stone before the objects was carved (red in fig. 3.1b).
Damages:	Many small pits and some other damages.
Carvings:	Two figures and three columns of text. These are carved besides the natural formed rings.
Origin:	Unknown.

(a) (b)

Figure 3.1: A1952/1.3

APM03221

Size: 26 x 12 mm.
Weight: 9.86 grams.
Material: Black-brown with white carvings, probably caused by contamination.
Damages: A part might have been broken off and is glued back on again. In addition, various small parts have been chipped and pits can be seen.
Carvings: Three columns of text and two large and two smaller figures.
Origin: Acquired in Iraq.

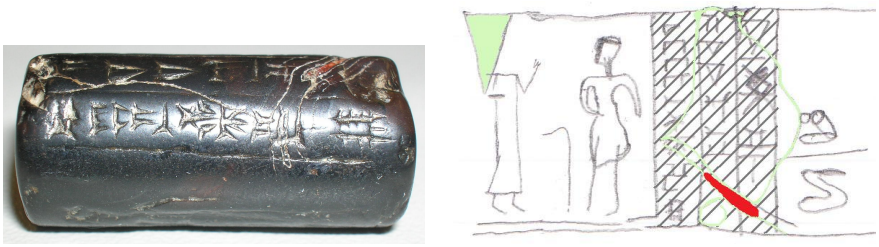

(a) (b)

Figure 3.2: APM03221

APM06361

Size: 23 x 9 mm.
Weight: 4.74 grams.
Material: Brown with many small white spots.
Damages: Undamaged except for a few pits.
Carvings: Three figures.
Origin: Acquired in Iraq.

(a) (b)

Figure 3.3: APM06361

APM06370

Size: 22 x 9 mm.
Weight: 3.87 grams.
Material: Dark brown with lighter carvings.
Damages: The bottom is slightly damages and a bit flattened.
Carvings: Two columns of text and two figures from which one with a stick-like symbol. Between the two figures sits an animal.
Origin: Acquired in Iraq.

(a) (b)

Figure 3.4: APM06370

APM06371

Size:	24 x 11 mm.
Weight:	7.54 grams.
Material:	Dark brown with lighter carvings.
Damages:	Slightly damaged in places.
Carvings:	Six figures, of which one is sitting at a throne. Two of the figures are smaller.
Origin:	Acquired in Iraq.

(a) (b)

Figure 3.5: APM06371

APM06372

Size:	20 x 10 mm.
Weight:	5.85 grams.
Material:	Between black, dark grey and brown.
Drilling hole:	Very flat, so might be modern.
Damages:	A few pits at the top and bottom.
Carvings:	The figures of this seal seems to be very different from those of the other seals, since they are much more rounded instead of just made of straight lines. One of the five figures has wings. This is probably an other style than the other seals.
Origin:	Acquired in Iraq.

(a) (b)

Figure 3.6: AMP06372

APM06377

Size: 25 x 14 mm.
Weight: 14.23 grams.
Material: Black to dark grey.
Damages: The top and bottom contain some pits and lines.
Carvings: The seal shows a figure on a throne, to the right possibly a sun with a moon crescent (personal communication M. de Vries, 2010), a small person, a figure with an animal, some unknown things and an other person. Then a line is drawn which divides the seal in two parts. Four unclear figures are visible below the line, while four things from which it is unclear what they are are visible at the top.
Origin: Acquired in Iraq.

(a) (b)

Figure 3.7: APM06377

APM13306

Size: 18 x 10 mm.
Weight: 3.18 grams.
Material: Black with light brown carvings.
Drilling hole: Very difficult to see, because of contamination.
Damages: Some scratches at the bottom and a crack and some wear at the top.
Carvings: Three figures, of which one on a thrown, and a few features between them.
Origin: Acquired in Egypt.

(a) (b)

Figure 3.8: APM13306

B1982/5.1324

Size: 25 x 18 mm.
Weight: 12.36 grams.
Material: Black, the carvings are light brown-white.
Damages: The object is broken in two and glued back together. Not only a few damages are visible at the bottom, but also a hole and a few scratches are visible at the object.
Carvings: One figure, unclear symbols and three columns of text.
Origin: Unknown.

(a) (b)

Figure 3.9: B1982/5.1324

B1982/5.1343

Size:	26 x 10 mm.
Weight:	7.33 grams.
Material:	Black, the carvings look red.
Drilling hole:	Drilled from two sides, it looks quite straight.
Damages:	A part, at which no carvings are visible, is glued to the rest of the seal.
Carvings:	Two figures and 3.5 column text.
Origin:	Unknown.

(a) (b)

Figure 3.10: B1982/5.1343

B1982/5.1366

Size:	28 x 11 mm.
Weight:	7.21 grams.
Material:	Black-grey, the carvings are white due to pollution.
Drilling hole:	Rings, possibly formed by drilling, can be seen in the two-side-drilled hole.
Damages:	The seal is intact, except for some scratches at the bottom.
Carvings:	Five figures and a few symbols.
Origin:	Unknown.

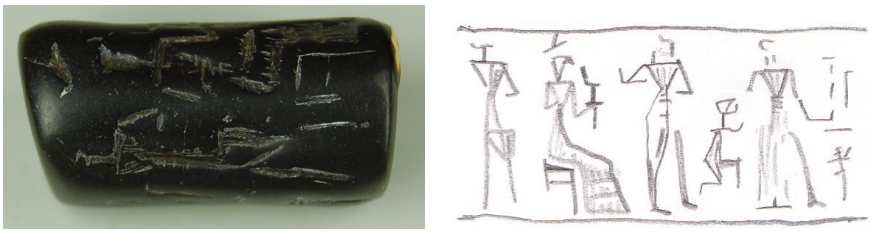

(a) (b)

Figure 3.11: B1982/5.1366

B1982/5.1368

Size: 21 x 10 mm.
Weight: 5.55 grams.
Material: Brown and black areas.
Damages: At both flat sides are some scratches visible.
Carvings: The carvings seem to be of an other style than those of the other seals, because unlike the others the figures are made of dots and stripes. Four figures and two other carvings are present in total.
Origin: Unknown.

(a) (b)

Figure 3.12: B1982/5.1368

B1982/5.1369

Size: 20 x 12 mm.
Weight: 5.99 grams.
Material: Black.
Drilling hole: A quite smooth drilling hole with rings in it.
Damages: Both flat sides are very smooth.
Carvings: A large part of the seal does not have carvings, and those present are not clear due to weathering.
Origin: Unknown.

(a) (b)

Figure 3.13: B1982/5.1369

B1982/5.1392

Size: 18 x 9 mm.
Weight: 4.43 grams.
Material: Black-grey.
Damages: Except for a few scratches, the seal is intact.
Carvings: Two of the five figures are carved upside down. The scene shows a fight with monsters or lions (personal communication M. de Vries, 2010).
Origin: Unknown.

(a) (b)

Figure 3.14: B1982/5.1392

B1982/5.1395

Size:	21 x 10 mm.
Weight:	6.20 grams.
Material:	Black-grey.
Drilling hole:	Rings are visible in the two-side-drilled hole.
Damages:	Intact and very smooth.
Carvings:	Four figures and many other small symbols.
Origin:	Unknown.

(a) (b)

Figure 3.15: B1982/5.1395

B1982/5.886

Size:	19 x 11 mm.
Weight:	6.06 grams.
Material:	Black-grey and quite matt, while the carvings have a light brown colour.
Drilling hole:	Dirt is present in the two-side drilled hole.
Damages:	The object is damaged on various places.
Carvings:	The intaglio does not seem to be very clear, no text is visible, 6 figures in total are carved. The style seems to be similar to that of APM06372.
Origin:	Unknown.

(a) (b)

Figure 3.16: B1982/5.886

B1987/5.2

Size:	21 x 9 mm.
Weight:	5.44 grams.
Material:	Grey.
Drilling hole:	Rings are visible in the two-side-drilled hole.
Damages:	Quite intact, the two flat sides are very smooth.
Carvings:	Five figures and a few symbols.
Origin:	Acquired in Syria.

(a) (b)

Figure 3.17: B1987/5.2

3.3 Duck weights

This paragraph shows the description of 12 duck weights.

A1932/7.138-A

Size:	23 x 14 x 13 mm.
Weight:	8.03 grams.
Material:	Very shiny and iron-like, black-grey.
Damages:	On the right side, when seen from above, is a long scratch visible which goes to the bottom of the object. The head is damaged in two spots, the tail has some smaller damaged areas and at the bottom of the left side is a red-brown spot visible.
Origin:	Unknown.

Figure 3.10: A1932/7.138-A

A1932/7.138-B

Size:	22 x 13 x 8 mm.
Weight:	5.65 grams.
Material:	Grey, lighter than A1932/7.138-A. Shiny, although less than A1932/7.138-A.
Damages:	A scratch at the right side of the duck, a small pit on the head and some scratches at the side of the neck and head. The last were probably made when creating the head.
Origin:	Unknown.

Figure 3.11: A1932/7.138-B

A1932/7.138-C

Size: 19 x 8 x 8 mm.
Weight: 3.25 grams.
Material: Light brown-grey and shiny. Yellow to light brown at the inside, at the place where the material has been broken off.
Damages: The neck has largely been broken off, only a small part of the head is still present.
Origin: Unknown.

Figure 3.12: A1932/7.138-C

A1932/7.138-D

Size: 20 x 10 x 10 mm.
Weight: 4.40 grams.
Material: Grey, iron like and very shiny. Light brown at the place where the material has been broken off.
Damages: The head has broken off and the bottom of the neck shows some damage.
Origin: Unknown.

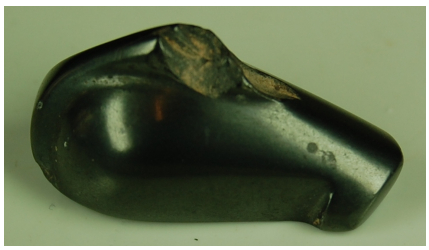

Figure 3.13: A1932/7.138-D

A1932/7.138-E

Size: 13 x 8.5 x 7 mm.
Weight: 1.78 grams.
Material: Black-grey. Not as shiny as some of the other objects. Light brown at scratches.
Creation: Instead of that the forming of the duck was done smoothly, the head and bottom of the duck weight are flat and near the tail carvings are clearly visible.
Damages: Scratches and pits are visible at various places.
Origin: Unknown.

Figure 3.14: A1932/7.138-E

A1932/7.138-F

Size: 17.5 x 7x 8 mm.
Weight: 2.42 grams.
Material: Shiny black-grey.
Damages: A few very small damages occur at the head and tail, while some larger damages occur at the bottom of the left side of the tail.
Origin: Unknown.

Figure 3.15: A1932/7.138-F

A1932/7.138-G

Size: 13 x 6.5 x 5 mm.
Weight: 0.93 grams.
Material: Dark brown, lighter brown at damages and carving areas.
Damages: Damages and the carving areas at both sides of the neck and between the tail and the body. Almost completely around the object are scratches or cracks visible.
Origin: Unknown.

Figure 3.16: A1932/7.138-G

A1932/7.138-H

Size: 14 x 5.5 x 5.5 mm.
Weight: 1.06 grams.
Material: Black-grey with an medium shine. Light brown at the damages.
Damages: Some damages along the tail and at the bottom a small pit is visible.
Origin: Unknown.

Figure 3.17: A1932/7.138-H

A1932/7.138-I

Size: 13 x 8.5 x 5 mm.
Weight: 1.32 grams.
Material: Black-brown and medium shining.
Damages: The right side is more weathered, so browner, than the left side. Many long scratches and a light brown pit are visible.
Origin: Unknown.

Figure 3.18: A1932/7.138-I

APM01768

Size: 23 x 11 x 11 mm.
Weight: 5.82 grams.
Material: Brown-grey.
Damages: The left side of the tail is broken off and at the bottom, the right side of the tail and the neck are some pits.
Origin: Acquired in Iraq.

Figure 3.19: APM01768

APM01770

Size: 19 x 10 x 11 mm.
Weight: 4.16 grams.
Material: Grey, iron like. Very shining, this is polished, not natural.
Damages: The tail and the bottom are slightly damaged and a few scratches are visible on the neck.
Origin: Acquired in Iraq.

Figure 3.20: APM01770

LB3502

Size:	51 x 28 x 27 mm.
Weight:	over 50 grams.
Material:	Black with a medium shine.
Damages:	Many damages, of which some are large pits. A part of the right side of the head has been broken off. A large pit with orange weathering is located at the right side of the weight at the side of the tail. In addition, a large pit with brown weathering, or a large pit filled up with brown material, appears in the middle of the object. Other pits appear at the middle/front of the left side of the weight and at the bottom of the side of the neck. The right side of the neck has been broken off.
Origin:	Unknown.

Figure 3.21: LB3502

3.4 Weights and half-fabricates

Half-fabricates and weights other than duck weights are taken together, because sometimes it is difficult to distinguish between half-fabricates and weights.

APM01777

Size:	43 x 12 mm.
Weight:	16.55 grams.
Description:	Grey with darker stripes on it which might be contamination and which make the object more dull. Elongated object, according to the Online database of the APM a rounded cylinder or cigar (Online database APM, no date). Since the object is very well shaped and rounded off, also at the sides, it is probably a weight and not a half-fabricate.
Damages:	Undamaged.
Origin:	Acquired in Iraq.

Figure 3.22: APM01777

APM01798

Size: 17 x 10 mm.
Weight: 4.36 grams.
Description: Brown-grey. According to the Online databases of the APM it is a rounded cylinder or a cigar. About half of the object is flat and at the top is also a flatter part of about a quarter of the length of the object. The front and back of the object are also flat. Although the object is a weight according to the Online database, it may also be a half-fabricate, because parts of the object are flattened off in order to shape the stone into something, instead of rounded off like at APM01777. On the other hand, it is very well polished, which suggests the object is finished, so that it is a weight.
Damages: Pits at various places.
Origin: Acquired in Iraq.

Figure 3.23: APM01798

APM06425a

Size: 24 x 6 mm.
Weight: 2.65 grams.
Description: It has a grey and iron like colour. It shines and the tips are flattened off. It is very smooth and rounded. According to the online database it is a cylinder cigar shaped weight. Because it is very well worked, it is probably a weight and not a half-fabricate. In addition, it is too small to make for example a cylinder seal from it.
Damages: A scratch or crack is visible through the length of the object.
Origin: Acquired in Iraq.

Figure 3.24: APM06425a

APM06425b

Size: 21 x 5 mm.
Weight: 1.41 grams.
Description: It is quite similar to a. It is also a small elongated cylinder cigar shaped (Online database APM) object, probably a weight, because it is to small to make an object from. The tips are flattened off and its colour is black-grey.
Damages: Unlike the previous it contains many pits. The shine disappeared because of all the pits.
Origin: Acquired in Iraq.

Figure 3.25: APM06425b

APM10958

Size: 61 x 20 mm.
Weight: 43.13 grams.
Description: Dark brown with lighter brown to red spots. One side is flattened off. Since it contains many cracks and spots and it is not well worked, it is probably a half-fabricate.
Damages: Many cracks and spots.
Origin: Found at an excavation at Selenkahiye in Syria on a floor of a room (Van Loon, 2001). More about Selenkahiye can be read in paragraph 3.5.

Figure 3.26: APM10958

APM10960

Size: 25 x 20 mm.
Weight: 19.01 grams.
Description: A short elongated brown object with lighter brown spots. It is probably a half-fabricate, because many areas are flattened, but no real shape is visible in it.
Damages: Pits and many light spots.
Origin: Found at an excavation at Selenkahiye in Syria, not related to any architectural characteristic (Van Loon, 2001).

Figure 3.27: APM10960

APM10961

Size: 15 x 7 mm.
Weight: 1.83 grams.
Description: Dark brown, cylinder shaped. Many flat sides are created in the length of the object. Because of the shape, it might be a half-fabricate of a cylinder seal.
Damages: A large crack runs through the length of the object.
Origin: Found at an excavation at Selenkahiye in Syria on a floor of a room (Van Loon, 2001).

Figure 3.28: APM10961

APM15888

Size: 29 x 21 mm.
Weight: 19.04 grams.
Description: It is a brown object with many lighter brown spots on it. In addition, a small green spot is visible on the object. Bi-conical according to the online database. The sides are flattened off, but the rest of the object is round. It is probably a half-fabricate, because it is flattened off and very well modeled, but it is not completely smoothened.
Damages: -
Origin: Unknown.

Figure 3.29: APM15888

APM15889

Size:	29 x 21 mm.
Weight:	5.27 grams.
Description:	Dark brown with many lighter spots on it. Cylinder according to the online database. It is, like APM15889, worked and flattened off, but not completely smoothened, so it is probably a half-fabricate.
Damages:	It contains a crack in the length of the object.
Origin:	Unknown.

Figure 3.30: APM15889

3.5 Selenkahiye

Although the exact original location of most objects is unknown, three of the half-fabricates were excavated at Selenkahiye in Syria (fig. 3.29).

Figure 3.31: Map that indicates the location of Selenkahiye (http://www.dijs.biz/kaart.gif).

The excavation at Selenkahiye was started by the University of Chicago Oriental Institute in 1967 in order to save the archaeological remains in the area, which would be flooded since a dam was build in the Euphrates at Tabqa (eth-Thawra). The excavation was continued by the University of Amsterdam in 1972, 1974 and 1975. The information in this paragraph is obtained from the final report of that excavation (Van Loon, 2001).

According to archaeological data, the settlement was assumed to have existed between 2400 and 1900 B.C.. The city had about 2000 inhabitants within the walled citadel area and possibly more in the surrounding area just outside the city. Since Selenkahiye was located at the crossing of the Euphrates and the main road from Aleppo to the east, the settlement controlled the trade routes along the river.

Ten cylinder seals and many cylinder rollings of 21 unique impressions were found. None were determined to be made of iron oxide stone. Eleven of the 16 scale weights found during the excavation were determined to be haematite. After analysis by Professor Dr. W. Stern of the Geochemical Laboratories of the University of Basle Mineralogic-Petrographic Institute, SLK 72-367, which is APM10958, turned out to be goethite. It is not mentioned in van Loon (2001) with which method the objects are determined. All but one weight were from the later phase of Selenkahiye. Only the three iron oxides weights from Selenkahiye that are measured in this research are nowadays located in the Allard Pierson Museum, the others can be found in Aleppo (Van Loon, 2001).

Chapter 4

Analytical methods and techniques

4.1 Introduction

A wide range of mineralogical, chemical and physical analysing techniques is available to gain more insight in the composition and texture of the objects studied here. However, the particular characteristics of the objects require certain features for the method.

Because the objects may not be damaged, since they are old and rare archaeological artefacts and borrowed from museums, a non-destructive method is needed. A quantitative method, which gives exact percentages of the elements or minerals that are analysed, is preferred to a qualitative method, which only shows the presence of elements and minerals and whether they occur often or not. In addition, a method is needed which does not only analyse the surface, but the entire sample, because when a sample is not homogeneous, a false composition will be found. The method should be able to detect minor and trace elements, because these are important in provenance studies. Due to this, differences can be seen in objects which looked similar with the naked eye. In order to see differences between objects, it is also useful to characterize an iron oxide as haematite, goethite and magnetite. As no method exists that can both distinguish the different iron oxides from each other and detect a suitable amount of trace elements, the characteristics of these methods are studied apart from each other.

Secondly, it is useful if the results from the measured objects can be compared with results of earlier measured objects. This requires to use the same methods as those used earlier in similar studies. In previous research neutron diffraction (De Vries-Melein et al., 2010), neutron tomography and neutron radiography (Dirk Visser), petrography (Joyner et al., 2006), PGAA (Institute of Isotopes), Raman microscopy (Joyner et al., 2006), XRD (Joyner et al., 2006), XRF (Cowell, 1985-86; Joyner et al., 2006 De Vries-Melein et al., 2010) were used.

Finally, the instruments have to be available.

Summarizing, the methods have to be useful (non-destructive, quantitative, entire object, trace elements, kind of iron oxide), preferably used earlier in similar studies and the instruments have to be available.

4.2 Method

At first the requirements of the methods will be examined.

Trace elements vs. identifying iron oxides

The ideal method could measure both the trace elements and identify which kind of iron oxide the sample is. Unfortunately, no method was found that can measure both. This means that at least two methods are needed if both functions will be used.

A method with which the atom structure can be studied, can show which elements are present, while a method with which the crystal structure or molecule structure can be studied, can distinguish different iron oxides.

The methods that measure trace elements, besides main and minor elements, are explained in paragraph 4.2.1, while the methods that can identify the type of iron oxide are explained in paragraph 4.2.2. Methods that can do neither, but might be useful in an other way are explained in paragraph 4.2.3.

Entire object vs. surface

In general, X-rays can only pass a few dozens of μms of iron oxide stone objects, while neutrons can go through the entire object. Radiation with lower energy levels and longer wavelengths than X-rays, like radio- and micro-waves, infrared radiation, visible light and ultraviolet radiation, can penetrate objects even less deep.

This means that methods which use X-rays or radiation with a lower energy level and longer wavelength can only measure the surface of iron oxide stone objects, while objects that use neutrons can measure the entire object.

Concluding, methods which use neutrons are preferred over methods that use X-rays or an other type of radiation. However, methods that use X-rays are generally speaking more easily available and cheaper than methods that use neutrons.

4.2.1 Methods with which trace elements can be measured

Instrument Neutron Activation Analysis (INAA)

The method INAA can achieve high accuracy and precision, depending on the element. Although only a small sample is required (50 mg for metals, 200 mg for silicates) (Rapp and Hill, 1998), the method can also be applied to the entire object, in a non-destructive way. There are no complex sample preparation or extraction techniques. The method uses neutron beams, so it can measure the composition of the entire object.

Radiochemical Neutron Activation Analysis (RNAA) is a variation of INAA which measures more sensitive (National Institute of Standards and Technology - NIST Center for Neutron Research (NIST-NCNR), 2002).

Prompt-Gamma Activation Analysis (PGAA)

PGAA is a variation of NAA (NIST-NCNR, 2001). It is a non-destructive technique. Objects of 5cm^3 can be measured with the instrument of the Institute of Isotope in Budapest, and even larger objects when the instrument is adjusted (R*é*vay et al., 2004). Databases exist for all natural elements (IAEA, 2003). PGAA and INAA together can measure all elements except for oxygen for the most common materials (IAEA, 2003). PGAA can determine elements that do not form radioactive products after irradiation and elements of which the half life is too long to be measured correctly with INAA (NIST-NCNR, 2002). PGAA can not differentiate between the different iron oxides (Tam*á*s and Kasztovszky, 2008).

Low energy electron diffraction (LEED)

This method is used to study the atomic structure (Cornell and Schwertmann, 2003), so it can show which elements are present in the object. Only the surface can be studied (Cornell and Schwertmann, 2003).

Particle-Induced X-ray Emission or Proton Induced X-ray Emission (PIXE)

PIXE is normally only non-destructive if the sample is less than a few millimeter (Garrison, 2003). However, sometimes, when the object may not be damaged, thick samples with no pre-treatment are used instead of thin samples. PIXE can measure trace elements, but it can only measure the surface and near surface material (Govil, 2001). It measures less deep than for example XRF. The method is very sensitive. Depth can be measured when PIXE is combined with other methods like Rutherford Back Scattering (RBS) (Govil, 2001), but this combined method still measures layers, not the whole sample (Bamford et al., 2007). The ideal sample is flat and has a uniform composition. Otherwise a number of spots is analysed and the average is taken (MRSEC, Harvard University, no date (online)).

Particle Induced Gamma-ray Emission (PIGE) is a variation of PIXE. High energy X-rays are emitted from the nucleus in this method. When X-rays are emitted from the nucleus they are called gamma rays. PIGE can only measure light elements (ANSTO, no date (online)).

X-ray fluorescence spectroscopy (XRF)

XRF can be non-destructive, since whole rock and powder can both be analysed with this method. But there are matrix and interference problems. The method is less sensitive than INAA (Rapp and Hill, 1998). The depth of analysis depends on the elements in the material and can range from a few micrometers to several millimeters (Malmqvist, 1986). XRF measures only the upper few dozens of μms of the surface of iron oxide objects (Cowell, 1985-86; De Vries-Melein et al., 2010). The costs of the XRF are lower than those of INAA.

4.2.2 Methods with which different iron oxides can be distinguished

X-ray diffraction (XRD)

According to Cornell and Schwertmann (2003), XRD is the most reliable tool for identification of a particular iron oxide, since it detects the long range order of the atoms, in contrast to most methods, which detect only the atoms and their nearby area. In contrast to most analyses, whereby the samples are powdered (Garrison, 2003; Cornell and Schwertmann, 2003), objects can also be examined non-destructively (ICN, no date (online)). XRD is rarely used as a quantitative method, because factors like texture, stress and crystal size can affect the intensities of the peaks (Da Costa et al., 2002). Only the surface can be measured with XRD.

Neutron diffraction (ND)

This method can, just like XRD, differ between haematite, goethite and magnetite (De Vries-Melein et al., 2010). ND can, unlike XRD, measure the entire object.

Magnetometry - Magnetic susceptibility

Magnetic properties can be used to characterize the different Fe oxides (Cornell and Schwertmann, 2003), although the methods which use these properties can not be used to determine the trace elements occurring in the sample. Since most methods in this category, for example isothermal remanent magnetization (IRM), alternating field demagnetization (AF) and Curie temperature analysis, are destructive (Bradák et al., 2009; Cornell and Schwertmann, 2003), only magnetic susceptibility is mentioned here.

Magnetic susceptibility χ differs between very low values, e.g. olivine, slightly higher values for the antiferromagnetic FeIII oxides haematite, goe- thite and lepidocrocite and very high values for magnetite and maghemite (Cornell and Schwertmann, 2003). So there are actually

only three groups, so not all iron oxides can be distinguished from all other iron oxides. Magnetic susceptibility can measure through a 2-3 mm thick patina on rocks, but objects smaller than 50 mm, which the objects to be measured are, can not be measured correctly (Bradák et al., 2009). Because of these two reasons, this method is not suitable for the research.

Infrared spectroscopy (IR)

Infrared spectroscopy can not determine impurities of elements other than oxalate, nitrate and carbonate, so this method, and its variations diffuse reflectance spectroscopy and Fourier-transform infrared spectroscopy (FTIR) (Cornell and Schwertmann, 2003), are not useful for detection of minor and trace elements. However, it is useful for the identification of iron oxides, because different iron oxides produce different bands in the spectra. IR can be used if the crystals of the iron oxide are too thin (<70nm) to be characterized by XRD (Cornell and Schwertmann, 2003). Since the iron oxides of this research can be measured with XRD, IR is not used. The infrared radiation can penetrate less deep than the X-rays.

Mössbauer spectroscopy

Mössbauer spectroscopy is non-destructive (Nayak et al., 2003). Mössbauer spectra can be made for about half of all elements (MEDC, 2008; RSC, 2008), while ^{57}Fe is the most studied isotope (RSC, 2008). The spectra are used for identification and characterization of iron oxides. The method is very useful when the concentration or crystallinity of the iron oxides is too low (Cornell and Schwertmann, 2003), for example in ochres. Mössbauer spectroscopy can be both quantitative and qualitative. It can identify oxides and (oxy)hydroxides (Vandenberghe et al., 2000). Disadvantages of Mössbauer spectroscopy are that the spectrum analysis is time-consuming and the Mössbauer spectrum is complex when iron is present in both reducing (Fe^{2+}) and oxidizing (Fe^{3+}) state (Nayak et al., 2003).

Photoelectron spectroscopy (PES)

Photoelectron spectroscopy (PES) can both determine the depth of the surface composition to a depth of less than 10 nm and distinguish the different kinds of iron oxides on a solid sample. The radiation comes from X-rays (XPS), which is carried out in vacuum and can therefore be destructive, or from ultraviolet (UPS) (Cornell and Schwertmann, 2003) with which can be measure less deep than for example XRD.

Raman spectroscopy

Similar to IR, Raman spectroscopy measures wavelengths in order to distinguish different iron oxides. Each band of wavelengths correspond to a certain iron oxide (Cornell and Schwertmann, 2003). The method can not detect minor and trace elements. It can measure a solid, but it is less widely used than for example IR (Cornell and Schwertmann, 2003). It can only measure the surface of an object (Smith and Clark, 2004).

Ultraviolet-visible spectroscopy (UV-Vis)

UV-Vis spectroscopy also distinguishes different kinds of iron oxide, because each iron oxide produces different bands of wavelengths. This method covers the Ultraviolet-visible area. Similar to Raman spectroscopy, UV-Vis spectroscopy measures a solid (Cornell and Schwertmann, 2003). This method can measure the objects to a lesser depth than methods that use X-rays.

X-ray absorption spectroscopy (XAS)

This method comprises X-ray absorption spectroscopy near edge structure (XANES) and extended X-ray absorption fine structure (EXAFS). EXAFS can only analyse the surface of an object, but can characterize different iron oxides. In addition, it can characterize adsorbates, mainly cations and oxyanions of Se, Cr and As (Cornell and Schwertmann, 2003), this does not mean that the method can measure main, minor and trace elements.

4.2.3 Other methods

The methods in this paragraph can not measure trace elements and can not distinguish different iron oxides, but they might be useful in an other way.

Neutron depth profiling (NDP)

NDP is a non-destructive technique. It determines the concentration of elements as a function of depth near the surface of various materials. The object has to have a flat surface (NIST-NCNR, 2003), in contrast to the round surface the objects that need to be analysed have.

Neutron Radio- and Tomography (NRNT)

Neutron tomography is a non-destructive method which measures differences in density. The method can not determine what elements are present in the sample. Neutron radiography measures through the whole object, while tomography mathematically reconstructs 3D images of individual slices. For example the homogeneity of the object can be observed with this method and whether different materials occur.

Scanning electron microscopy (SEM)

A sample can be viewed with a large magnification when using scanning electron microscopy (SEM). It gives information about the morphology of the surface of an object (Cornell and Schwertmann, 2003). It is too time consuming to use it to decide which elements are present in an object or what kind of iron oxides the object is.

4.2.4 Conclusion

Table 4.1 shows an overview of the non-destructive methods described in this paragraph.

INAA, RNAA and PGAA can measure the entire object for trace elements, while PIXE and XRF can only measure the surface. ND can measure the entire object to distinguish iron oxides, XRD does the same, but can only measure the surface.

4.3 Methods used earlier in haematite research

It is useful to use the same methods as in previous research, since the results can then be compared with the results of earlier projects. It is even better when the measurements are done at the same locations and when the same instruments are used.

Previous research done on iron oxide stone artefact is already presented in chapter two, but is summarized in table 4.2.

Function	Method	Entire object
Measuring trace elements	INAA	+
	RNAA	+
	PGAA	+
	PIXE	-
	XRF	-
Distinguishing iron oxides	XRD	-
	ND	+
	RAMAN	-
	IR	-
	UV-VIS	-
	Mössbauer	-
	Magnetometry	-
	Photoelectron	-
Other	NRNT	+

Table 4.1: Overview of non-destructive methods.

Methods	Locations	References
Neutron radio- and tomography	FRM II, Garching, Germany.	Unpublished
Neutron diffraction	ROTAX and INES at ISIS, Didcot, United Kingdom.	De Vries et al. (2010)
Petrography	Department of Conservation, Documentation and Science, The British Museum, London, United Kingdom.	Joyner et al. (2006)
Prompt-gamma activation analysis	Institute of Isotopes, Budapest, Hungary.	Unpublished
Raman microscopy	Department of Conservation, Documentation and Science, The British Museum, London, United Kingdom.	Joyner et al. (2006)
X-ray diffraction	Department of Conservation, Documentation and Science, The British Museum, London, United Kingdom.	Joyner et al. (2006)
X-ray fluorescence spectroscopy	The British Museum Research Laboratory, London, United Kingdom.	Cowell (1985-86)
	Department of Conservation, Documentation and Science, The British Museum, London, United Kingdom.	Joyner et al. (2006)
	ICN, Amsterdam, The Netherlands.	De Vries et al. (2010)

Table 4.2: Summary of methods used in previous research.

4.4 Availability of the methods

Methods that use neutrons require beam time, the time in which you are allowed to use the neutron beam, which takes a lot of time to arrange.

The XRF was the easiest to plan. Not only did it take just one day to measure a single set of artefacts, it could also be done nearby. The set of artefacts of the Allard Pierson Museum in Amsterdam was measured at the ICN also in Amsterdam. The other set of artefacts was at the Rijksmuseum van Oudheden (National Museum of Antiquities) in Leiden. Because the XRF is a hand held, it could easily be taken along. One set of the objects could be measured with the XRF in November 2008 and the other set in February 2009.

Neutron radio- and tomography was more difficult to plan, due to available beam time, other time schedules and maintenance of the machines. The objects from the RMO could eventually be measured in April 2009 and the measurements could be analysed in May of that year.

4.5 Selecting methods

4.5.1 Discussion

At least two methods are needed. One with which the trace elements can be measured and with which the iron oxide can be identified.

The method with which the trace elements can be measured should be XRF. INAA is more sensitive than XRF (Rapp and Hill, 1998) and methods that use neutrons can measure the entire object, while methods that use X-rays measure only the surface, so depending on the properties INAA or PGAA were preferred over XRF. However, XRF was available in short term and it was easy to arrange this, because it was nearby. In contrast, beam time should be arranged for INAA and PGAA, which takes long. In addition, XRF was also done in previous research at the same location and with the same instrument. So this is very useful to compare the results with each other.

An advance of that XRF does not measure the entire object is that the object codes that are drawn at some of the objects do not have to be measured. When the entire object would have been measured for material composition, these codes had to be removed.

The best method that can distinguish between the different kind of iron oxides is neutron diffraction, since it can measure the entire object. However, no beamtime could be acquired for these measurements, so this could not be used. In addition, it was not done because the logistics were more difficult to arrange than for example for XRF.

X-ray diffraction is also a reliable and often used method to identify iron oxides (Cornell and Schwertmann, 2003). Although this could also easily be done at the ICN in Amsterdam, XRD was not performed, because neutron diffraction is better than XRD and this may be done later. In addition, this research project is only a part of the research about iron oxide artefacts, so not everything could be done in this project.

Neutron radio- and tomography was also chosen to be done, because this method is useful to determine whether the objects are homogeneous. Since only the surface is measured with XRF, it is not sure whether the composition acquired from the measurements is the same as the real composition of the object. When the object is homogeneous according to the neutron radio- and tomography results, than the XRF results are valid for the entire object. When neutron diffraction was used, the composition of the entire object was known, but an average composition was taken, so nothing was known about the homogeneity. In addition, since neutron radio- and tomography can distinguish different stones, it may be noticed when a part of an artefact is fake. The painted codes on the objects are no problem for NRNT because this method makes a 3D reconstruction of the object in which the densities can be seen. The codes can be located on the images and will not be confused with the object.

4.5.2 Conclusion

The conclusion (table 4.3) is that the methods X-ray Fluorescence (XRF) and neutron radio- and tomography (NRNT) will be used in this research project. Prompt Gamma Activation Analysis (PGAA), Neutron Diffraction (ND) and XRF have already been applied to several objects in previous research related to the PhD project of Martine de Vries (chapter 2). Both PGAA and NRNT have also already been done on some objects, but the data analysis has not yet been analysed. INAA and XRD may be used later on the objects, because these methods are useful.

Methods		INAA	ND	NRNT	PGAA	XRD	XRF
Object	amount						
APM	18	-	L	L	M	-	+
DLB	13	-	P	L	P	-	P
RMO	20	-	L		L	-	+
- Duck weights	10			+			
- Inscribed seals	3			+			
- Not-inscribed seals	7			-			
Tell Bazi set 1	3	-	-	M	P	-	P
Tell Bazi set 2	14			M			

Table 4.3: Overview of the analysis done on different kind of objects. P: done previously (chapter 2), +: done and presented in this research project, M: measurements done, but data analysis is not yet finished, L: will probably be done later.

4.6 Chosen methods

This paragraph presents information about the methods used in this project. These methods are XRF and neutron radio- and tomography.

4.6.1 XRF

4.6.1.1 General information

XRF is generally applied on powder samples, which makes the method destructive. It can also be applied on whole rocks (Rapp and Hill, 1998) as a non-destructive method. The depth of analysis depends on the elements in the material and can range from a few micrometers to several millimeters (Malmqvist, 1986). XRF measures only the upper few dozens of μms of the surface of iron oxide objects (Cowell, 1985-86; De Vries-Melein et al., 2010).

The instrument emits X-rays and measures returning X-rays which have a different wavelength depending on the elements present in the object. A spectrum of different wavelengths, each belonging to a different element, is produced.

The primary energy, the X-ray that is emitted, comes from an X-ray tube (Henderson, 2000). When the primary X-ray collides to the sample, it will be absorbed by an atom. If the X-ray brings enough energy along, the innermost electron is emitted (fig. 4.1a) (Buckman-Ellis, 2004).

Because of the emission of the electron, an empty spot is formed in the inner shell which makes the atom unstable. An electron from the outer shell will move to the empty spot. This movement will cause the emission of an X-ray (fig. 4.1b). The energy of this secondary X-ray is the difference between the binding energy of the shells and hence it is unique for each atom (Buckman-Ellis, 2004).

The primary X-rays interact with each element at the surface of the sample. The secondary X-rays are observed by a detector, which converts the X-ray energy pulses to electrical pulses. Different energies represent different elements (Henderson, 2000).

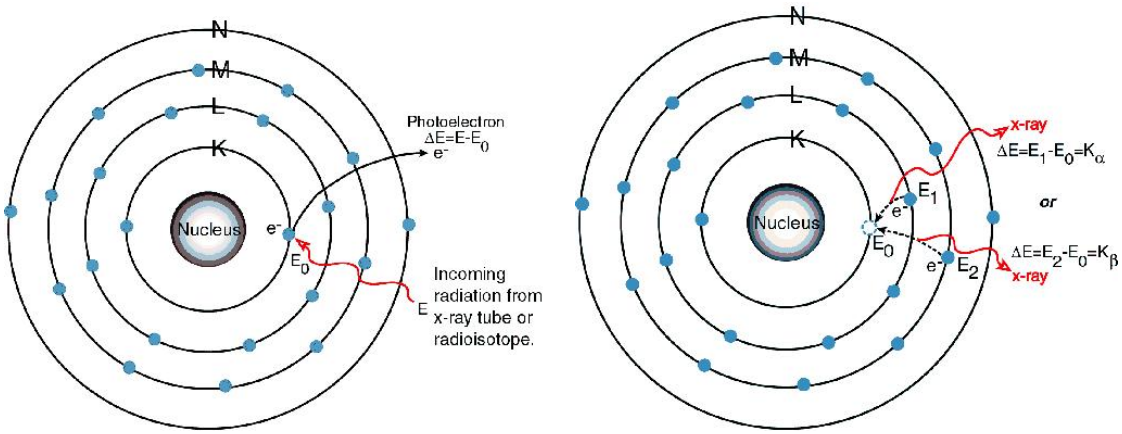

Figure 4.1: XRF principle (Buckman-Ellis, 2004).

When the instrument is calibrated for the material type which is measured, quantitative results can be obtained. The instrument used in this study was not calibrated.

4.6.1.2 Settings used for this study

XRF is done at the ICN with a Bruker Tracer III-V handheld X-ray fluorescence spectrometer with a Rhodium tube (fig. 4.2), because this instrument was also used for the measurements of the De Laigre Böhl artefacts (De Vries-Melein et al., 2010). When the De Laigre Böhl artefacts were analysed, the Bruker Tracer III-V handheld was the only available X-ray fluorescence spectrometer at the ICN (personal communication L. Megens, ICN, 2009). Standard were not available for this kind of samples, so the results could not be quantitative. The instrument can measure the elements from Al to Sr, when ordering on atomic number.

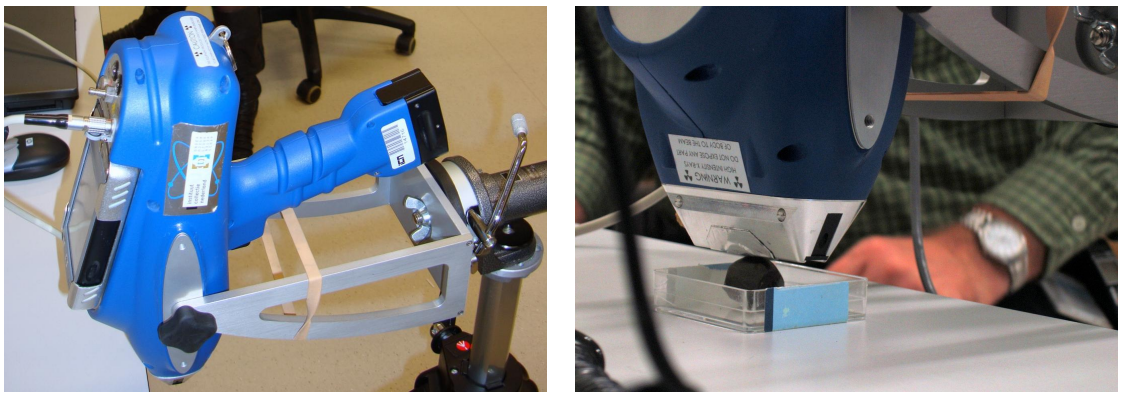

(a) (b)

Figure 4.2: The XRF instrument used (©Ron Leenheer, Allard Pierson Museum).

Measurements are done at least two times on the same object, in order to check whether the values are consistent. The handheld XRF measures areas of 5x6 mm (personal communication L. Megens, ICN, 2008).

The objects of the Allard Pierson Museum (APM) and the Dutch National Museum of Antiquities (RMO) were measured with tube settings of 15kV tube voltage and 15μA tube current. Because the De Laigre Böhl (DLB) objects were analysed with 40kV tube current and 2.2μA tube current, some objects were measured with both settings. No significant differences were observed.

The objects APM10960, LB3502 and A1932/7.138-C were not only measured with 15kV tube voltage and 15μA tube current, but APM10960 was also measured with 35kV tube voltage and 2.2μA tube current, LB3502 with 40kV tube voltage and both 2.2μA and 1.1μA tube current and A1932/7.138-C also with 40kV tube voltage and 1.1μA tube current. A1932/7.138-A and -B were only measured with 40kV tube voltage and 1.1μA tube current.

The current determines the intensity of the beam, the higher the current, the more photons are produced, while the energy and wavelength do not change. The tube voltage is presented in kV, while the measured energy of the fluorescing röntgenbeams is presented in keV.

The maximum energy is 40 keV (kiloelectron Volt). This energy is shown on the x-axis of the spectra and all elements show a different keV. The number of channels was 1024, this is the number of measurements done in the spectrum. So, measurements are done with 40 keV over 1024 measuring points. No filter was used. The livetime is how long a measurement took, this was 60,76 sec.

4.6.2 Neutron radio- and tomography

4.6.2.1 General information

Neutron tomography is non-destructive and it is a quite new method for archaeology. The first study in which neutron tomography was applied to archaeological samples was reported by B. Schillinger et al. in 1996 (Kardjilov et al., 2008).

The advantage of this method is that neutrons can easily transmit through large, dense samples (Kardjilov et al., 2008). Different densities can be observed at the neutron radio- and tomography results, so differences in material can be seen. However, it can not be said which material or which element is present (personal communication D. Visser, 2009).

Principle

The object to be measured is put on a rotation table (fig. 4.3a). A neutron beam, which is bigger than the object to be measured, is set to collide with the object. One part of the beam is absorbed in the object, while a second part is scattered out of the object and a third part goes trough the object, it is transmitted (fig. 4.3b) The neutrons which go through the object are converted to light by a plate (yellow in fig. 4.3a), because neutrons can not be detected directly. The converter material, ^{6}Li or Gd, captures the neutrons and emits X-rays or α-particles, which are converted to light by scintillating material such as ZnS. The light beam is reflected to a mirror and goes through a lens to the CCD camera which records it (Kardjilov et al., 2006).

Various measurements (e.g. 400) will be done while the object is turning. An image of a measurement is a slice from the material from the axis to the outside of the object. First, the first half of the object, from 0 ° to 180 °, is measured and than the second half to 360 °.

The neutron beam can come either from a reactor, like at FRMII in Garching (Germany) or an accelerator (synchrotron), like at ISIS in Didcot (UK) (personal communication R. Mole, FRMII, 2009).

Neutrons are produced by fission of uranium, in case of the reactor. Because neutrons with a high energy are produced, water surrounds the reactor to moderate the neutrons to lower energies. A reactor produces neutrons continuously (Kardjilov et al., 2006).

Neutrons are coming from a heavy-target, Ta or W, in a sychnotron. These are then accelerated. The fast neutrons are slowed down by collision to a moderator. The neutrons of this sources are produced in pulses (Kardjilov et al., 2006).

It is called 'cold source' when the neutrons are moderated at a very low temperature. In that case, cold neutrons are obtained, which have a higher attenuation coefficient due to their

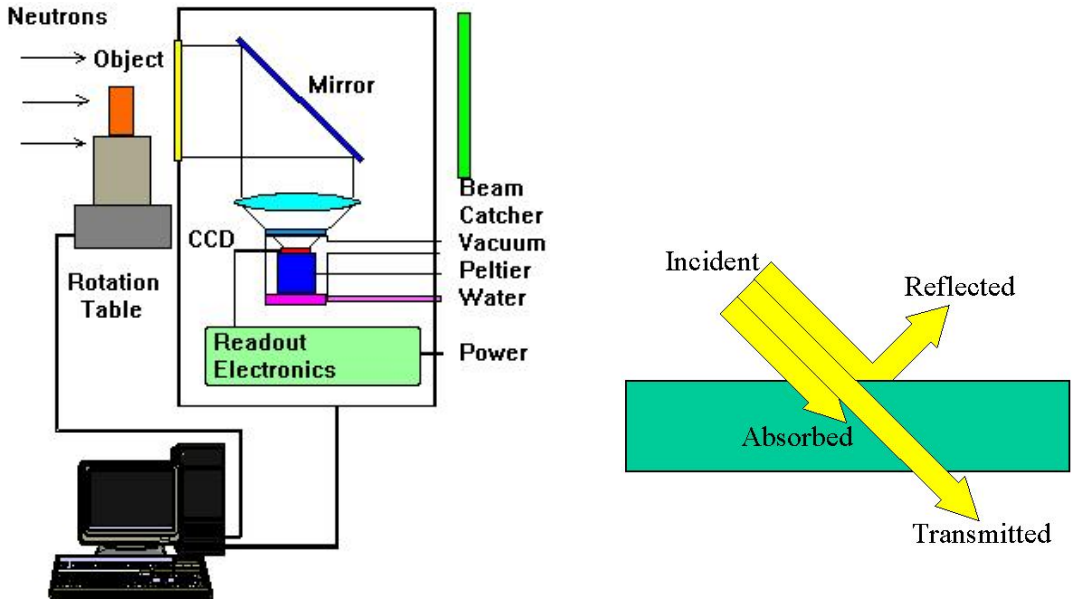

(a) (b)

Figure 4.3:
a: Schematic overview of the radiography system (Ph-TUM, no date (online)).
b: Radiation absorbed, scattered and transmitted (NOAA, no date (online)).

low energy (Kardjilov et al., 2006). The intensity of the energy beam will be more reduced with a higher attenuation coefficient when the beam goes through an object. The neutrons are called fast neutrons when they are not moderated at a very low temperature (personal communication R. Mole, FRMII, 2009).

The closer an object is to the detector, the better the resolution. However, the object has to be a few centimeters away from the plate. Many measurements are done and after each measurement the object will rotate a few degrees. Material with a lower density let a higher percentage of radiation through the object which is shown as darker spots in the image (personal communication D. Visser, 2009).

After this radiography the tomography starts, which is completely done with the computer. The tomography images have to be calculated mathematically. At first the 0° and 180° radiography images have to be set at the same point, because the object might not have been positioned precisely in the middle of the rotation table. After that, the reconstruction can be calculated mathematically. A sinogram (fig. 4.4b) is made from the radiography image (fig. 4.4a). The horizontal direction of the sinogram represents the measurements going from the outside to the middle of the object. A digital 3D model (fig. 4.4c) is made based on the sinograms, existing of a lot of pixels with density data. Digital slices can be made of that 3D model (personal communication D. Visser, 2009).

Reconstruction artefacts

Mistakes can occur in the reconstruction of the 3D model. Reconstruction artefacts are mistakes which occur in the model as rings of different density. Rings can always be seen after the reconstruction of a 3D object, but it depends on the object whether the rings are also visible in the object itself or whether they are only visible in the reconstruction. Some properties of the object increase or decrease the rings. Properties that might influence the rings are the material

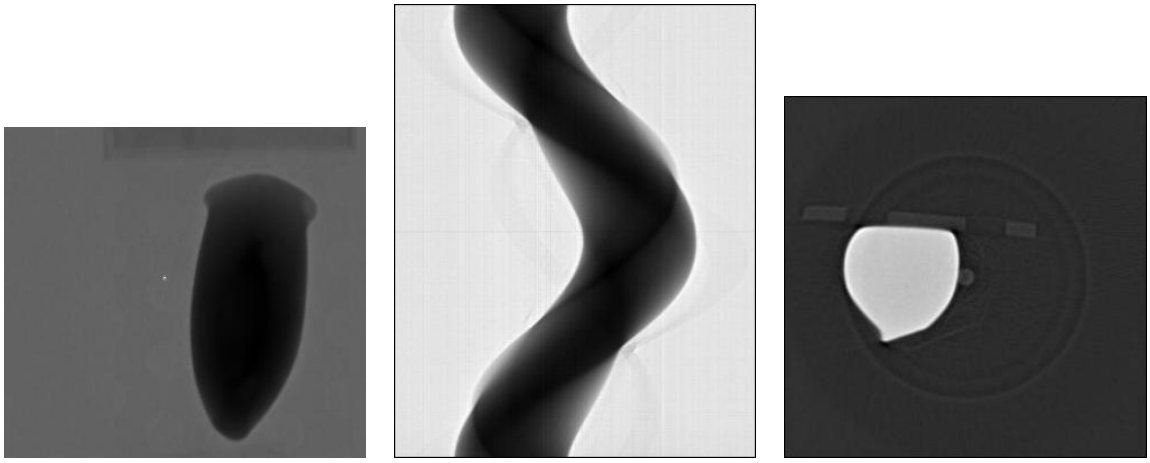

(a) Radiography image (b) Sinogram (c) Reconstruction

Figure 4.4: From left to right the image from the radiography measurement (179,100° of 360°), the sinogram and reconstruction (the 145th images of 291 in total) of A1932/7.138-D.

and the size of the object, the position of the object to the rings and whether the object is placed in the center during the measurements. The reconstruction rings can be reduced by using a filter as can be seen in figure 4.5 (personal communication D. Visser, 2009).

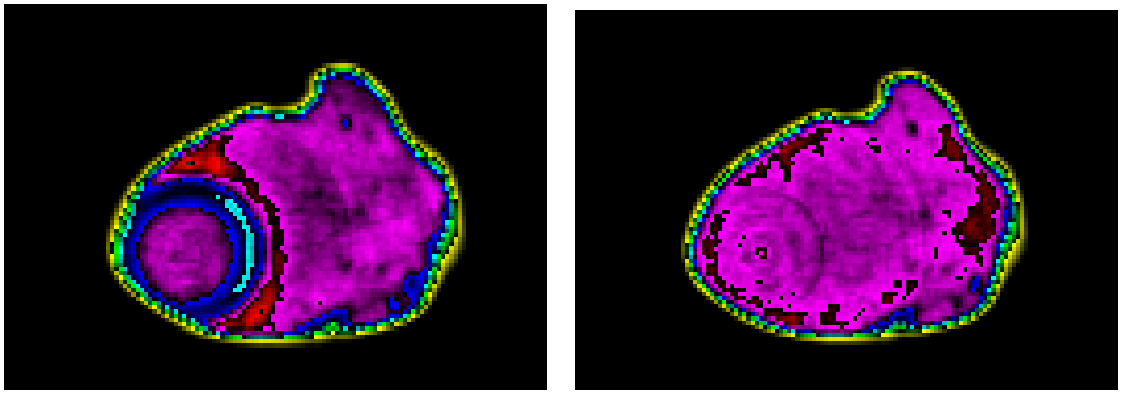

(a) Axial slice of A1932/7.138-G without ring filter. (b) Axial slice of A1932/7.138-G with ring filter.

Figure 4.5: Axial slices of A1932/7.138-G with and without ring filter.

Half voxels

The tomography image can be surrounded by a thin layer of a very low density (fig. 4.5). This layer is not necessarily material with a very low density, it can also be a half of a voxel. The 3D image is build of voxels which are 3D pixels. This voxel might be only a half voxel at the border of the object. Therefore, the value of this voxel is also seen as half. For example when a voxel has the value of 60, the half of the voxel is interpreted as a whole voxel with the value of 30, and so it presents a lower density (personal communication D. Visser, 2009).

Radiation

The objects can not be handled for a few days after the neutron radiography images are made, because radiation can come from the objects.

When a neutron collides with an atom, the isotope of the element can change. It depends on the element if that is a problem. For example, when uranium or cobalt split, it takes a long

time before the isotope falls back. But it is not a problem when for example iron splits, because this falls back after a short amount of time (personal communication D. Visser, 2009).

4.6.2.2 Settings used for this study

The radiography measurements have been done at the FRM (Forschungsreaktor München) II from the Technische Universität München in Garching, Germany. The instrument ANTARES (Advanced Neutron Tomography And Radiography Experimental System) was used in this project.

The neutrons are produced in a reactor core and moderated by heavy water. They are cold source neutrons, the energy is also reduced by cooled liquid deuterium (Ph-TUM, no date (online)).

400 measurements are done in the 360 rotation of the objects. The number of projections needed depends on the sample size (Kardjilov et al. 2008). The pixel size of the images is 0,082812 mm. The camera range was 2048x2048 pixels.

First, measurements are done without the objects in order to check both the camera and the beam. This was done five times with the beam on, which resulted in the open beam images, and five times with the beam off, the dark images.

Three series of measurements were done for this research. The first contained four duck weights, the second two duck weights and three cylinder seals and the third four duck weights.

The objects of one series were taped to an aluminium plate with aluminium tape. This tape contained some organic material, but this could be filtered during the analysis (personal communication D. Visser, 2009).

The tomography reconstruction is done with the computer program 'Verknüpfung mit all in one' and the program 'VGStudioMax', which is a program for voxel analysis and visualisation, is used to separate different areas of density in the objects and to add colours to these parts.

Three different sections have been made of the 3D model. The axial, in which the width is x and the height is y (fig. 4.6a), the sagittal, in which the width is y and the height is z (fig. 4.6b) and the frontal section, in which the width is x and height is z (fig. 4.6c). The axial slices are made by cutting the 3D image of the object in slices following the z axis as path. For making the sagittal slices, the x axis was used as path and for the frontal axis, the y axis was used as path. The length of x, y and z is different per object and can be seen in table 4.4.

Objects	x	y	z
A1932/7.138-A	192	183	301
A1932/7.138-B	172	130	287
A1932/7.138-C	145	148	266
A1932/7.138-D	124	120	248
A1932/7.138-E	114	131	228
A1932/7.138-F	118	110	176
A1932/7.138-G	128	91	65
A1932/7.138-H	89	87	185
A1932/7.138-I	95	86	169
A1952/1.3	193	185	332
B1982/5.1324	210	193	337
B1982/5.1343	174	162	349
LB3502	383	400	678

Table 4.4: Maximum x, y and z for each object.

The axial slices of the duck weight are taken through the z-axis, from the front to the back of the object, if you consider the front the side to which the duck is not looking. The bottom

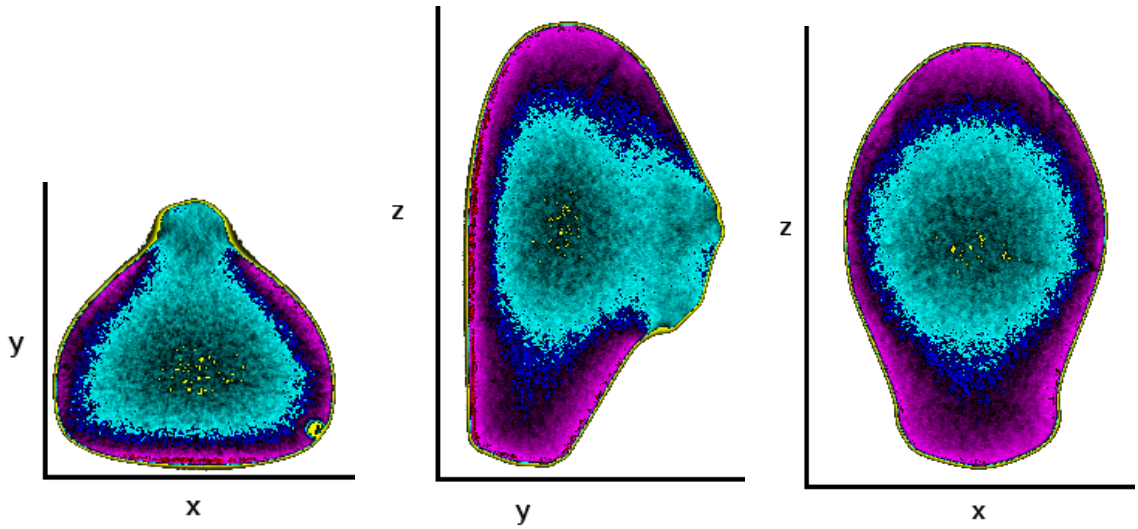

(a) Axial slice 155 (b) Sagittal slice 96 (c) Frontal slice 57

Figure 4.6: Axial, sagittal and frontal slices of object A1932/7.138-a, indicating the different sections in relation to the axes.

is below in this view. The x-axis goes from the left to the right through the object, if you see the object from above. The back is below in this view. The measurements were going from the bottom to the top in the frontal view. The backside was down in the image. The location of the x-, y- and z-axis in relation to the duck weight is shown in fig. 4.7a.

The z-axis of the cylinder seals is going through the length of the object while, the x- and y-axis are going through the short end of the object. Where they exactly go depends per object. Fig. 4.7b shows the three axes in a cylinder seal.

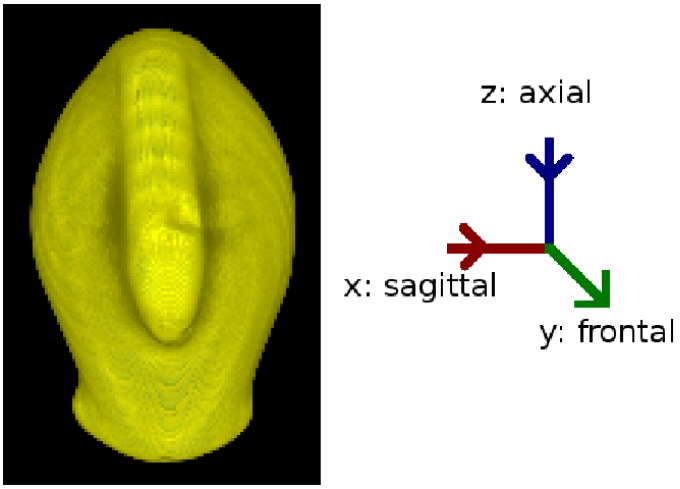

(a) A1932/7.138-a

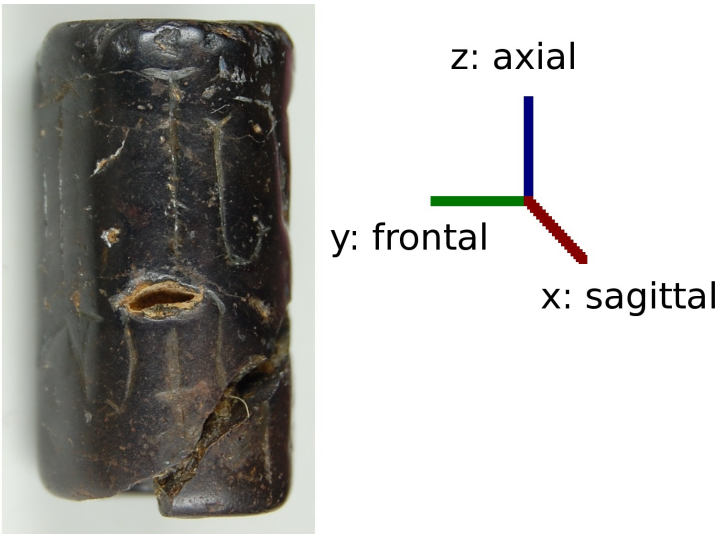

(b) B1982/5.1324

Figure 4.7: A duck weight and a cylinder seal with their axes indicated.

Chapter 5

Results

5.1 Introduction

The 38 objects described in chapter 3 are measured with XRF. In addition, 10 duck weights and 3 cylinder seals are measured with neutron radio- and tomography. First the results of the XRF and than the results of the NRNT will be shown in this chapter.

5.2 XRF

The 38 objects are measured with X-ray Fluorescence (XRF). The spectra of these measurements can be seen in fig. 5.2-5.12. The results are also presented in table 5.1.

At least two measurements on different areas were done at all samples in order to check whether the values are consistent. The first measurement is presented as a black spectra, while the second is presented as a red spectra. A third measurement (blue spectra) is done at both A1932/7.138-C and B1982/5.1324. The third measurement of B1982/5.1324 was done in order to see whether the two parts of the seal, which seemed to be glued together, had the same composition, while the third measurement of A1932/7.138-C was done after changing the XRF settings. Even a fourth measurement (yellow spectra) was done on APM10960 and LB3502, because, since these objects were the first to be measured, the right settings had to be found.

Since the peaks in the spectra of APM13306, B1982/5.1343, B1982/5.1369 and B1982/5.886 are higher than those of other objects, the scale of the spectra in the figures has been changed in order to get a better view of the peaks.

When peaks are high, they can cause other peaks, like at the Fe peaks in most measured objects. Not only the Kα and Kβ peaks of Fe are visible, but also an escape peak, an edge effect peak and sum peaks at Kα+Kα, Kα+Kβ and Kβ+Kβ (fig. 5.1). In addition, a small Cu peak and a Rh peak are caused by the XRF instrument. The height of the Rh peak differs per object, because different materials give different reflections. Peaks that do not represent elements are not mentioned further in this report.

The elements are subdivided in main, minor and trace elements. Although the method is not quantitative the height of the peaks gives an indication. The main element of all samples is iron, except for APM13306 of which the main element is calcium.

Some objects show similar XRF results. Three groups of objects could be formed based of these results. The groups are described in the paragraphs 5.2.1 to 5.2.3. The XRF results of the remaining objects are presented in paragraph 5.2.4.

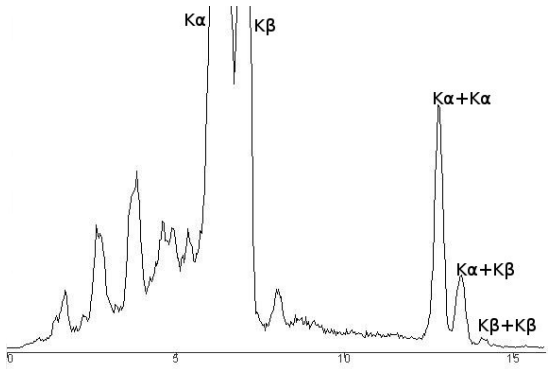

Figure 5.1: The Kα and Kβ peaks at the left and the escape peaks at the right.

5.2.1 Group 1

Core

The largest group that can be formed is the group of objects which contain besides iron, the elements Al, Si, S, K, Ca, V, Mn and Cr. This group contains the objects A1932/7.138-F, -G and -H, APM06370, APM06371, APM06377, B1982/5.1366, B1982/5.1392 and B1982/5.1395 (fig. 5.2 and 5.3).

Mn is a minor element in all the samples. The Mn peaks of APM06371 and APM06377 are very high and very close to the Fe peak, so not visible in the figure. The peak of Mn is the second highest peak in all samples. Ca is a minor element in all samples, it is present in only one measurement of A1932/7.138-F. V is a trace element in APM06370, but a minor element in all other samples. Si is minor element in APM06371 and A1932/7.138-H, but a trace element in the other objects. Al, S, K and Cr are trace elements in all objects. The Al peak of APM06370 and the Cr peak of A1932/7.138-F are not very clear.

Other objects

APM01768, APM01798, APM10958 and B1982/5.1324 may also occur in group 1, since they differ only in one element from the composition of the other objects in this group.

APM01768 (fig. 5.4a). This object contains all elements present in the objects on which group 1 is based, without Ca. This is only one element, but a relative large difference, since Ca is a minor element in the other objects. Furthermore, S and Mn can only be observed in the first measurement of this object. Concluding, the object contains V and Mn as minor elements and Al, Si, S, K, and Cr as trace elements. Almost all peaks of the first measurement are higher than those of the second measurement.

APM01798 (fig. 5.4b). The spectra show peaks at the same places as at the initial objects. Only Cr is not present in this object. This does not matter, because Cr is unclear in many spectra and it is only a trace element in the initial objects of group 1. Summarising, Ca and Mn are present as minor elements and Al, Si, S, K and V as trace elements.

APM10958 (fig. 5.4c). This object contains the same element as the core objects, except for Mn. Mn is a minor element in all the initial objects, so it is quite important. Ca is a minor element in this object, while Al, Si, S, K, V and Cr are trace elements. Some peaks of the second measurement are slightly higher than those of the first measurement.

B1982/5.1324 (fig. 5.4b). All elements from the core objects of group 1 occur in this object, except for V. V is quite important, since it is a minor element all but one objects. This object contains Ca and Mn as a minor element and Al, Si, S, K and possibly Cr as trace elements. The peak of Cr is very unclear.

The compositions of the objects A1932/7.138-D, APM03221, APM06361, APM06377, B1982/5.886 and B1987/5.2 differ in two elements from the composition of the objects in the core of group 1.

In group 1, the present of Ca, V and Mn is very dominant. Therefore, A1932/7.138-D, APM03221, APM06372, B1987/5.2 are not placed in this group. A1932/7.138-D does not contain Ca, but Ti is present in one of the measurements. APM03221 does not contain V and Mn. APM06372 misses Ca and Mn and B1987/5.2 misses V and Cr.

APM06361 and B1982/5.886 may be present in this group. APM06361 only misses Cr and contains Ti and B1982/5.886 contains P instead of S.
Summarising:

APM06361 (fig. 5.5a). This object contains Si, Ca, Ti, V and Mn as minor elements and S, K and possibly Al as trace elements. The peak of Al is not very clear and Ti can only be seen in one of the measurements.

B1982/5.886 (fig. 5.5b). The spectra show the minor elements Ca, V and Mn and the trace elements Al, Si, P, K and Cr. P is only visible in the first measurement. The Ca peak is much higher in the first than in the second measurement.

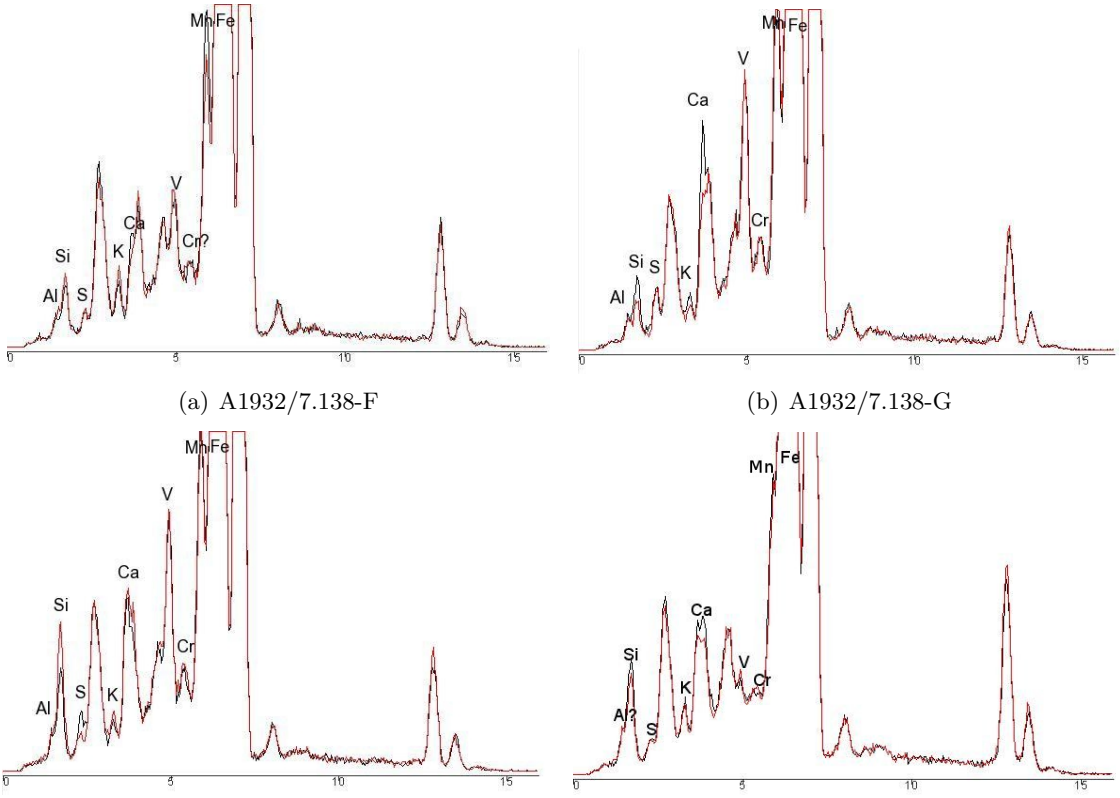

(a) A1932/7.138-F

(b) A1932/7.138-G

(c) A1932/7.138-H

(d) APM06370

Figure 5.2: XRF spectra of group 1.

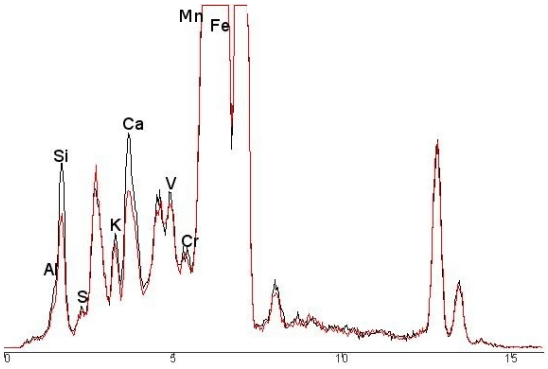

(a) APM06371

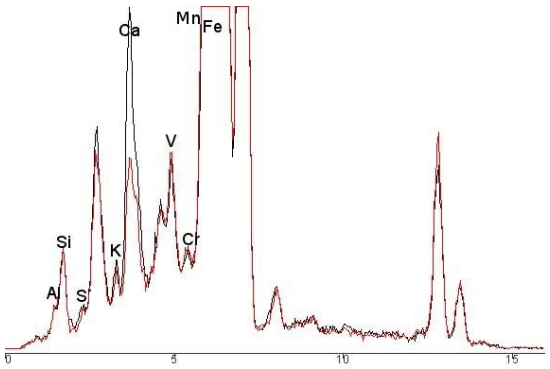

(b) APM06377

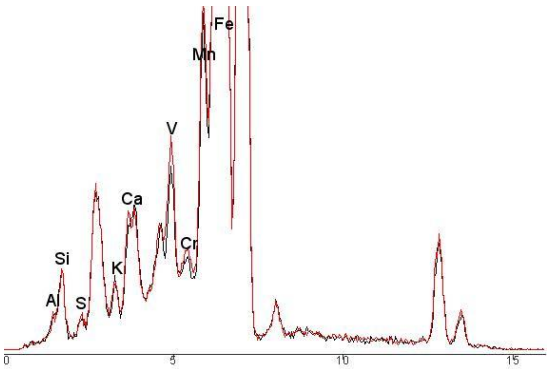

(c) B1982/5.1366

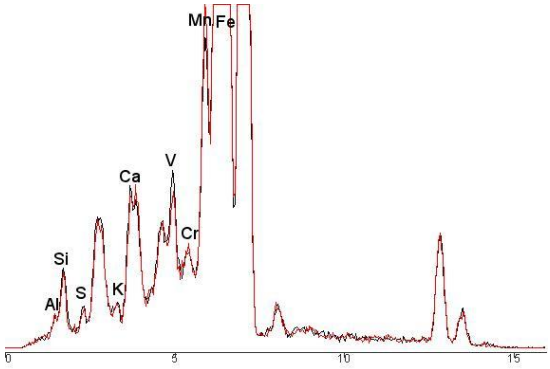

(d) B1982/5.1392

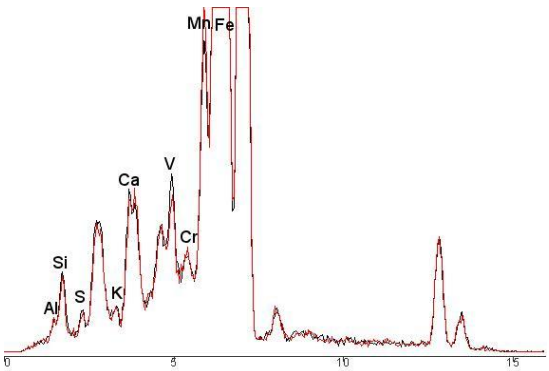

(e) B1982/5.1395

Figure 5.3: XRF spectra of group 1.

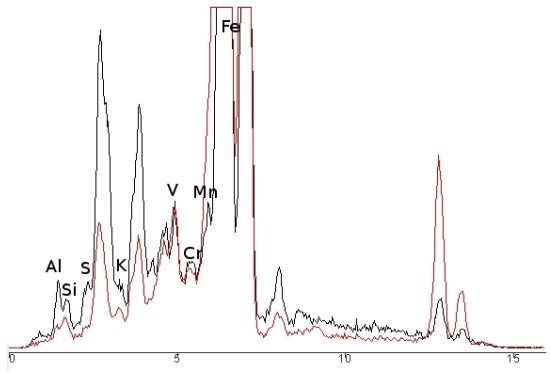

(a) APM01768

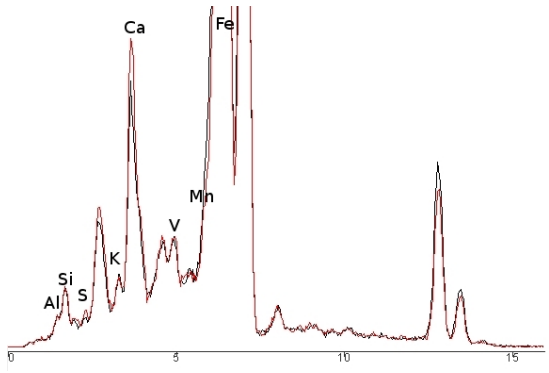

(b) APM01798

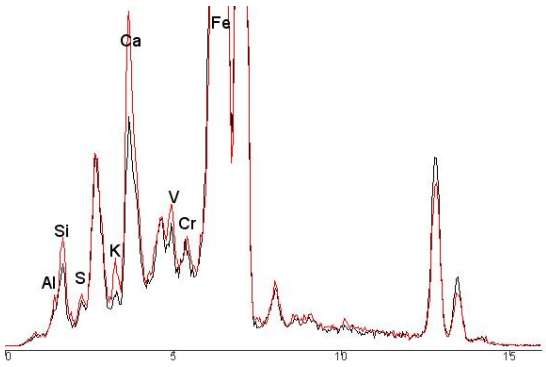

(c) APM10958

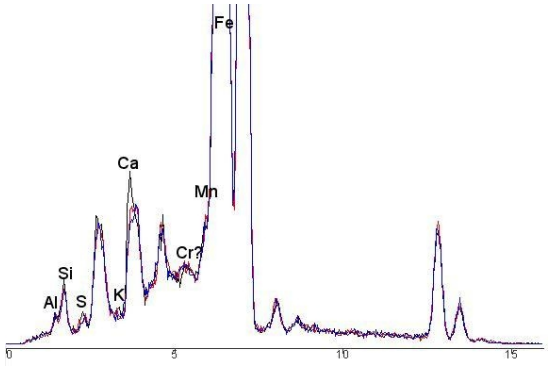

(d) B1982/5.1324

Figure 5.4: XRF spectra of objects possibly present in group 1, differing in 1 element1 from the core objects.

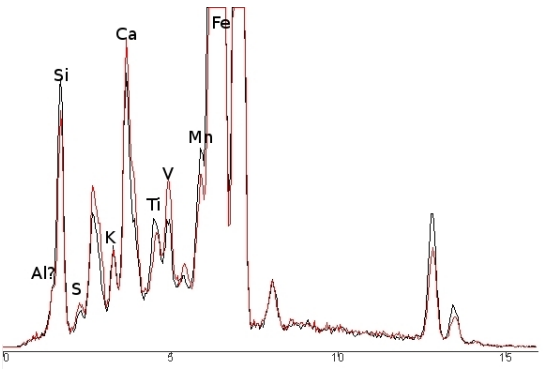

(a) APM06361

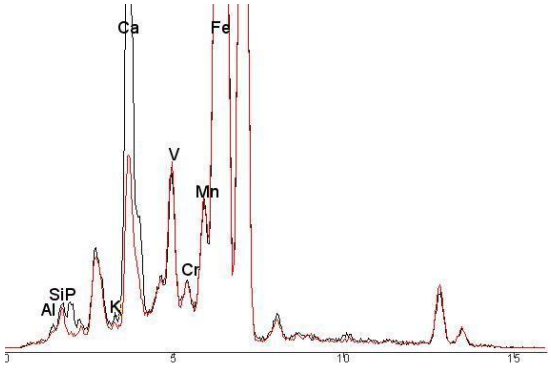

(b) B1982/5.886

Figure 5.5: XRF spectra of objects possibly present in group 1, differing in 2 elements from the core objects.

5.2.2 Group 2

Core

The object B1982/5.1343 exists of two parts, which are both measured. The part at which the second measurement of B1982/5.1343 was done and the object B1982/5.1369 are in the second group. These are the only measured objects which contain some Ni (fig. 5.6), furthermore, they contain Si, S, K, Ca, Cr and Mn.

The scales of the figures 5.4 a and b are set differently, in order to gain the best view for each object. When looking to the three measurements relative to each other, the peaks of Si and Ni are almost the same height. The Ca and Cr peaks of B1982/5.1343 are only a bit higher than those of the measurements of B1982/5.1369.

Si and Ni are minor elements in the objects. Ca and Cr are minor objects in B1982/5.1343, while they are trace elements in B1982/5.1369. S, K and Mn are trace elements in both objects.

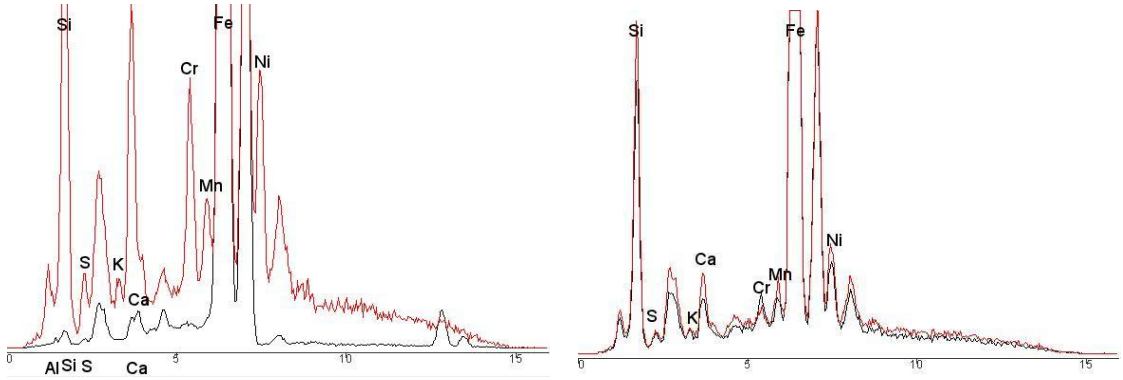

(a) B1982/5.1343 (b) B1982/5.1369

Figure 5.6: XRF spectra of group 2.

Other objects

None of the other objects differs in one element from group 2. Only the object B1982/5.1324 differs in 2 elements from group 2, but it differs also in one element from group 1. Unlike the other objects of this group it contains Al and does not contain Ni. Since the presence of Ni is, together with a high Si peak, the largest characteristic of this group, B1982/5.1324 does not belong to group 2.

5.2.3 Group 3

Core

The third group consist of the objects APM06425-a and b (fig. 5.7). These objects contain the elements Al, Si and S. Cr might be present as a trace element, but the peak is not clear. The Al peak of APM06425b is also not very clear, but a shoulder can certainly be distinguished.

Other objects

APM10961 (fig. 5.8) may also belong to this group, since it contains the same elements as APM06425-a and b, and a small K peak. It contains traces of Al, Si, S, K and maybe Cr, of which the peak is not very clear are shown in the spectra.

A characteristic of group 3 is that the spectra contain few small peaks of trace elements. A1932/7.138-I, APM03221 and APM06372 contain relative large peaks of respectively Ca, Ca

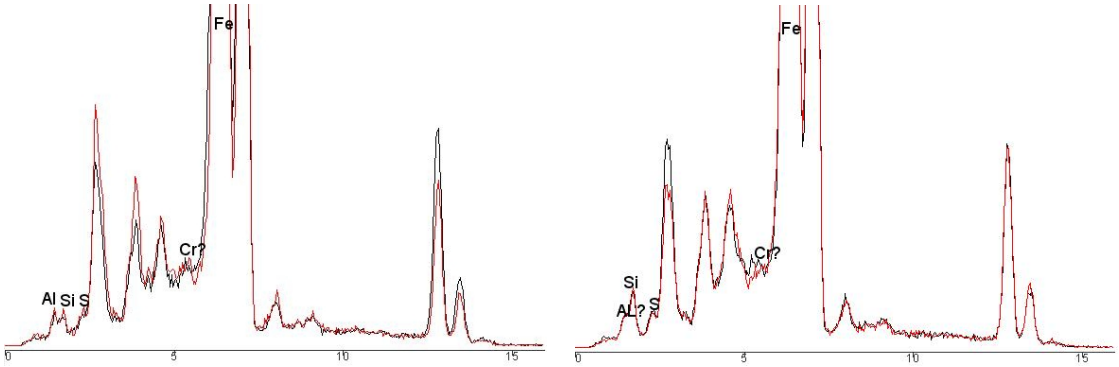

(a) APM06425a (b) APM06425b

Figure 5.7: XRF spectra of group 3.

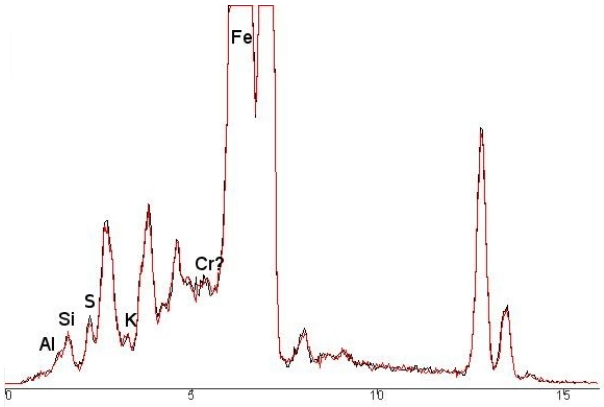

Figure 5.8: APM10961, possibly present in group 3, differing in 1 element from the core objects.

and V. Because of this, these objects are not placed in group 3. Further differences are that A1932/7.138-I misses Cr and APM03221 and APM06372 contain traces of K.

APM01777 and APM10960 can be places in group 3, since APM01777 only misses the trace elements Al and Cr and APM10960 has a trace of V instead of Cr.

Summarising:

APM01777 (fig. 5.9a). This object contains Si as a minor element and S as a trace element.

APM10960 (fig. 5.9b). The spectra present trace elements of Al, Si, S and V. The peaks of the third and fourth measurement are a bit higher than those of the first and second measurement.

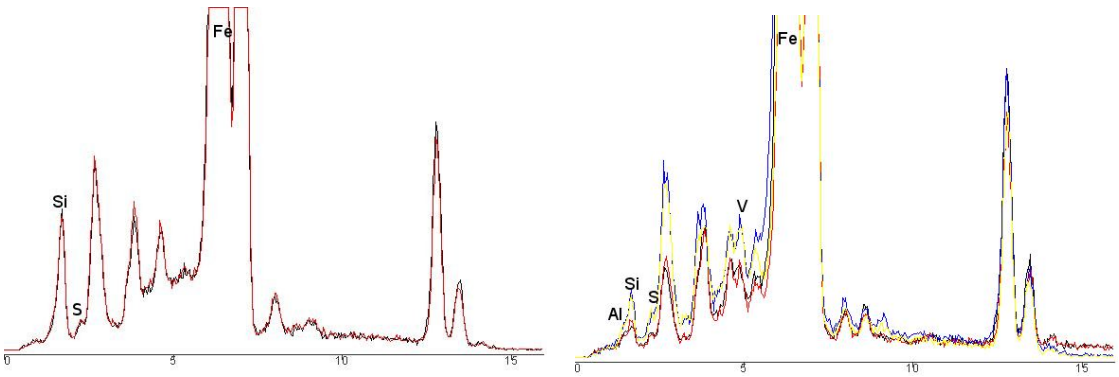

(a) APM01777 (b) APM10960

Figure 5.9: XRF spectra of objects possibly present in group 3, differing in 2 elements from the core objects.

5.2.4 Other objects

The other objects differ in 3 or more elements from the objects on which the groups are based or differ in 2 elements and are rejected from the groups in the previous paragraphs.

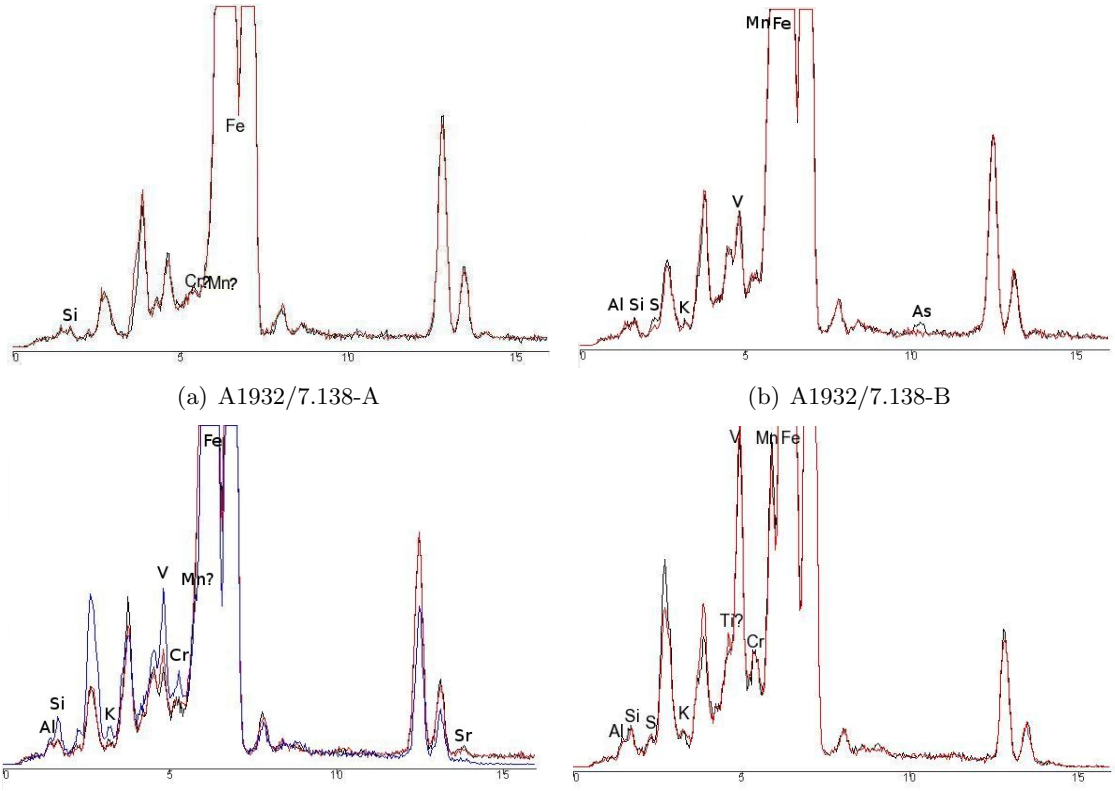

(a) A1932/7.138-A

(b) A1932/7.138-B

(c) A1932/7.138-C

(d) A1932/7.138-D

Figure 5.10: XRF spectra.

A1932/7.138-A (fig. 5.10a). These spectra shows an unclear peak of an trace of Cr and no peak of Mn, but a small broadening of the base of the Fe peak is visible, which indicates that a trace of Mn might be present. In addition, a small peak of Si is visible, which indicates a trace of Si.

A1932/7.138-B (fig. 5.10b). This object contains the minor elements V and Mn and traces of Si, S, K and As. As is only shown in one measurement.

A1932/7.138-C (fig. 5.10c). V and possibly Mn are present as a minor element and Al, Si, K, Cr and Sr as trace elements. Cr and Sr are only visible in one of the measurements. The peak of Mn is unclear, but in the third measurement a small peak is visible. Some peaks are higher in one of the measurements than in the others.

A1932/7.138-D (fig. 5.10d). The spectra present, apart from Fe as main element, V, Mn, Cr and possibly Ti as minor element and Al, Si, S and K as trace elements. Ti is only present in one measurement.

A1932/7.138-E (fig. 5.11a). Ca and Mn are present as minor element and Al, Si and S as trace elements.

A1932/7.138-I (fig. 5.11b). Ca is possibly a minor element in this object. It is difficult to see, because the peak is not clear and next to an escape peak of Fe. Si is a trace element according the first measurement and a minor element according the second measurement. Since the average of the two peaks is as high as a trace elements, Si is considered to be a trace element in this object. Al and S are present as trace elements. The S peak is only visible in one of the measurements.

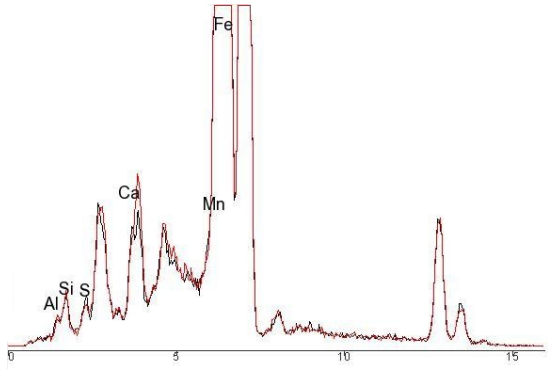

(a) A1932/7.138-E

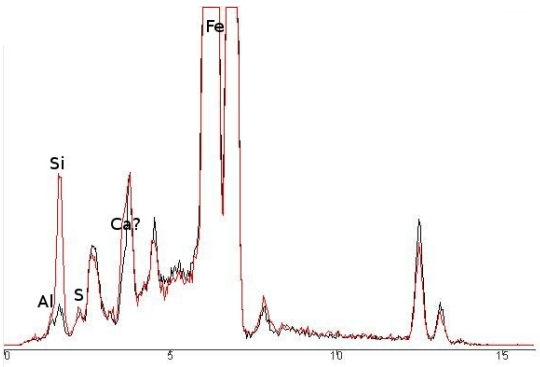

(b) A1932/7.138-I

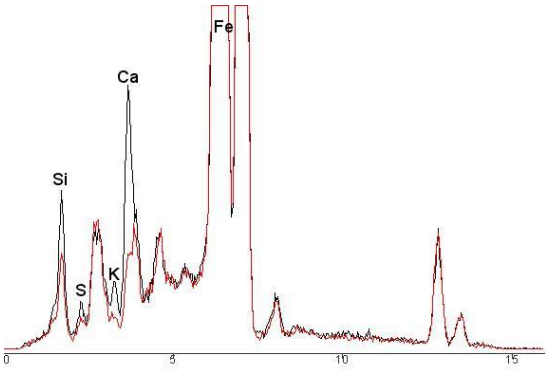

(c) A1952/1.3

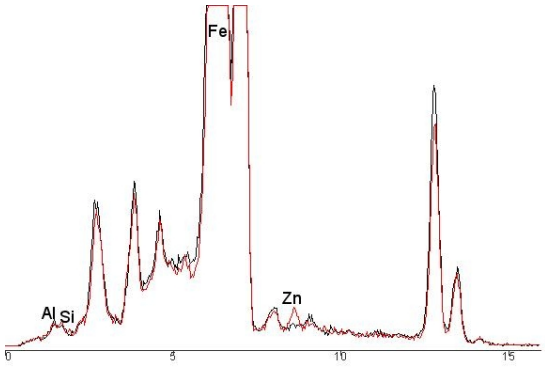

(d) APM01770

Figure 5.11: XRF spectra.

A1952/1.3 (fig. 5.11c). Ca and Si are present as minor elements and S and K as trace elements. The peaks of those elements are a bit higher in the first measurement than in the second.

APM01770 (fig. 5.11d). The spectra present the trace elements Al and Si. In addition, the trace element Zn is shown only in the second measurement of this object.

APM03221 (fig. 5.12a). Traces of Al, Si, S, K and maybe Cr are present, although the Cr peak is not very clear in both measurements. In addition, the object contains the minor element Ca, although the peak is not very clear in the second measurement.

APM06372 (fig. 5.12b). Peaks of the minor element V and trace elements Al, Si, S, K and Cr can be seen.

APM13306 (fig. 5.12c). This object is the only one that has Ca as main element instead of Fe. Furthermore, it contains the minor elements Fe and Si and traces of Ti, V, Cr and Mn. The peaks of Fe and Ti are a bit higher in the second measurement than in the first.

In **APM15888** (fig. 5.12d). Ca and Si can be observed as minor elements and Al, S and K as trace elements.

APM15889 (fig. 5.12e). The spectra present Ca as minor element and Al, Si and V as trace elements.

B1982/5.1343 (fig. 5.6a). The first measurement contains Al, Si, S, Ca and Mn as trace elements, while its second measurement contains Si, Cr and Ni as minor elements and S, K and Mn as trace elements. In addition, the second measurement presents much higher peaks than the first. Since the artefact seemed to exist out of two different stones glued together and the two measurements are very different, they are shown separately in table 5.1.

B1982/5.1368 (fig. 5.12f). Ca is present as a minor element and Si and S as trace elements. The Ca peak is much higher in the second than in the first measurement.

B1987/5.2 (fig. 5.12g). Peaks of the minor elements Ca and Mn and the trace elements

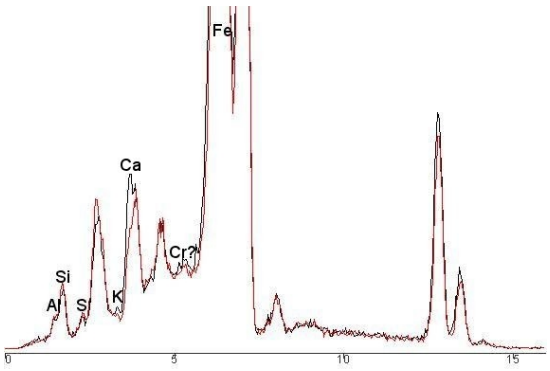

(a) APM03221

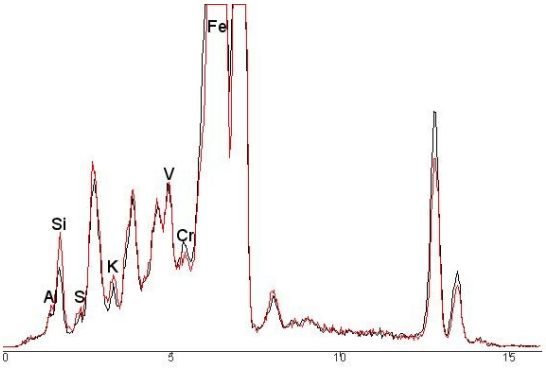

(b) APM06372

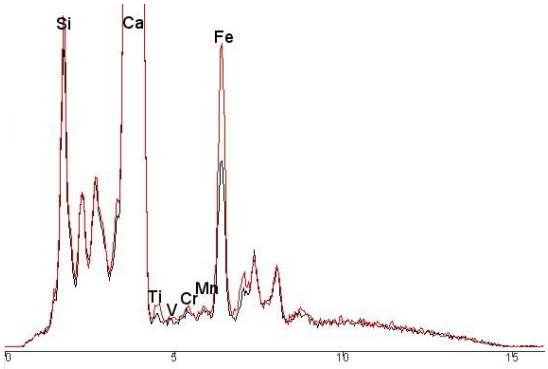

(c) APM13306

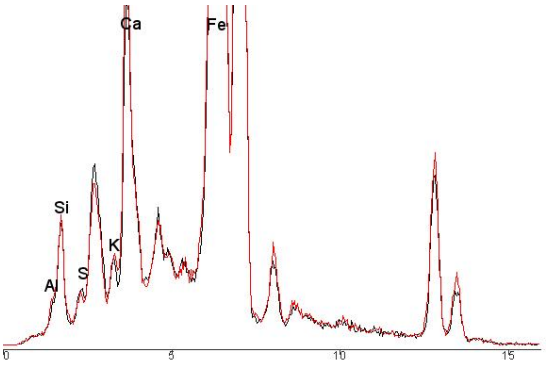

(d) APM15888

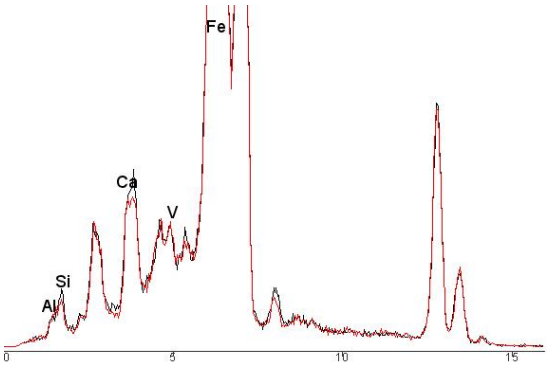

(e) APM15889

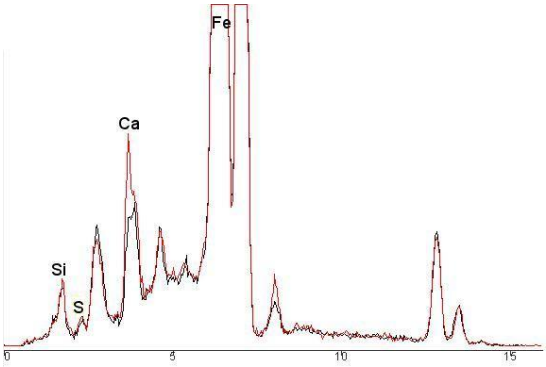

(f) B1982/5.1368

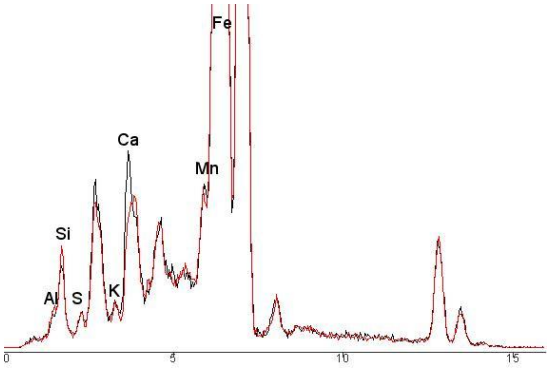

(g) B1987/5.2

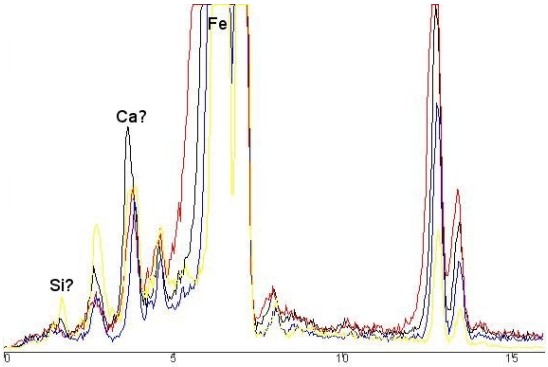

(h) LB3502

Figure 5.12: XRF spectra.

Al, Si, S and K can be seen. The Ca peak is, also at this object, a bit higher in the first than in the second spectrum.

LB3502 (fig. 5.12h). Besides Fe, a peak of trace element Si can be seen in the fourth measurement and peak of minor element Ca in the first measurement. There are lumps of in Si and Ca in the other measurements, but that are not clear peaks. So it is not sure whether the elements Si and Ca are present in the object. The height of the peaks variate much, because the settings were different during the different measurements.

Object	Elements															Group
	Al	Si	P	S	K	Ca	Ti	V	Cr	Mn	Fe	Ni	Zn	As	Sr	
A1932/7.138-a		x							x$^{?}$	x$^{?}$	++					
A1932/7.138-b	x	x		x	x			+		x	++			x^{1}		
A1932/7.138-c	x	x			x			+	x^{1}	+$^{?}$	++				x^{1}	
A1932/7.138-d	x	x		x	x		+^{1}	+	+	+	++					
A1932/7.138-e	x	x		x		+				+	++					
A1932/7.138-f	x	x		x	x	+^{1}		+	x$^{?}$	+	++					1 c
A1932/7.138-g	x	x		x	x	+		+	x	+	++					1 c
A1932/7.138-h	x	+		x	x	+		+	x	+	++					1 c
A1932/7.138-i	x	x		x^{1}		+$^{?}$					++					
A1952/1.3		+		x	x	+					++					
APM01768	x	x		x^{1}	x			+	x	+^{1}	++					1
APM01770	x	x									++		x^{1}			
APM01777		+		x							++					3
APM01798	x	x		x	x	+		x		+	++					1
APM03221	x	x		x	x	+			x$^{?}$		++					
APM06361	x	+		x	x	+	+^{1}	+		+	++					1
APM06370	x$^{?}$	x		x	x	+		x	x	+	++					1 c
APM06371	x	+		x	x	+		+	x	+	++					1 c
APM06372	x	x		x	x			+	x		++					
APM06377	x	x		x	x	+		+	x	+	++					1 c
APM06425-a	x	x		x					x$^{?}$		++					3 c
APM06425-b	x$^{?}$	x		x					x$^{?}$		++					3 c
APM10958	x	x		x	x	+		x	x		++					1
APM10960	x	x		x				x			++					3
APM10961	x	x		x	x				x$^{?}$		++					3
APM13306		+				++	x	x	x	x	+					
APM15888	x	+		x	x	+					++					
APM15889	x	x				+		x			++					
B1982/5.1324	x	x		x	x	+			x$^{?}$	+	++					1
B1982/5.1343-1	x	x		x		x				x	++					
B1982/5.1343-2		+		x	x	+			+	x	++	+				2 c
B1982/5.1366	x	x		x	x	+		+	x	+	++					1 c
B1982/5.1368		x		x		+					++					
B1982/5.1369		+		x	x	x			x	x	++	+				2 c
B1982/5.1392	x	x		x	x	+		+	x	+	++					1 c
B1982/5.1395	x	x		x	x	+		+	x	+	++					1 c
B1982/5.886	x	x	x^{1}		x	+		+	x	+	++					1
B1987/5.2	x	x		x	x	+				+	++					
LB3502		x$^{?}$				+$^{?}$					++					

Table 5.1: Major, minor and trace elements of the measured objects. The three groups of objects that can be distinguished based on their composition are marked with different shades of grey.
++: main element ^{1}: element present in 1 measurement
+: minor element $^{?}$: element might be available in the object
x: trace element c: the core of the group

5.3 Neutron radio- and tomography

The duck weights (LB3502, A1932/7.138-A to I) and cylinder seals with a text inscribed (A1952/1.3, B1982/5.1324 and B1982/5.1343) have been measured with neutron radio- and tomography. The results are described in this chapter. In addition, the Tell Bazi objects (set 1: 1, 2 and 3 and set 2: 14 objects) and all objects from the DLB collection were measured, but the data have not yet been analysed. The other objects will be measured later.

Tomography measures the density of the material of an object. Different densities are displayed as different colours in the figures. The density increases from yellow to green, cyan, blue, white, magenta and red. The density increases from left to right in the histogram, while to the top the frequency of a determined density increases. The colours in the histograms are yellow for the first horizontal area, green for a slope, cyan for a peak before the main peak, blue for the main peak, or the middle peak if there are three peaks, white for an extra area between blue and magenta if necessary, magenta for a peak after the main peak or a slope and red for the densest area. In these coloured areas the colour becomes darker with decreasing density. Usually, not all these colours were needed.

In all tomography images a thin yellow rim can be seen around the object in all tomography images, which is caused by the half pixels at the border of the object. This phenomenon is explained in chapter four. Because it is visible in all objects it will not be pointed out in the descriptions.

Reconstruction artefact were observed in A1932/7.138-A, -B, -D, -E, -G, -H, -I, A1952/1.3, B1982/5.1324 and B1982/5.1343 and possibly in LB3502. Because of these reconstruction artefacts, the tomographies of A1932/7.138-E and -G were also made using a ring filter. The phenomenon reconstruction artefact has also been explained in chapter four.

A selection of images is put in this chapter. More images are presented in the appendix.

A1932/7.138-A

This object is quite homogeneous. The material of the object is less dense at the inside than at the outside. The head of the duck has no dense outer rim, like the rest of the duck has. A yellow circle can be seen at the axial slice in fig 5.13a, which is probably a reconstruction artefact. When with macroscopic analysis a hole can be seen in the object at exactly that place, than it is, instead of a reconstruction artefact, a hole filled with less dense material. A very dense area is visible at the bottom of the object, which may be some contamination.

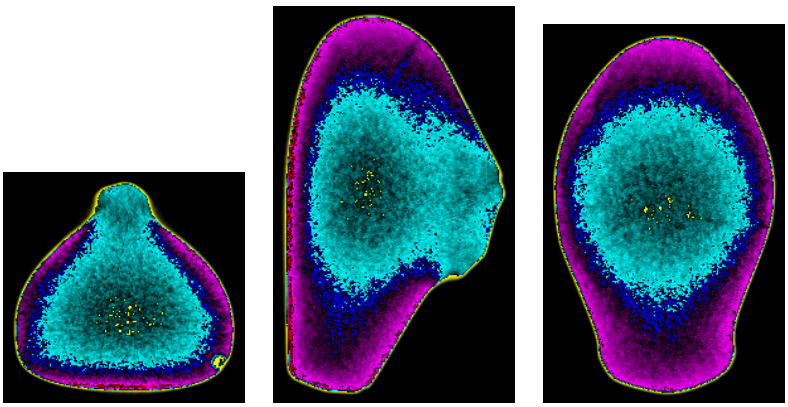

(a) Axial slice 155 (b) Sagittal slice 96 (c) Frontal slice 57

Figure 5.13: From left to right: axial slice 155, sagittal slice 96 and frontal slice 57 of A1932/7.138-A.

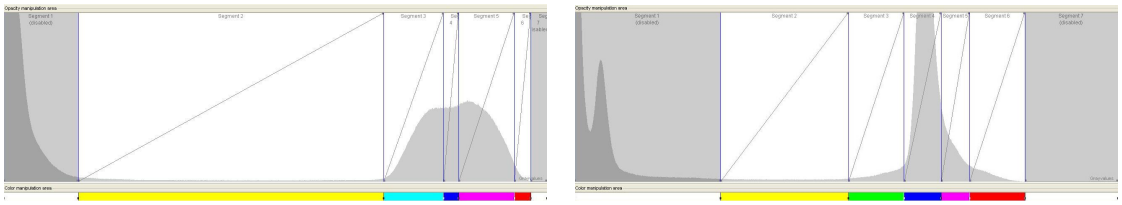

(a) A1932/7.138-A (b) A1932/7.138-B

Figure 5.14: Histograms of A1932/7.138-A and -B.

A1932/7.138-B

This object is quite homogeneous, almost the entire duck weight has the same density. The small ring at the right of axial slice 70 (fig. 5.15a) and the ring at the right of frontal slice 25 (fig. 5.15c) are reconstruction artefacts. A more dense outer rim might be present, but this may also be a contamination layer.

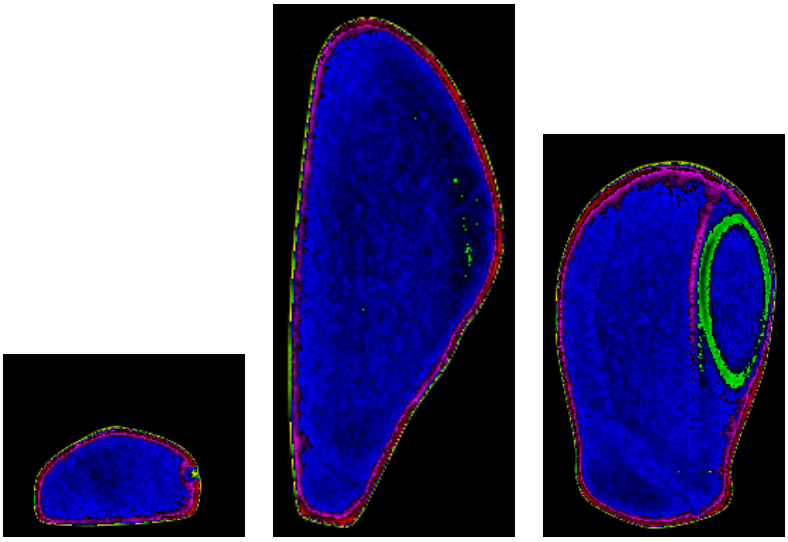

(a) Axial slice 70 (b) Sagittal slice 86 (c) Frontal slice 28

Figure 5.15: From left to right: axial slice 70, sagittal slice 86 and frontal slice 28 of A1932/7.138-B.

A1932/7.138-C

The density is very divided in this object. Spots of low density can be seen at the left both the axial and frontal images and at the top of the sagittal image (fig. 5.16). A line of higher density can be seen at the right of both the axial and frontal images. The bottom of the sagittal image is a bit more dense than the rest of the image. In addition, the head of the duck has a low density.

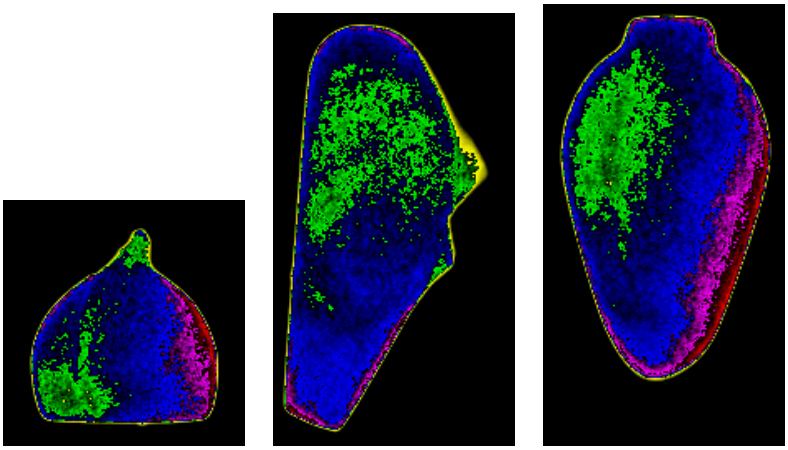

(a) Axial slice 133 (b) Sagittal slice 61 (c) Frontal slice 60

Figure 5.16: From left to right: axial slice 133, sagittal slice 61 and frontal slice 60 of A1932/7.138-C.

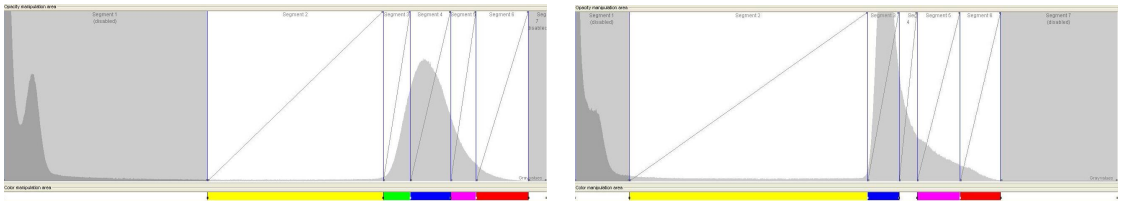

(a) A1932/7.138-C (b) A1932/7.138-D

Figure 5.17: Histograms of A1932/7.138-C and -D.

A1932/7.138-D

This object is a quite homogeneous artefact. The core is slightly less dense than the rest of the artefact, a few spots of low density can be seen, while the outer layer is a bit more dense, with increasing density to the outside.

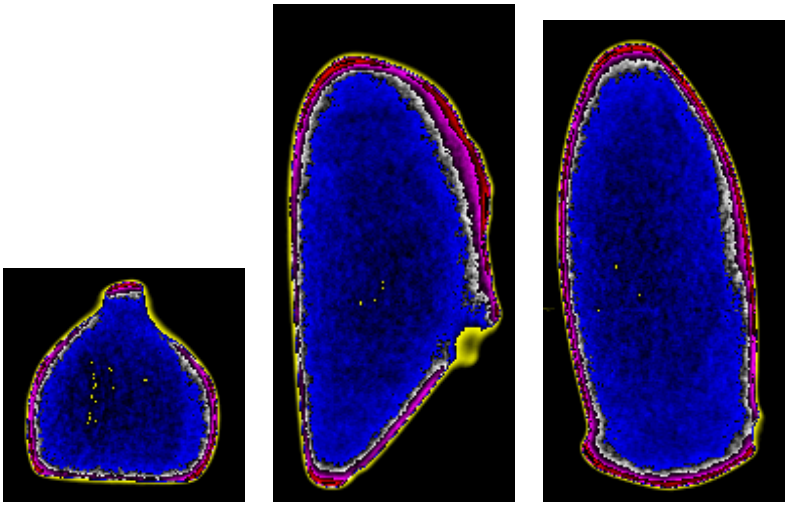

(a) Axial slice 90 (b) Sagittal slice 70 (c) Frontal slice 33

Figure 5.18: From left to right: axial slice 90, sagittal slice 70 and frontal slice 33 of A1932/7.138-D.

A1932/7.138-E

Object E has quite much material with a low density in it. The shape of the less dense material is very much influenced by the reconstruction artefacts in the images made without a ring filter (5.20 a, b and c), this can be seen by comparing these images with the images made with a ring filter (5.20 d, e and f). The circular shape is almost gone due to the ring filter. Both the neck and head of the duck seems to contain less dense material than the duck in general. The material is also less dense in the center of the object than in the area surrounding it.

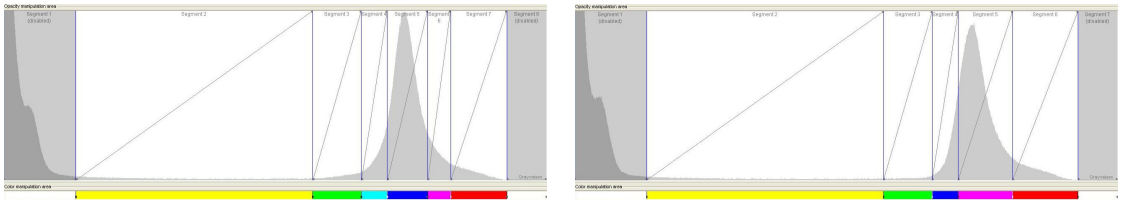

(a) A1932/7.138-E without ring filter (b) A1932/7.138-E with ring filter

Figure 5.19: Histograms of A1932/7.138-E.

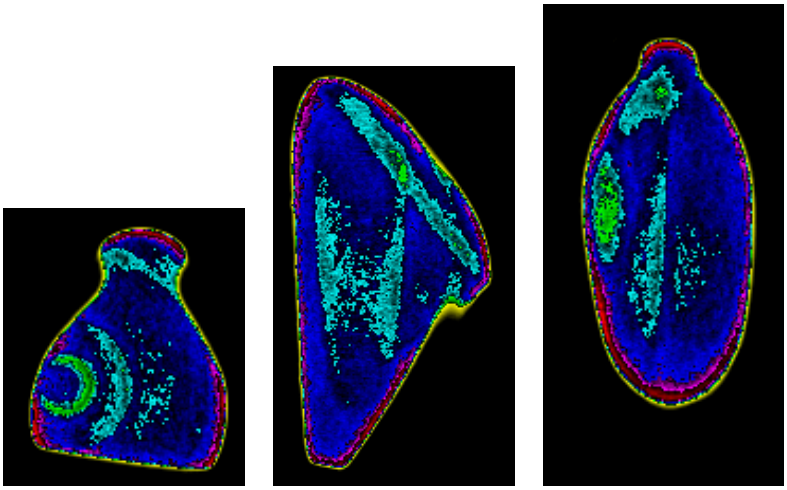

(a) Axial slice 120 without ring filter

(b) Sagittal slice 50 without ring filter

(c) Frontal slice 60 without ring filter

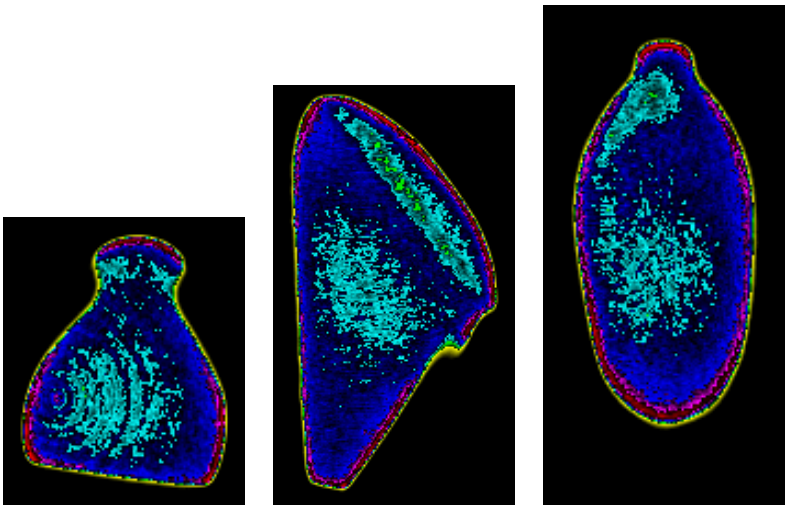

(d) Axial slice 120 with ring filter

(e) Sagittal slice 50 with ring filter

(f) Frontal slice 60 with ring filter

Figure 5.20: various images of A1932/7.138-E.

A1932/7.138-F

This artefact looks different from the others. Instead of a large spot of less dense material in the middle, it has both denser bands and small spots and spots of a smaller density on various places. Holes seem to occur at the ends of the dense bands.

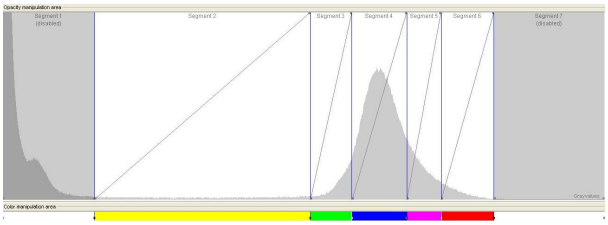

Figure 5.21: Histogram of A1932/7.138-F

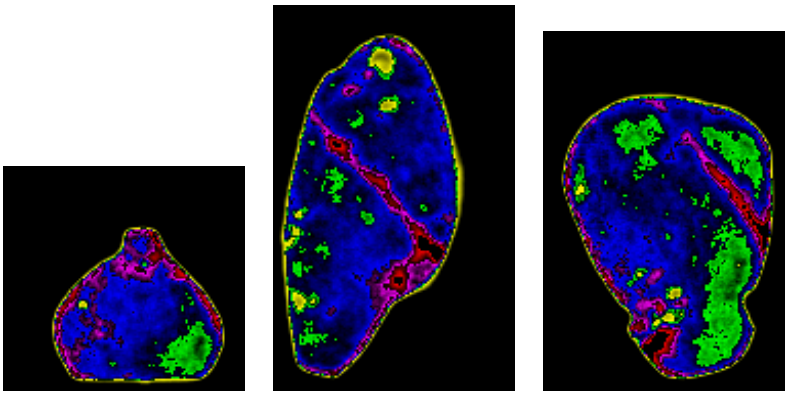

(a) Axial slice 60 (b) Sagittal slice 74 (c) Frontal slice 22

Figure 5.22: From left to right: axial slice 60, sagittal slice 74 and frontal slice 22 of A1932/7.138-F.

A1932/7.138-G

A filter is placed on this artefact, just like on A1932/7.138-E. The reconstruction artefacts can clearly be seen in the images without a ring filter (5.24 a-c) when comparing them to images with a ring filter (5.24 d-e). The density is very divided in this artefact. A large density is mainly visible at the top, back and outer layer of the object (so at the top of the axial slices and right side of the sagittal images), while a small density is mainly found at the bottom and center of the duck weight. A lot of variation can be seen in this area with a small density.

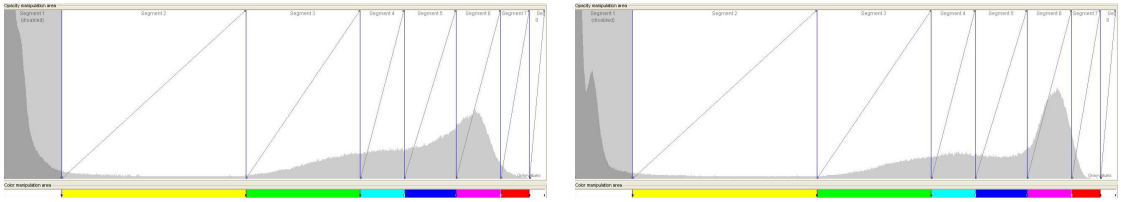

(a) A1932/7.138-G without ring filter (b) A1932/7.138-G with ring filter

Figure 5.23: Histograms of A1932/7.138-G.

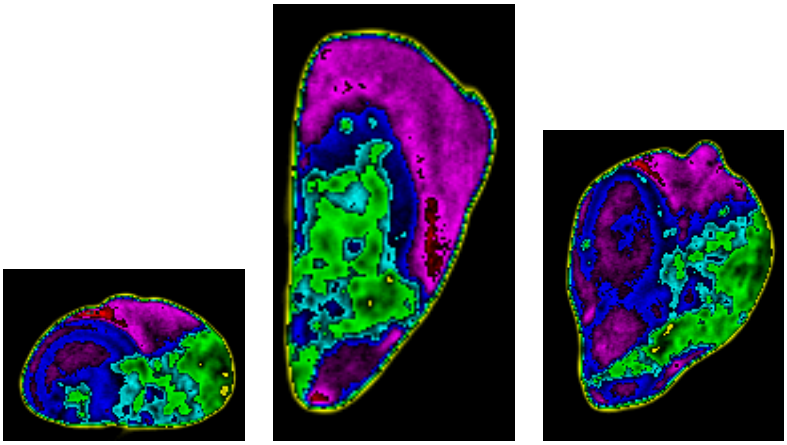

(a) Axial slice 92 without ring filter

(b) Sagittal slice 68 without ring filter

(c) Frontal slice 43 without ring filter

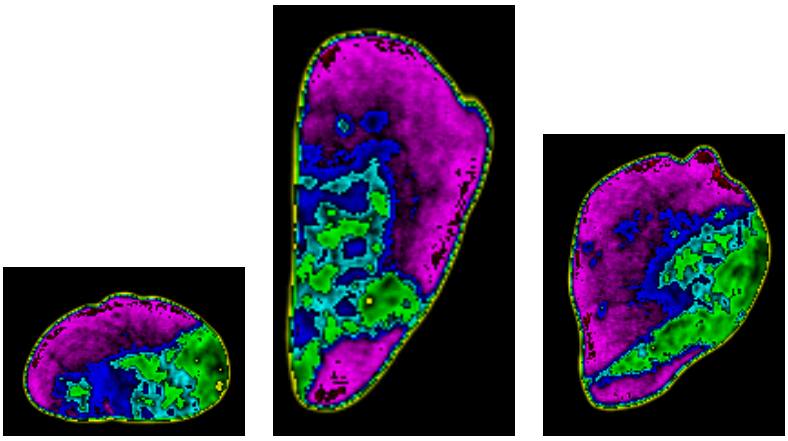

(d) Axial slice 92 with ring filter

(e) Sagittal slice 68 with ring filter

(f) Frontal slice 43 with ring filter

Figure 5.24: various images of A1932/7.138-G.

A1932/7.138-H

The inner side is less dense than the outer side. In addition, a small variation can be seen in the density of the less dense area. A reconstruction artefact can for example be seen at slide 104 of the axial images (fig. 5.25a).

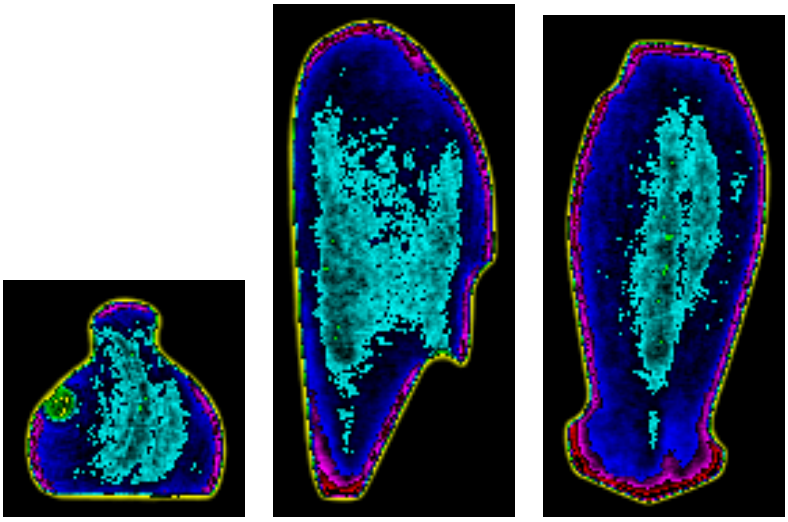

(a) Axial slice 104 (b) Sagittal slice 43 (c) Frontal slice 22

Figure 5.25: From left to right: axial slice 104, sagittal slice 43 and frontal slice 22 of A1932/7.138-H.

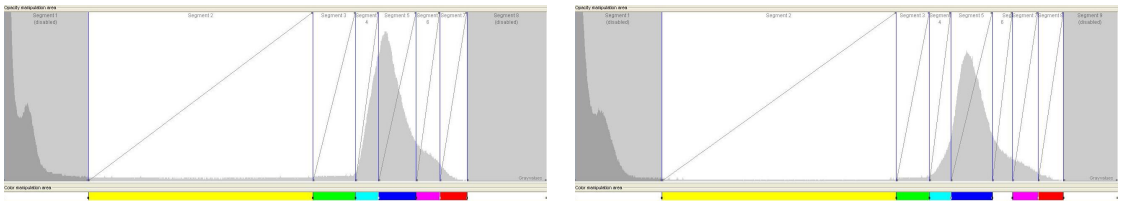

(a) A1932/7.138-H (b) A1932/7.138-I

Figure 5.26: Histograms of A1932/7.138-H and -I.

A1932/7.138-I

Like many other artefacts, this object is less dense at the inside than at the outside. The shape of the less dense area might be a bit reformed by the reconstruction artefact, which is visible at axial slice 101 (fig. 5.27a).

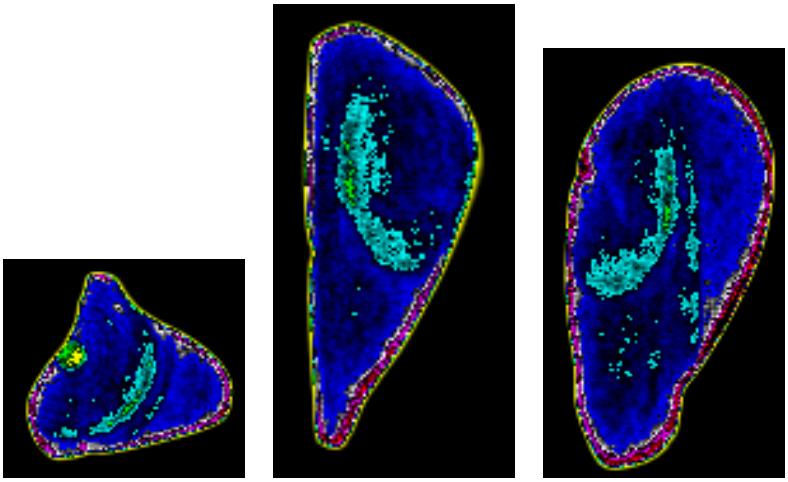

(a) Axial slice 101 (b) Sagittal slice 49 (c) Frontal slice 26

Figure 5.27: From left to right: axial slice 101, sagittal slice 49 and frontal slice 26 of A1932/7.138-I.

A1952/1.3

In the 3D figures of this seal are clearly a figure and inscriptions visible. The density of this object increases from the inside to the outside. The moon-shaped figure in the axial slice (fig. 5.28a) is a reconstruction artefact. The borders of the drilling hole have a low density. The hole is probably drilled from two sides, it is closer at the outside than at the inner side. It is more curved than that of B1982/5.1343, but it is straighter than that of B1982/5.1324.

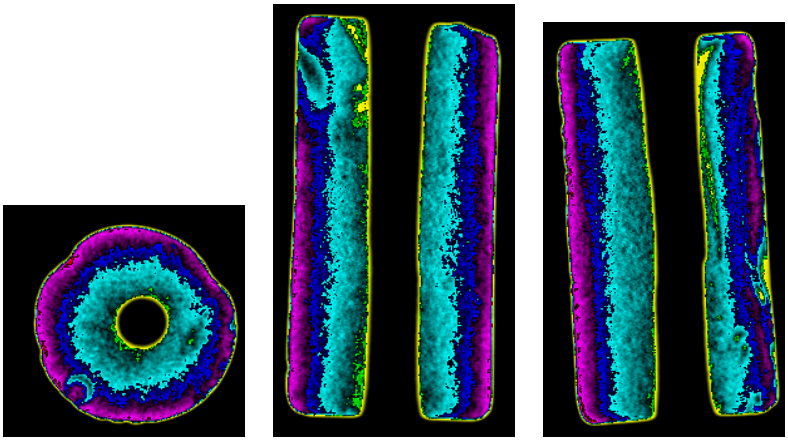

(a) Axial slice 60 (b) Sagittal slice 105 (c) Frontal slice 92

Figure 5.28: From left to right: axial slice 60, sagittal slice 105 and frontal slice 92 of A1952/1.3.

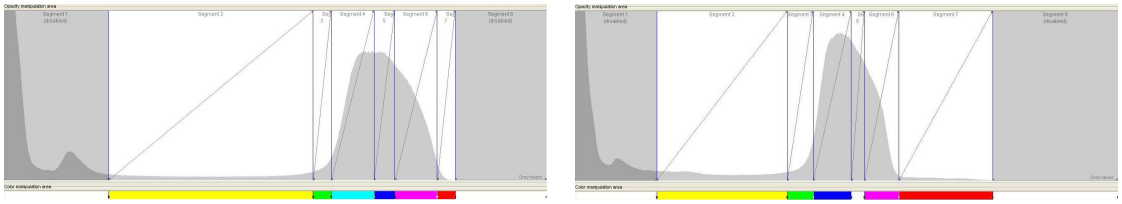

(a) A1952/1.3 (b) B1982/5.1324 (1342)

Figure 5.29: Histograms of A1952/1.3 and B1982/5.1324.

B1982/5.1324

The density increases from the center to the outside. Spots of a lower density are visible through the seal. Dirt and dust, with a low density, can be seen in the drilling hole. The hole has been drilled from two side, it is curved drilled. The bore hole is not completely circular, as can be seen in axial slice 179 (fig. 5.30a). The seal exists of two parts. Between the two parts is a very dense line visible, so apparently the glue, used for gluing both parts together, is very dense. Holes can be seen in that dense line, which are probably air bubbles. The small blue circle, visible in the axial slice, is a reconstruction artefact.

The inscriptions and figures are not clearly visible in the 3D images, probably because the resolution of the measuring instrument was not high enough, or because the inscriptions were not very visible on the seal itself either.

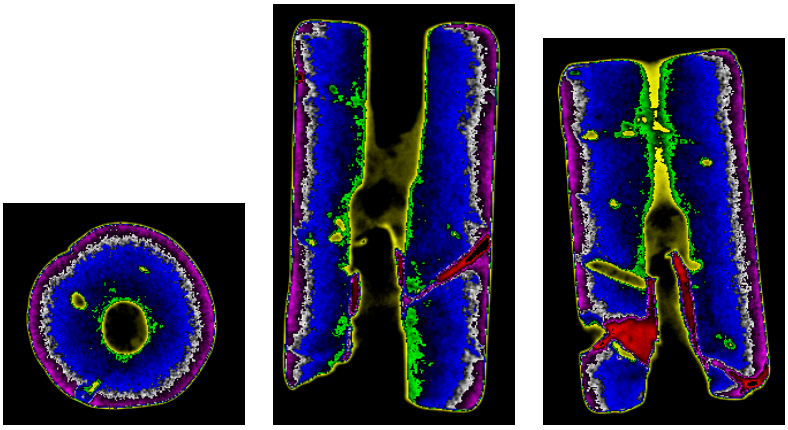

(a) Axial slice 179 (b) Sagittal slice 106 (c) Frontal slice 73

Figure 5.30: From left to right: axial slice 179, sagittal slice 106 and frontal slice 73 of B1982/5.1324.

B1982/5.1343

Two very different materials are present in this object. This can be seen both at the difference in colour in the slice images (fig. 5.31) and in the histogram (fig. 5.32a), which has two peaks. A hole is visible between the two different parts. The main part (blue in the images) is homogeneous except for a few less denser spots and a denser layer at the outside. The second part is white in the images and contains some material of a lower density. The drilling hole has been bored from two sides, one much further in the seal than the other. The hole is very rounded and very straight.

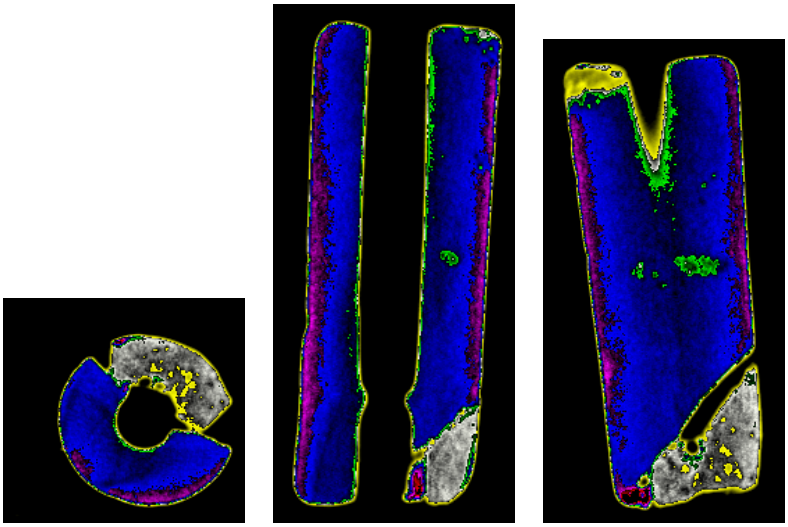

(a) Axial slice 40 (b) Sagittal slice 90 (c) Frontal slice 105

Figure 5.31: From left to right: axial slice 179, sagittal slice 106 and frontal slice 73 of B1982/5.1343.

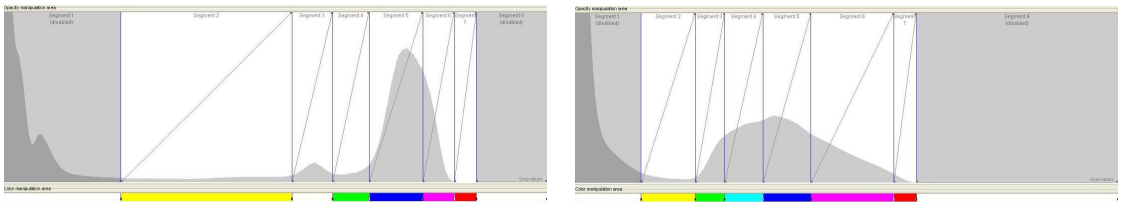

(a) B1982/5.1343 (b) LB3502

Figure 5.32: Histograms of B1982/5.1343 and LB3502.

LB3502

This object shows different grades of density, from dense at the outside to less dense at the inside. Material of a very low density can be seen near the head (axial slide 400 and sagittal slice 49) and at the left of frontal slice 161. This is probably dirt, filling up holes and carvings. This indicates that quite a deep hole is present in the duck weight.

All objects that have been measured with neutron radio- and tomography have been described in this paragraph. In the next chapter, the objects are grouped, based on the results, and the results are discussed.

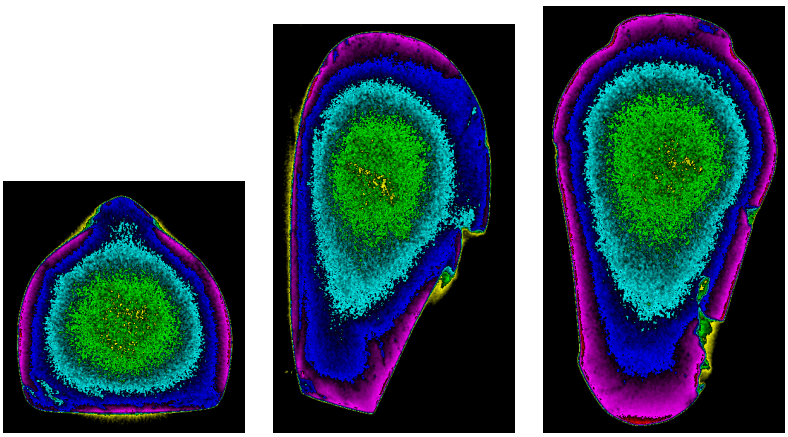

(a) Axial slice 400 (b) Sagittal slice 219 (c) Frontal slice 161

Figure 5.33: From left to right: axial slice 400, sagittal slice 219 and frontal slice 161 of LB3502.

Chapter 6

Discussion

6.1 Introduction

In order to find the provenance of iron oxide artefacts, the compositions of these artefacts have to be compared with each other and with raw material. Groups have been formed bases on the results of the analyses. These groups are presented in this chapter. The results of the analyses of different kind of artefacts are compared with each other. In addition, particularities found after analysing the objects are shown.

6.2 XRF

6.2.1 Grouping, classification based on composition

The objects can be divided into different groups according to the results of the XRF measurements.

Group 1 has core objects containing the elements Fe, Al, Si, S, K, Ca, V, Cr and Mn. The objects A1932/7.138-F, -G and -H, APM06370, APM06371 and APM06377, B1982/5.1366, B1982/5.1392 and B1982/5.1395 are in this group. Objects with a slightly different composition that could be in this group are APM01768, APM01798, APM06361, APM10958, B1982/5.1324 and B1982/5.886.

B1982/5.1369 and the part of B1982/5.1343 on which the second measurement has been done form the second group of objects, containing Fe, Si, S, K, Ca, Cr, Mn, Mg and Ni.

The core of the third group is formed by the objects APM06425-a and -b. These contain Fe, Al, Si, S and possibly Cr. Other objects that might be in this group are APM01777, APM10960 and APM10961.

According the results of the DLB artefacts in chapter 2, only one group is found at the DLB artefacts, those which include the elements Fe, Mn and V. This group includes the objects DLB 45, 46, 47 and 59.

Many artefacts did not have a composition similar to an other artefact, so these could not be grouped.

Surprisingly, the compositions of the artefacts measured in this research and those of the DLB artefacts measured in previous research seems to differ. More elements seem to be detected at the artefacts measured in this research than at the DLB artefacts. In addition, no Al, Si or S can be observed in the spectra of the DLB artefacts, while Si is present in all artefacts measured in this research and Al and S in most artefacts. The same instrument is used and the different settings used for both sets are checked with each other, so the differences have to appear in the different sets of artefacts. This indicates that larger more-covering groups might be made based on the presence of light elements in the spectra.

6.2.2 Comparing different groups

Comparing source material

In order to compare the objects that have a provenance with each other, the XRF results are presented below. The Selenkahiye objects are measured in this research (chapter 4), while the Tell Bazi artefacts are measured in previous research (chapter 2).

Composition of Selenkahiye half-fabricates:

- APM 10958: The main element is Fe. Also much Ca, and smaller amounts of Al, Si, S, K, V and Cr are present.
- APM 10960: The main element is Fe. It contains small amounts of Al, Si, S and V.
- APM 10961: The main element is Fe. It contains small amounts of Al, Si, S, K and may contain Cr.

Composition of Tell Bazi artefacts:

- Tell Bazi 1: The main element is Fe and traces of Zn, Sr and possibly As are present.
- Tell Bazi 2: The main element is Fe, it also contains traces of V, Cr, Mn, Zn, As and Sr.
- Tell Bazi 3: The main element is Fe. Furthermore, a large amount of Cl is present, which might be contamination. It also contains traces of Zn, As and Sr.

The objects from Selenkahiye are not exactly similar to each other. Their only resemblance is that they all contain Al, Si and S, but most of the objects measured in this research contain these three elements. The objects from Tell Bazi are also not exactly the same. They all contain Zn, As and Sr, but Tell Bazi 2 and 3 also contain other elements. This indicates that iron oxide objects with the same provenance do not necessarily have to have the exact same composition.

The groups are very different from each other, no element except iron is present in all six objects. Although the compositions in a group are not exactly the same, differences between the two groups can clearly be seen: the Selenkahiye half-fabricates contain Al, Si and S and the Tell Bazi artefacts contain Zn, As and Sr.

These objects with a provenance do not show exact resemblance with other artefacts that are measured. No artefact has a composition identical to an object with an provenance. Since all artefacts measured in this research contain Si, and most contain Al and S, and the elements Zn, As and Sr do not occur together in one of the artefacts, the compositions of the Selenkahiye artefacts are more similar to the artefacts measured in this research than the compositions of the Tell Bazi artefacts are. The Selenkahiye artefacts are even present in groups made based on the XRF results, although in two different groups.

To be sure about the provenance, more source material and more artefacts have to be measured. Consider that the two groups both exist of only three objects, so they may not be representative for the location. When groups of artefacts can be made depends among others of how fixed the boundaries of the groups are made. Except for the results in this paragraph, it is not exactly known how much the compositions of artefacts differ per source area.

It is improbable, but it might be suspected that the similarity in composition between the Selenkahiye half-fabricates and the other artefacts measured in this research exists because these objects are measured in the same set, while the DLB and Tell Bazi artefacts are measured in a different set. The same instrument is used and the different settings are checked, but some mistakes might have occurred here.

Comparing kinds of objects

There are no large differences between the different sorts of objects. The only relative large differences are that calcium (Ca) seems to occur more in cylinder seals than in duck weights and the group of half-fabricates and weights (15 out of 18 (94%) against 6 out of 12 (50%) and 4 out of 9 (44%)) and that manganese (Mn) seems to occur less in half-fabricates and weights than in duck weights and cylinder seals (1 out of 9 (11%) against 9 out of 12 (75%) and 14 out of 18 (78%)).

The reason for differences in composition between different sorts of objects could be that other material was used for the different groups on purpose, but it could also be a coincidence. The different groups of objects could have been produced on various locations, resulting in the use of different material. Unfortunately, the provenance of most objects is unknown, so we can not ascertain that.

In addition, too few objects are available to get reliable statics. It is not certain whether the differences in composition are per group or per object. No element is present in all objects of one group and in none of the other.

6.2.3 Particularities

Calcium as main component

Surprisingly, one of the object of the DLB collection measured in previous research and one of the objects measured in this research had calcium as main component instead of iron. These objects are seal DLB55 and seal APM13306.

Limestone, which contains calcium, apparently can be used instead of iron oxide, because this material can also be black and can look like haematite. The difference might not have been noticed in ancient times. The seals may also be imitated, because either iron oxide was not available in the area where these seals were made, or the material was very expensive. They could have been made from local black material, because that was much cheaper and easier to make. This occurred for example in Cyprus (Joyner et al., 2006).

Different material in one object

Both the seals B1982/5.1343 and B1982/5.1324 consist of two parts. It can clearly be seen that a part of the seal has broken off and has been glued back on again, or an other part has been glued on.

Two XRF measurements have been done on both seals, one measurement on each part. In contrary to B1982/5.1324 which shows the same composition for both parts, the material of both parts of B1982/5.1343 differs.

The first measurement was done on the larger part, the second measurement was done on the smaller part that had been glued on the larger part. Various differences can be noted in the two spectra of B1982/5.1343. Both spectra show silicon (Si), sulfur (S), calcium (Ca) and manganese (Mn), but aluminium (Al) can only be seen in the first measurement, while potassium (K), chromium (Cr) and nickel (Ni) can only be observed in the second spectrum. In addition, the height of the peaks is different.

It can be conclude that the glued part is not the original piece, but that it has been glued on the seal later. Since the composition of the part that has been glued on the artefact is similar to the composition of object B1982/5.1369, that artefact might also be not as old as expected.

6.2.4 Possibilities of occurrence of elements in material

The following elements were detected with the XRF in the iron oxide artefacts: Al, Si, P, S, K, Ca, Ti, V, Cr, Mn, Fe, Ni, Zn, As and Sr. This paragraph presents which elements can occur

naturally in iron oxide artefacts.

To see whether an element originally occurred in an artefact or whether it is contaminated by humans after the artefact was made, it has to be known which elements can occur in iron oxide artefacts naturally.

The measured iron oxides consist of Fe-O bonds. In these bonds the Fe can be substituted by an other element (Cornell and Schwertmann, 2003; see table 6.1). Apart from this substitution any elements can occur next to the Fe-O bonds as a free-standing mineral. For example Si can not substitute Fe, but it can occur in an iron oxide. Concluding, any element can occur naturally in the measured iron oxides.

Oxide	Substituting cation
Goethite	Ni^{2+}, Zn^{2+}, Cd^{2+}, Al^{3+}, Cr^{3+}, Ga^{3+}, V^{3+}, Mn^{3+}, Co^{3+}, Sc^{3+}, Pb^{4+}, Ge^{4+}
Lepidocrocite	Al^{3+}
Akaganéite	Cu^{2+}, Si^{4+}, Mn^{3+}, Ni^{2+}
δ-FeOOH	Mn^{3+}, Ni^{2+}, Co^{2+}, Zn^{2+}, Cd^{2+}, Mg^{2+}, Ca^{2+}
Haematite	Al^{3+}, Cr^{3+}, Mn^{3+}, Rh^{3+}, Ga^{3+}, In^{3+}, Nd^{3+}, Ni^{2+}, Cu^{2+}, Ge^{4+}, Sn^{4+}, Ti^{4+}
Magnetite	Al^{3+}, Mn^{2+}, Ni^{2+}, Cu^{2+}, Co^{2+}, Zn^{2+}, Ca^{2+}, Ge^{4+}
Maghemite	Al^{3+}, Ti^{4+}, Sn^{4+}

Table 6.1: Cations substitution for FeIII in various Fe oxides (Cornell and Schwertmann, 2003).

6.3 Neutron radio- and tomography

6.3.1 Grouping, classification based on density

The objects can be divided in four groups based on the neutron radio- and tomography analysis.

The first group exists of objects which have a much smaller density in the core than at the outside. In this group are the objects A1932/7.138-A, A1952/1.3, LB3502 and maybe B1982/5.1324. The last is between group 1 and 2.

The objects of the second group are very homogeneous. Almost only one colour is visible at the images. This group contains the objects A1932/7.138-B, A1932/7.138-D, B1982/5.1343 and maybe B1982/5.1324, which is between group 1 and 2.

The density is also heterogeneous in the third group, but instead of increasing density from the core to the outside, as in group one, an area of less dense material is visible at one side of the object. The objects that belong to this group are A1932/7.138-C, -E, -H and -I.

The material of the artefacts in group four is heterogeneous. Smaller spots of different density appear in the material, in contrary to the larger spots that appear in the first and third group. A1932/7.138-F and -G are in this group.

The groups that have been made of the results show that the hypothesis, that the weights should have a homogeneous composition, so the size is related to the weight of the object, can be rejected. This paragraph shows three groups of heterogene artefacts and only one group of homogene artefacts. Only two duck weights are present in that last group.

6.3.2 Comparing the tomography results with the objects

Tomography images were made of all duck weights and three cylinder seals. Some particularities in the tomography images could not be identified without the object itself. For example, a less denser area could be a hole in the object, or a difference in the material. Therefore, the objects were re-examined to find this out.

Objects of which no particularities were found in the tomography images and the object are left out of this paragraph.

A reconstruction artefact could be seen at the tomography images of A1932/7.138-A (fig. 5.12a). No gap was visible at that same spot at the artefact, so this indicates that indeed a reconstruction artefact was made during the process.

A1932/7.138-F was very heterogeneous at the tomographies (fig. 5.22). It had very large differences in density and something that seems to be a hole was visible, but nothing of this can be seen at the object itself.

A streak is surrounding duck weight A1932/7.138-G (fig. 3.16), but this can not be seen at the tomographies (fig. 5.24). The streak divides the front and the back of the object, while a difference in density is present between the top and the bottom of the artefact.

The gaps of LB3502 are well visible in both the tomography images and the object itself (fig. 3.21). For example, frontal slice 161 (fig. 5.33c) shows two holes at the right side very well which are also present in the object. One of the holes is very deep. It is unknown how they are formed.

Rings are visible in the material of cylinder seal A1952/1.3 (fig. 3.1a). The rings in the tomography, for example in sagittal slice 122 (fig. 6.1b), may be the same rings. This indicates that these rings are no reconstruction artefact.

In cylinder seal B1982/5.1324 occurs a gap (fig. 3.9) which is possibly also visible in the tomographies, for example in axial slice 132 (fig. 6.1b) is a less dense line visible at the left. The crack of the object is also very well visible (fig. 5.30c).

The tomographies (fig. 5.31) clearly show that the two different parts of B1982/5.1343 are made from different material. However, this can not be seen with the naked eye.

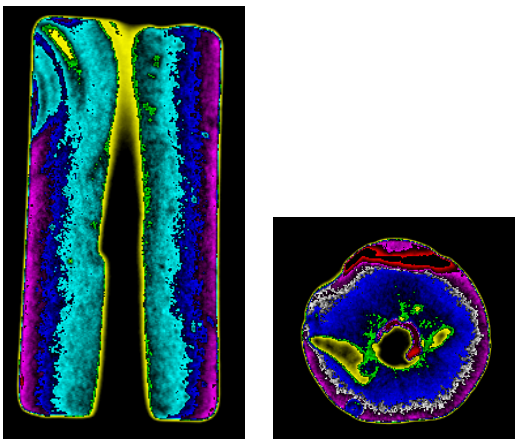

(a) Sagittal slice 122 of A1952/1.3

(b) Axial slice 132 of B1982/5.1324

Figure 6.1: Objects which show similarities in tomography and macroscopic analysis.

6.4 Comparing XRF and neutron radio- and tomography results

The XRF and radio- and tomography results can not completely be compared with each other, because not all objects that are measured with XRF are also measured with neutron radio- and tomography.

At first an overview of the different groups that can be made. Many objects could not be assigned to a group on the basis of the XRF-measurements.

XRF:

- Group 1:
  Core: A1932/7.138-F, -G and -H, APM06370, APM06371, APM06377, B1982/5.1366, B1982/5.1392 and B1982/5.1395.
  Others: APM01768, APM01798, APM06361, APM10958, B1982/5.1324 and B1982/5.886.
- Group 2: B1982/5.1343-2 and B1982/5.1369.
- Group 3:
  Core: APM06425-a and -b.
  Others: APM01777, APM10960 and APM10961.

Radio- and tomography:

- Group 1: A1932/7.138-A, A1952/1.3, LB3502 and maybe B1982/5.1324.
- Group 2: A1932/7.138-B, A1932/7.138-D, B1982/5.1343 and maybe B1982/5.1324.
- Group 3: A1932/7.138-C, -E, -H and -I.
- Group 4: A1932/7.138-F and -G.

This overview shows that the groups of the XRF and NRNT results are not the same. The only similarity is that A1932/7.138-F and -G are in the same groups at both the measurements.

Most objects that are places in a group based on the XRF results are not measures met neutron radio- and tomography and most objects in the neutron radio- and tomography groups could not be placed in groups based on the XRF results.

It can be said that measuring with both XRF and neutron radio- and tomography not necessarily results in the formation of the same groups. And the elements that are present at the outside of the objects do not say anything about the density of the whole object.

Chapter 7

Conclusion

Based on a study to find adequate methods, X-ray fluorescence and neutron radio- and tomography were chosen to use for this research. X-ray fluorescence was applied to 17 cylinder seals, 12 duck weights and 9 weights or half-fabricates, of which three had a known archaeological source. In addition, 10 duck weights and 3 cylinder seals were analysed with neutron radio- and tomography.

Only small differences in composition could be seen between some of the duck weights and cylinder seals, but too few objects could be compared for reliable conclusions. The hypothesis, that weights should have a homogeneous composition, is rejected. Most weights analysed in this research had a heterogeneous composition.

The XRF results show that most artefacts measured in this research are more similar in composition to the Selenkahiye half-fabricates than to the Tell Bazi objects. Further research is necessary to be sure about the provenance of the artefacts, for example to know how much the composition of objects differs per region. Based on the XRF results of six objects, it can be concluded that iron oxide objects with the same provenance do not necessarily have to have the exact same composition, but similarities can be observed between them.

It has also been shown that groups made of XRF results and groups made of neutron radio- and tomography results do not necessarily exist of the same objects. The composition and density of the objects are not related to each other.

Further research

A lot of research is currently being done. For example Radio- and Tomography has been done on three Tell Bazi objects in April 2009, PGAA has been done on the objects from the Allard Pierson Museum in July 2009. The data of these measurements has not yet been analysed.

Other methods might be applied to the objects to gain even better insight in them. More raw material with a known geological source has to be measured.

In addition, 14 more pieces of raw material have recently been found in Tell Bazi, these will soon be analysed, probably with PGAA. This looks promising, I am looking forward to the results.

References

Bibliography

Bamford, S., P. Kregsamer, S. Fazinic, M. Jaksic, D. Wegrzynek, E. Chinea-Cano, and A. Markowicz (2007). Complementarities of Nuclear-based Analytical Techniques for the Characterization of Thin Film Technological Materials. *Nuclear Instruments and Methods in Physics Research Section B:Beam Interactions with Materials and Atoms 261*(1-2), 541–543.

Bradák, B., G. Szakmány, S. Józsa, and A. Prichrystal (2009). Application of Magnetic Susceptibility on Polished Stone Tools from Western Hungary and the Eastern part of the Czech Republic (Central Europe). *Journal of Archaeological Science 36*(10), 2437–2444.

Collon, D., M. Sax, and C. B. F. Walker (1986). Cylinder Seals III Isin-Larsa and Old Babylonian Periods. In D. Collon (Ed.), *Catalogue of the Western Asiatic Seals in the Britisch Museum.*, Volume 3. London.

Cornell, R. M. and U. Schwertmann (2003). *The Iron Oxides: Structure, Properties, Reacions, Occurences and Uses.* Weinheim.

da Costa, G. M., V. G. de Resende, and N. M. Toríbio (2002). Quantitative Phase Analysis of Iron Ore Concentrates. *Rem: Revista Escola de Minas 55*(4), 263–266.

Cowell, M. (1985-86 (unpublished)). Report on the Analysis of some Haematite Cylinder Seals (Dept. of Western Asiatic Antiquities). The Britisch Museum Research Laboratory, London.

Garrison, E. G. (2003). *Techniques in Archaeological Geology.* Heidelberg.

Govil, I. M. (2001). Proton Induced X-ray Emission - A Tool for Non-destructive Trace Element Analysis. *Current Science 80*(12), 1542–1549.

Henderson, J. (2000). *The Science and Archaeology of Materials: an Investigation of Inorganic Materials.*

Joyner, L., R. S. Merrillees, and C. Xenophontos (2006). The Materials of the Cypriote Bronze Age Cylinder and Stamp Seals in the Department of Greek and Roman Antiquities, the British Museum, London. *Report of the Department of Antiquities, Cyprus*, 127–154.

Kardjilov, N., F. Fiori, G. Giunta, A. Hilger, F. Rustichelli, M. Strobl, J. Banhart, and R. Triolo (2006). Neutron Tomography for Archaeological Investigations. *Journal of Neutron Research 14*(1), 29–36.

Kardjilov, N., A. Hilger, I. Manke, V. Benfante, F. L. Celso, R. Triolo, I. Ruffo, and S. Tusa (2008). Neutron Tomography in Modern Archaeology. *Notiziario Neutroni e Luce di Sincrotrone 13*(2), 6–9.

van Loon, M. N. (2001). *Selenkahiye. Final Report on the University of Chicago and University of Amsterdam Excavations in the Tabqa Reservoir, Northern Syria, 1967-1975.* Istanbul.

Malmqvist, K. G. (1986). Comparison Between PIXE and XRF for Applications in Art and Archaeology. *Nuclear Instruments and Methods in Physics Research B14*, 86–92.

Moorey, P. R. S. (1994). *Ancient Mesopotamian Materials and Industries. The Archaeological Evidence.* Oxford.

Mulder, J. J. (2008). Potential Sources of Iron Oxides found in Mesopotamia. Bachelor's thesis. IGBA, VU University Amsterdam.

Nayak, P. K., D. Das, P. Singh, and V. Chakravortty (2003). ^{57}Fe Mössbauer Spectroscopy of Banded Iron Formations from Eastern India. *Journal of Radioanalytical and Nuclear Chemistry 260*(1), 19–26.

Otto, A. (2006). Alltag und Geselschaft zur Spätbronzezeit: eine Fallstudie aus Tall Bazi (Syrien). In *Subartu XIX.* Turnhout.

Pittman, H. (1995). *Civilization of the Ancient Near East.*, Volume III, Chapter Cylinder Seals and Scarabs in the Ancient Near East., pp. 1589–1604. Chapter: Cylinder Seals and Scarabs in the Ancient Near East. In book: Civilization of the Ancient Near East.

Rapp, G. and C. L. Hill (1998). *Geoarchaeology: the Earth-science Approach to Archaeological Interpretation.*

Révay, Z., T. Belgya, Z. Kasztovszky, J. L. Weil, and G. L. Molnár (2004). Cold neutron PGAA facility at Budapest. *Nuclear Instruments and Methods in Physics Research 213*, 385–388.

Roaf, M. (1990). *Cultural Atlas of Mesopotamia and the Ancient Near East.* New York.

Smith, G. D. and R. J. H. Clark (2003). Raman Microscopy in Archaeological Science. *Journal of Archaeological Science 31*, 1137–1160.

Tamás, B. and Z. Kasztovszky (2008). Research Report. Technical report, Institute of Isotopes, Budapest.

Vandenberghe, R. E., C. A. Barrero, G. M. da Costa, E. V. San, and E. D. Grave (2000). Mössbauer Characterization of Iron Oxides and (Oxy)Hydroxides: the Present State of the Art. *Hyperfine Interactions 126*, 247–259.

de Vries-Melein, M. M., D. Visser, J. J. Mulder, L. Megens, S. Imberti, and W. Kockelmann (2010). Mesopotamian "Haematite" Seals in a New Light. In *Proceedings of the 6th International Congress on the Archaeology of the Ancient Near East (Rome, 5th-10th May 2008).*

Websites

ANSTO (no date). Australian Nuclear Science and Technology Organisation. *Particle Induced Gamma-ray Emission (PIGE).* http://www.ansto.gov.au/research/institute_of_environmental_research/

Ph-TUM (no date). Physik Department - Technische Universität München. *ANTARES.* http://www.ph.tum.de/antares/

Freunde von Bazi e.V. (no date). *Bazi. Ausgrabungen im Syrischen Euphrattal. Project in Bazi of the Institut für Vorderasiatische Archäologie of the Ludwig-Maximilians-Universität München.* http://www.vaa.fak12.uni-muenchen.de/BAZI/bazi.htm

Buckman-Ellis, J. (2004). University of Minnesota. *X-Ray Fluorescence (XRF) - Theory.* http://mxp.physics.umn.edu/s04/Projects/s04xrf/theory.htm

http://www.dijs.biz/kaart.gif

IAEA (2003). International Atomic Energy Agency. *Database of Prompt Gamma Rays from Slow Neutron Capture for Element Analysis.* Vienna. http://www-nds.iaea.org/pgaa/.

ICN (no date). Instituut Collectie Nederland. http://www.icn.nl/

MEDC (2008). Mössbauer Effect Data Center. *Properties of Isotopes Relevant to Mössbauer Spectroscopy.* http://orgs.unca.edu/medc/Resources.html

MRSEC (no date). Materials Research Science and Engineering Center, Harvard University. *PIXE.* http://www.mrsec.harvard.edu/cams/PIXE.html

Microsoft Virtual Earth (2009). http://maps.live.com/ or www.bing.com/maps/

NIST-NCNR (2001). National Institute of Standards and Technology - NITS Center for Neutron Research. *Prompt-Gamma Activation Analysis (PGAA) Spectrometer.* http://www.ncnr.nist.gov/instruments/pgaa/

NIST-NCNR (2002). National Institute of Standards and Technology - NITS Center for Neutron Research. *Analytical Techniques.* http://www.ncnr.nist.gov/div8395/analytical_tech.html

NIST-NCNR (2003). National Institute of Standards and Technology - NITS Center for Neutron Research. *Neutron Depth Profiling.* http://www.ncnr.nist.gov/div8395/ndp.html

NOAA (no date). National Oceanic and Atmospheric Administration - Coastal Service Center. *Remote Sensing Fundamentals.* http://www.csc.noaa.gov/products/gulfmex/html/rsdetail.htm

Online database APM (no date). Online inventory database of the Allard Pierson museum. http://opc.uva.nl/

RSC (2008). Royal Society of Chemistry. *Introduction to Mössbauer Spectroscopy.* http://www.rsc.org/Membership/Networking/InterestGroups/MossbauerSpect/Intropart1.asp

Appendix A

XRF spectra

DLB objects

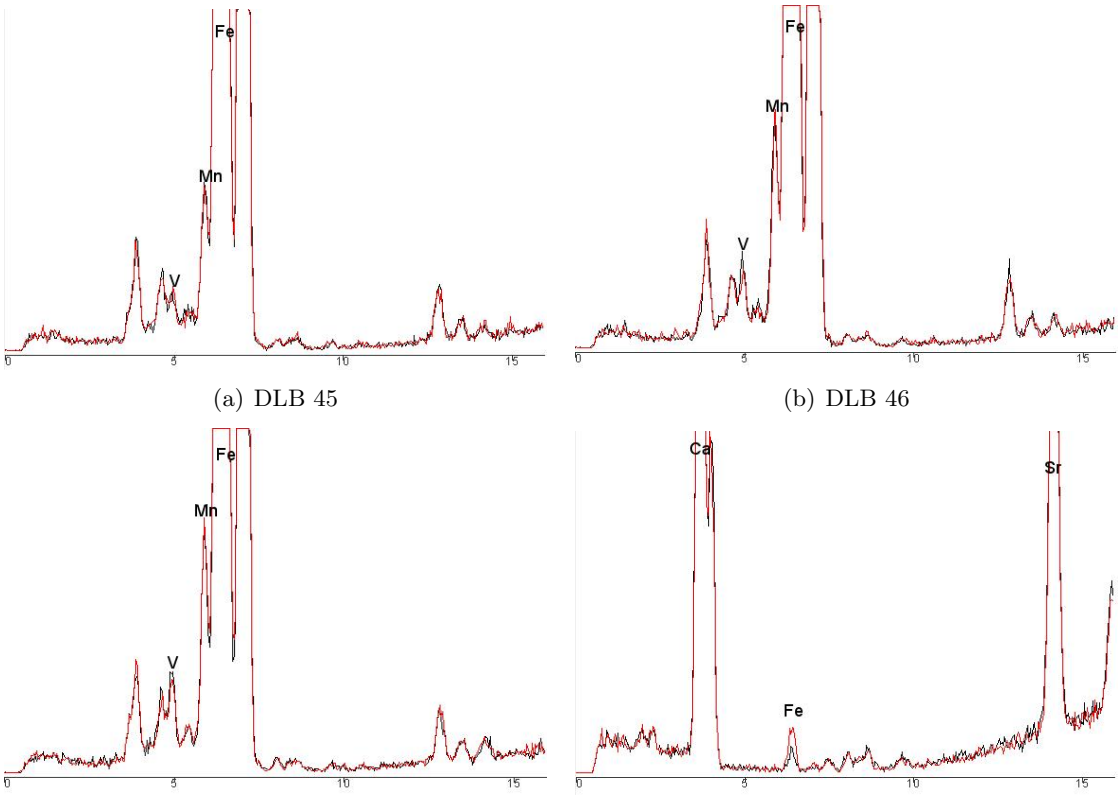

(a) DLB 45

(b) DLB 46

(c) DLB 47

(d) DBL 55

Figure A.1: XRF spectra from De Liagre-Böhl (DLB).

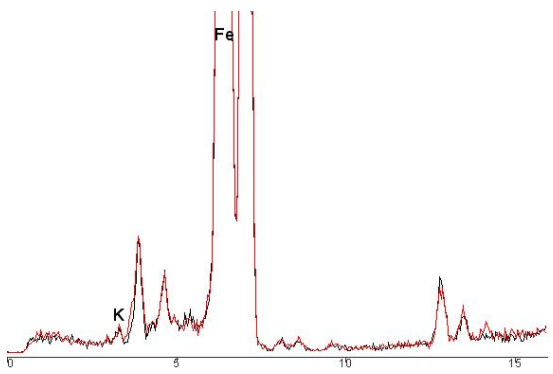

(a) DBL 57

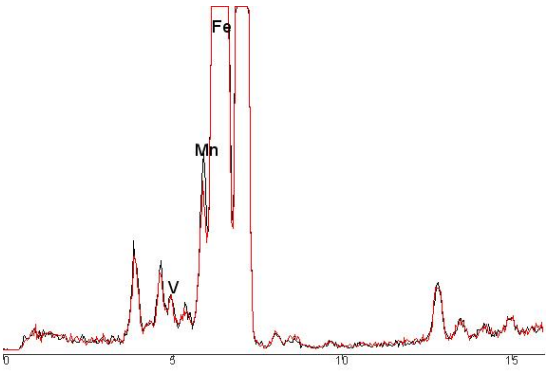

(b) DLB 59

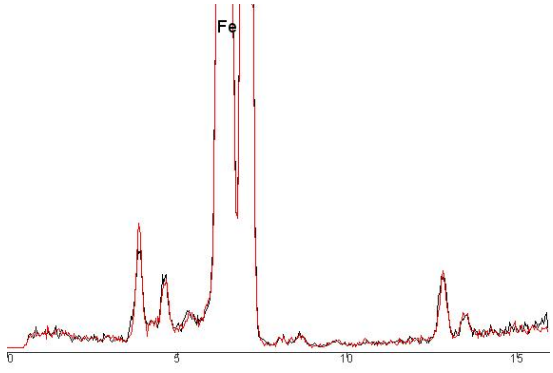

(c) DBL 61

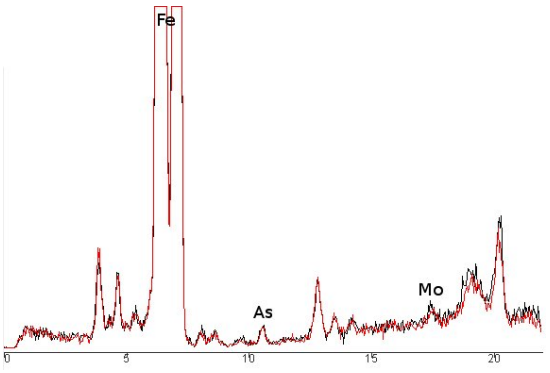

(d) DBL 62

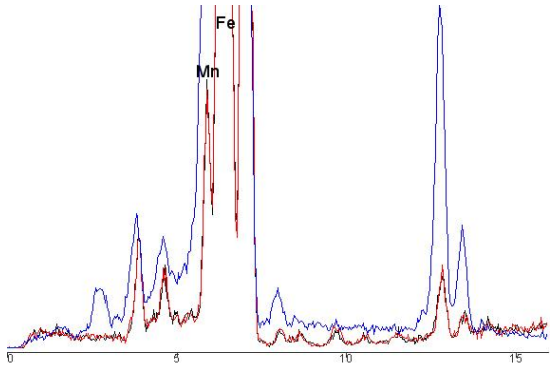

(e) DBL 66

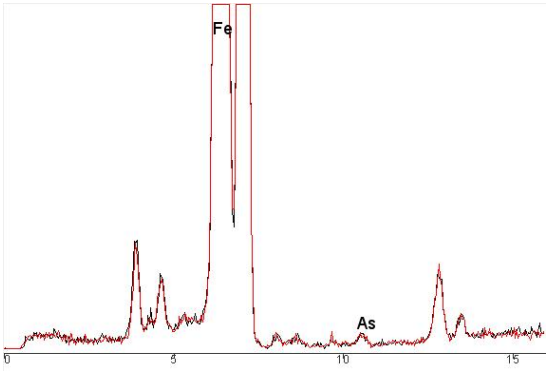

(f) DBL 67

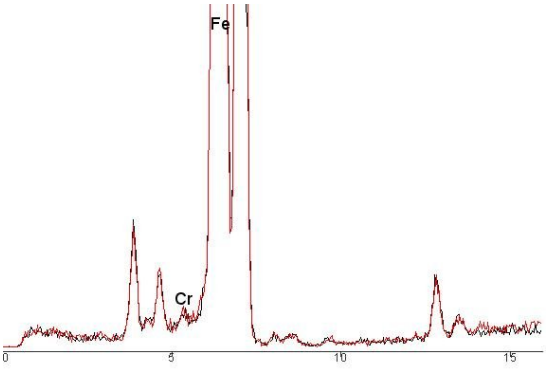

(g) DBL 75

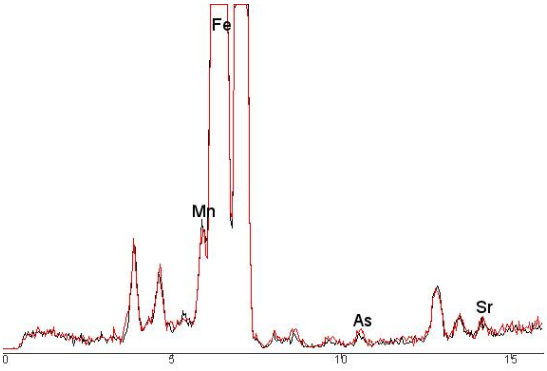

(h) DLB 84

Figure A.2: XRF spectra from De Liagre-Böhl (DLB).

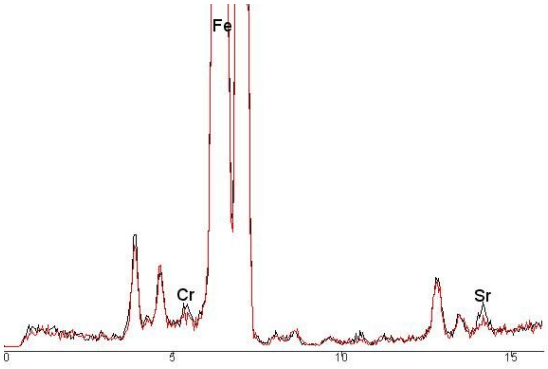

(a) DBL 118

Figure A.3: XRF spectra from De Liagre-Böhl (DLB).

Tell Bazi half-fabricates

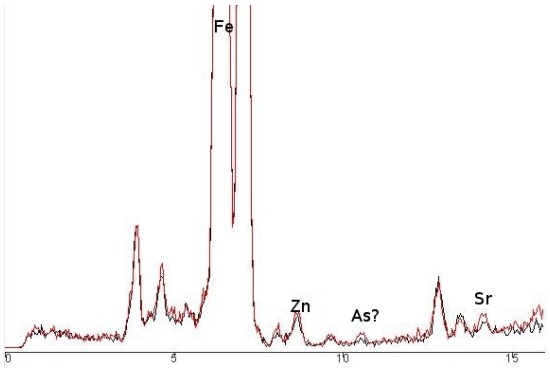

(a) Tell Bazi 1

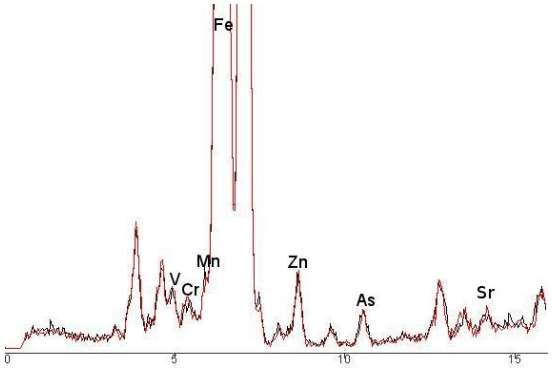

(b) Tell Bazi 2

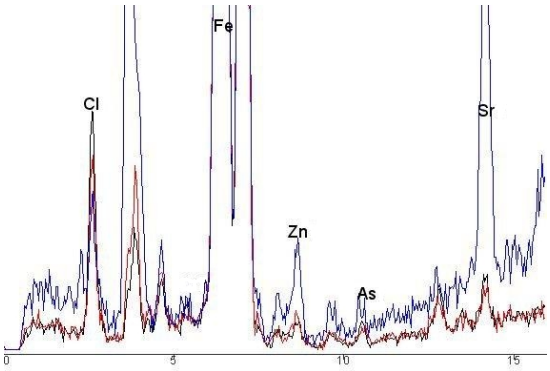

(c) Tell Bazi 3

Figure A.4: XRF spectra of three Tell Bazi artefacts.

Allard Pierson Museum objects

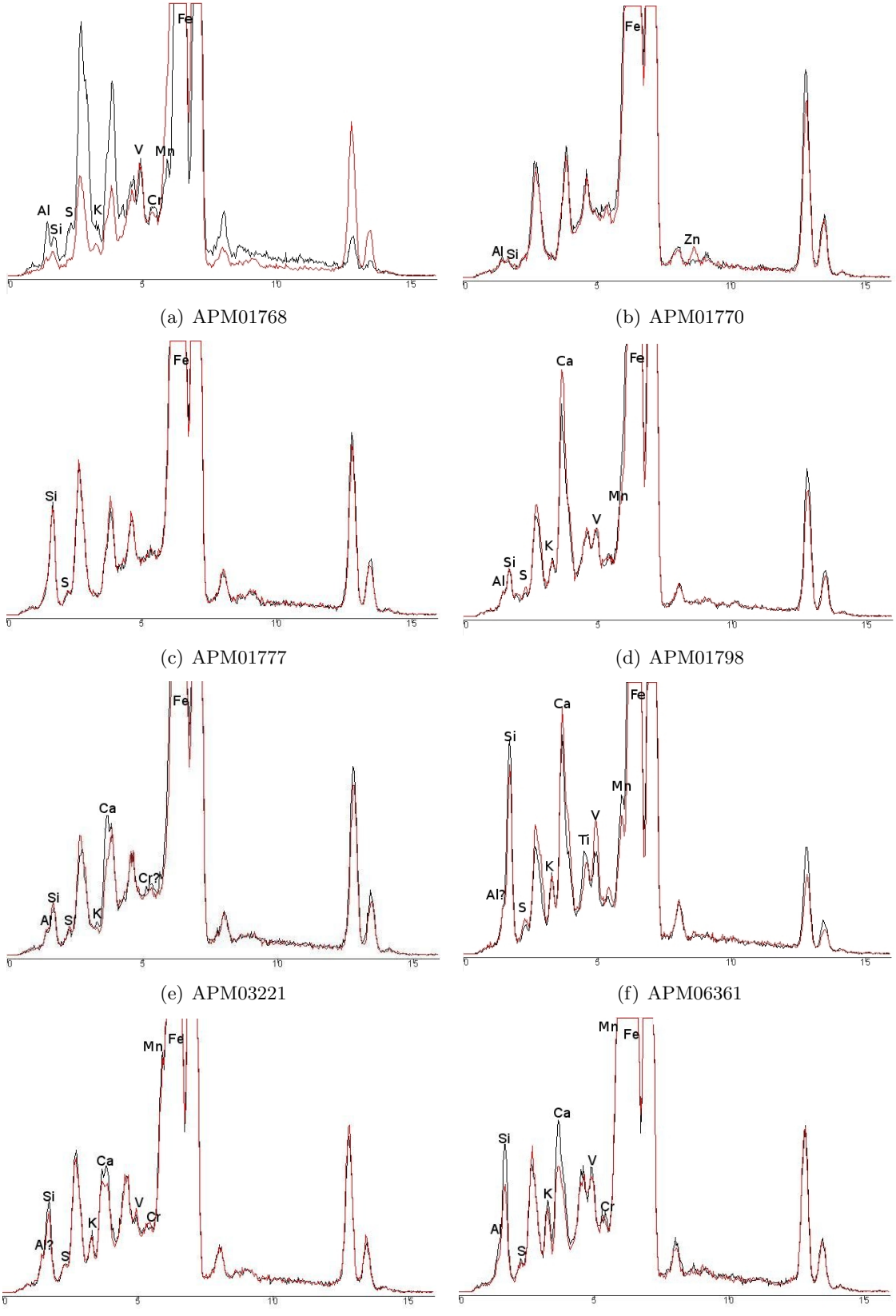

(a) APM01768

(b) APM01770

(c) APM01777

(d) APM01798

(e) APM03221

(f) APM06361

(g) APM06370

(h) APM06371

Figure A.5: XRF spectra of artefacts of the Allard Pierson Museum (APM).

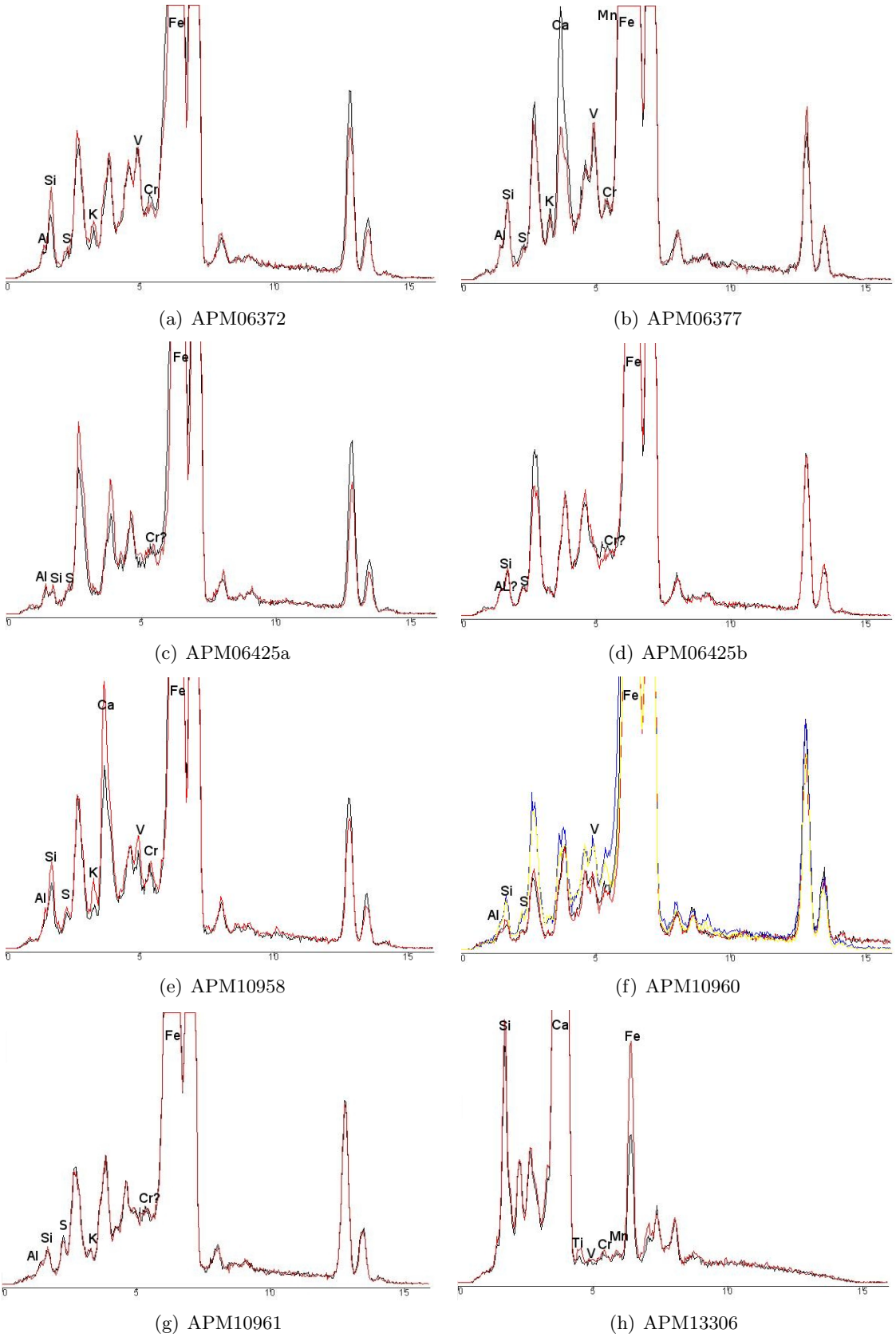

(a) APM06372

(b) APM06377

(c) APM06425a

(d) APM06425b

(e) APM10958

(f) APM10960

(g) APM10961

(h) APM13306

Figure A.6: XRF spectra of artefacts of the Allard Pierson Museum (APM).

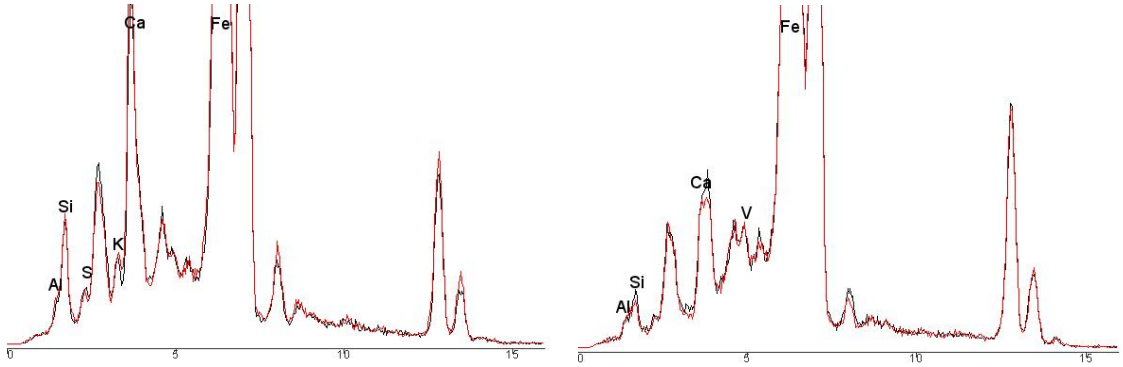

(a) APM15888 (b) APM15889

Figure A.7: XRF spectra of artefacts of the Allard Pierson Museum (APM).

The Dutch National Museum of Antiquities objects

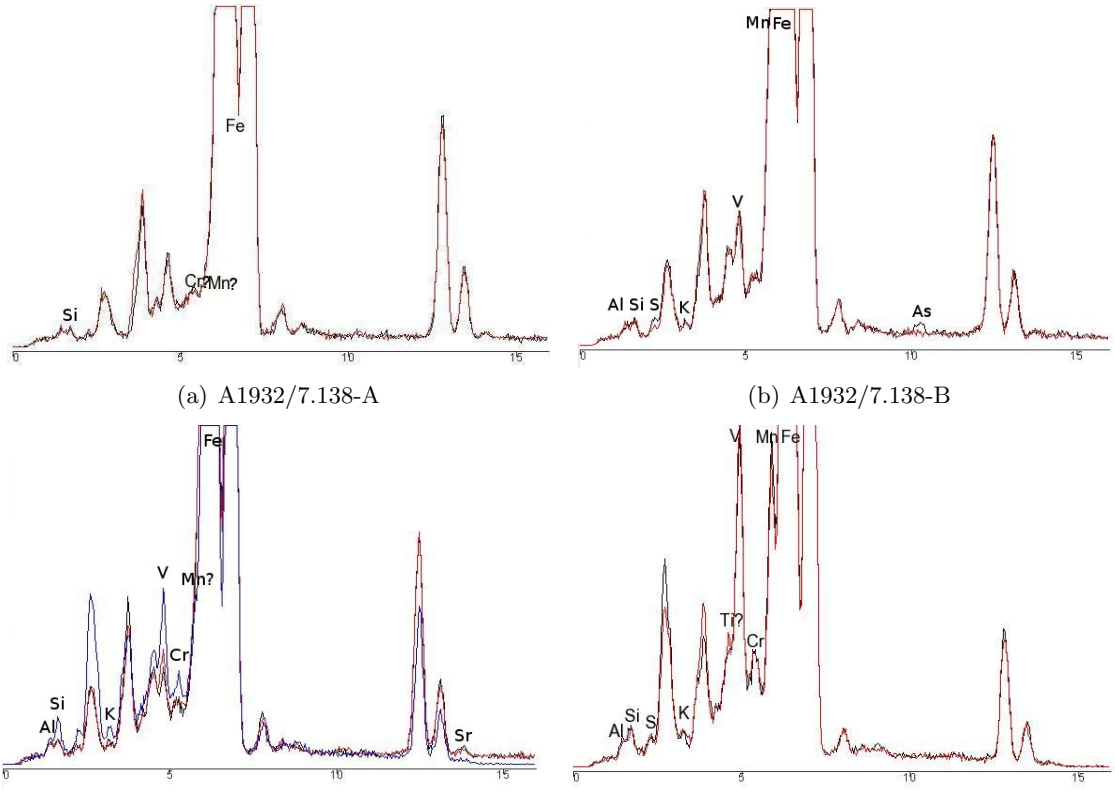

(a) A1932/7.138-A (b) A1932/7.138-B

(c) A1932/7.138-C (d) A1932/7.138-D

Figure A.8: XRF spectra of artefacts of The Dutch National Museum of Antiquities (Rijksmuseum van Oudheden, RMO).

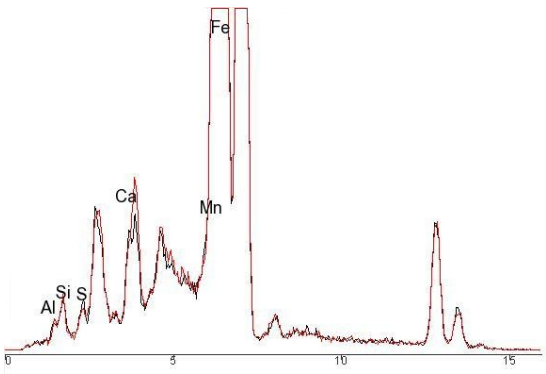

(a) A1932/7.138-E

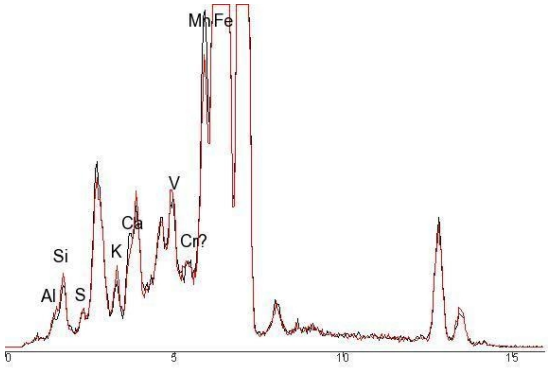

(b) A1932/7.138-F

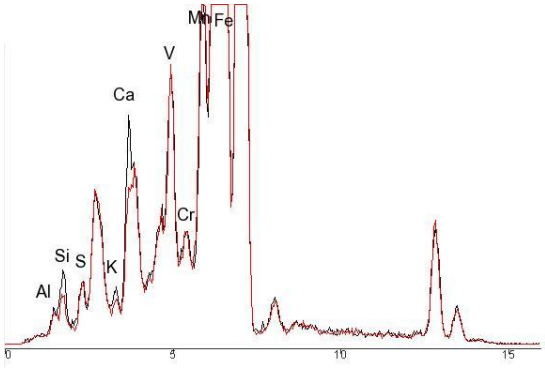

(c) A1932/7.138-G

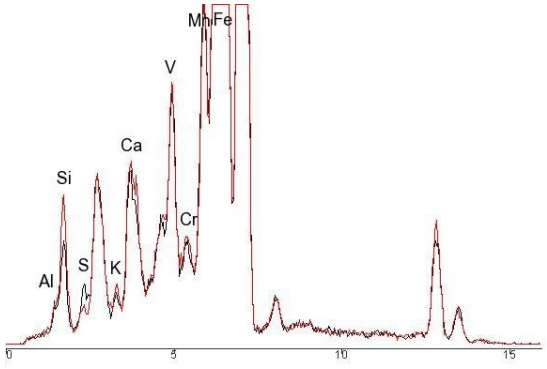

(d) A1932/7.138-H

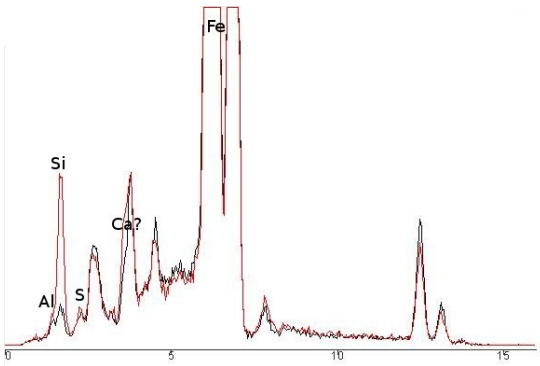

(e) A1932/7.138-I

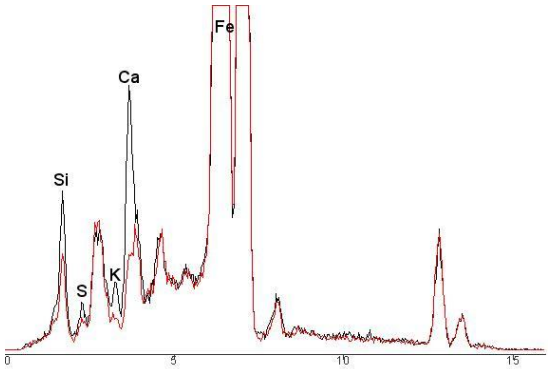

(f) A1952/1.3

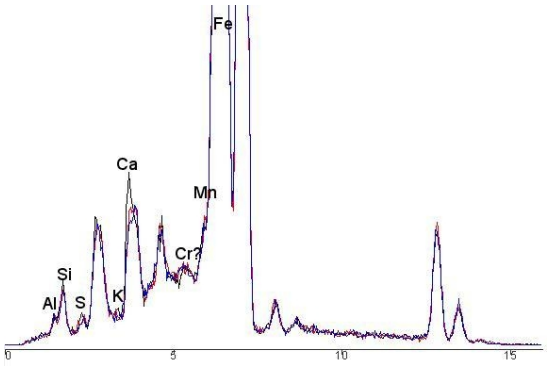

(g) B1982/5.1324

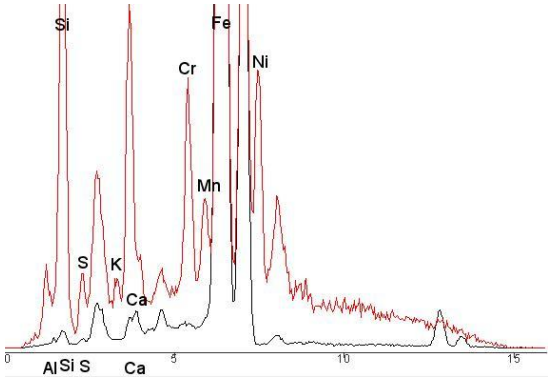

(h) B1982/5.1343

Figure A.9: XRF spectra of artefacts of The Dutch National Museum of Antiquities (Rijksmuseum van Oudheden, RMO).

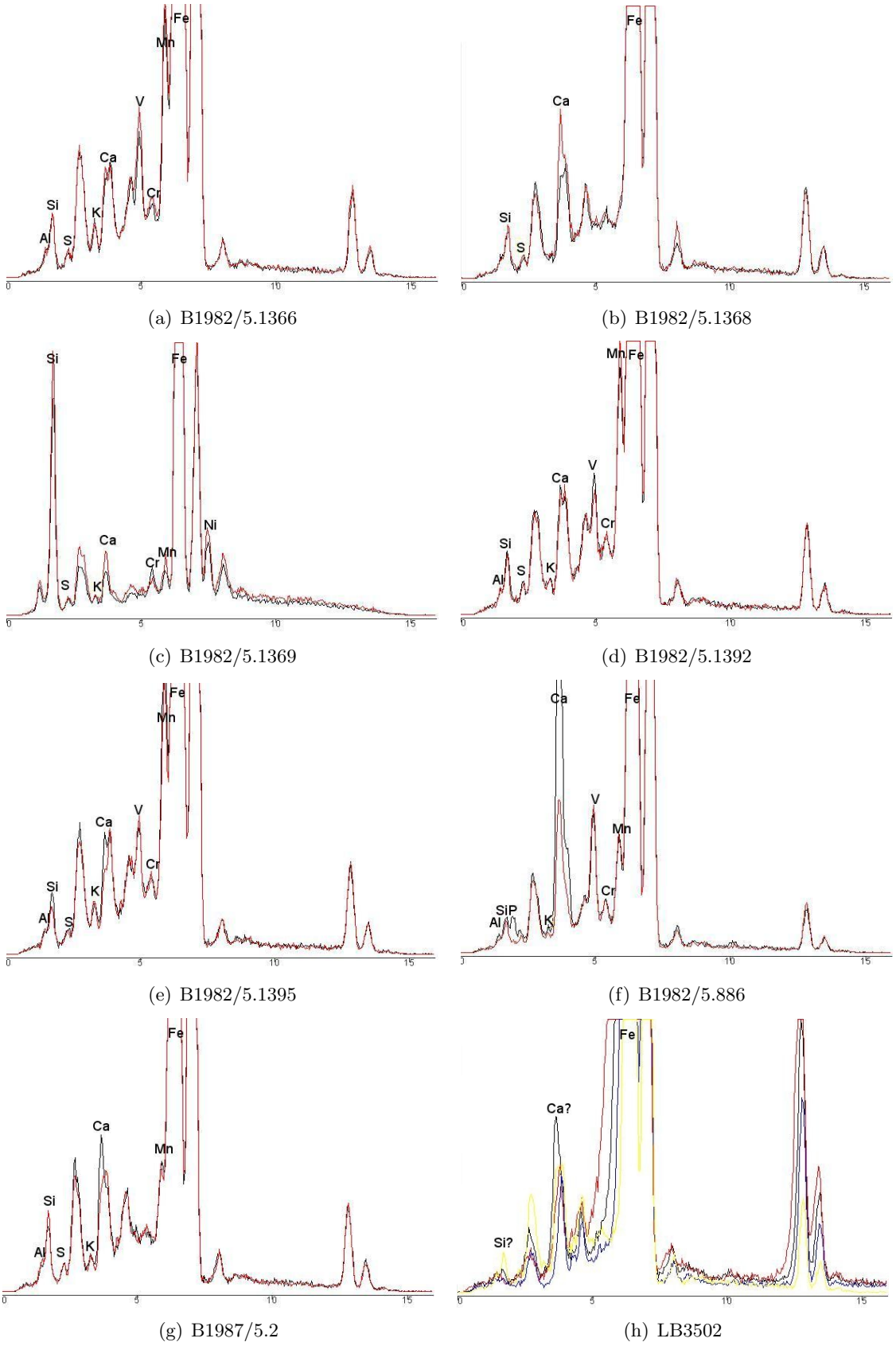

(a) B1982/5.1366

(b) B1982/5.1368

(c) B1982/5.1369

(d) B1982/5.1392

(e) B1982/5.1395

(f) B1982/5.886

(g) B1987/5.2

(h) LB3502

Figure A.10: XRF spectra of artefacts of The Dutch National Museum of Antiquities (Rijksmuseum van Oudheden, RMO).

Appendix B

Radio- and Tomography

B.1 Histograms

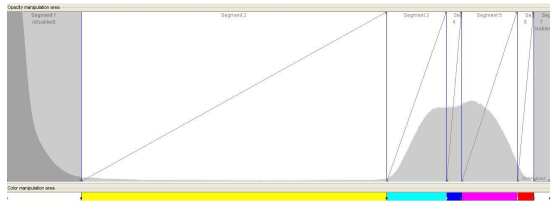

(a) A1932/7.138-A

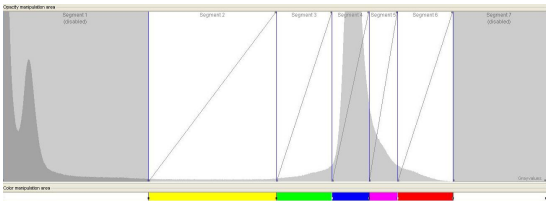

(b) A1932/7.138-B

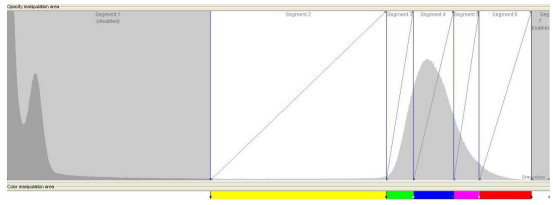

(c) A1932/7.138-C

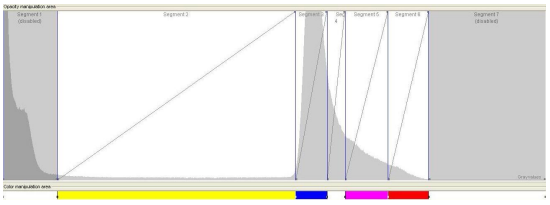

(d) A1932/7.138-D

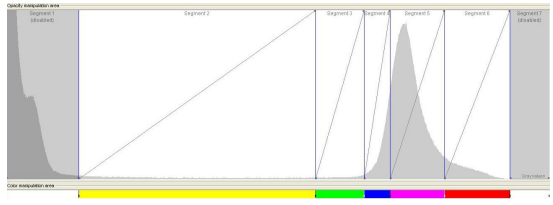

(e) A1932/7.138-E with ring filter

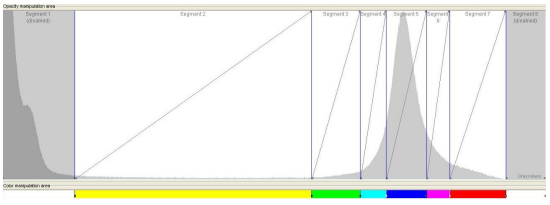

(f) A1932/7.138-E without ring filter

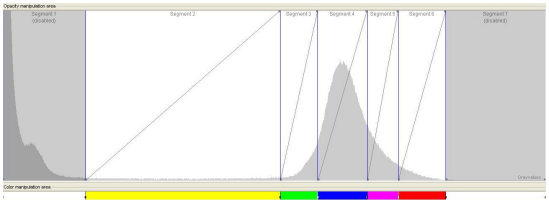

(g) A1932/7.138-F

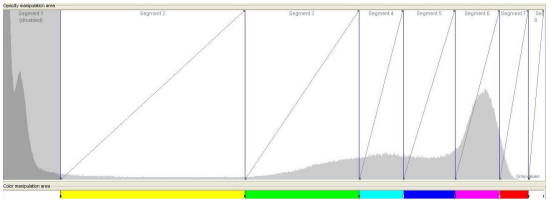

(h) A1932/7.138-G with ring filter

Figure B.1: Histograms of the Radio- and Tomography measurements

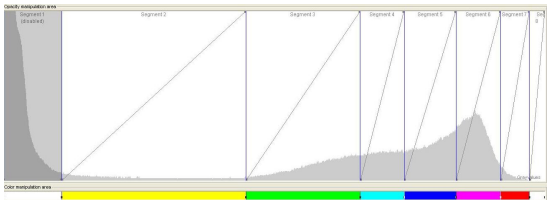

(a) A1932/7.138-G without ring filter

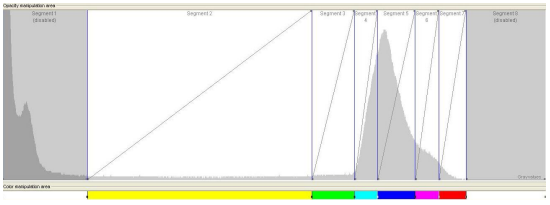

(b) A1932/7.138-H

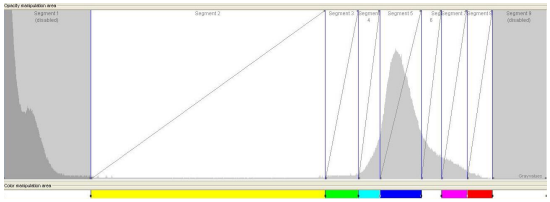

(c) A1932/7.138-I

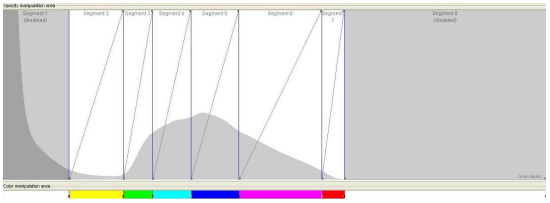

(d) LB3502

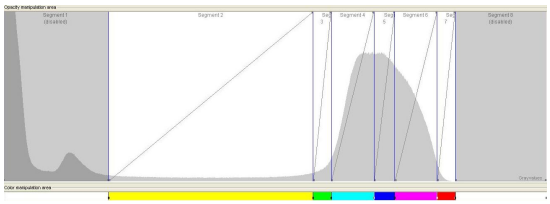

(e) A1952/1.3

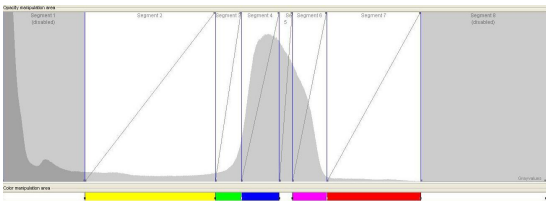

(f) B1982/5.1324 (1342)

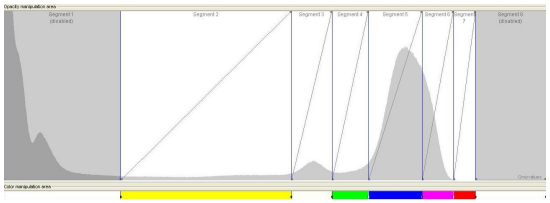

(g) B1982/5.1343 (1362)

Figure B.2: Histograms of the Radio- and Tomography measurements

B.2 Tomography

A1932/7.138-A

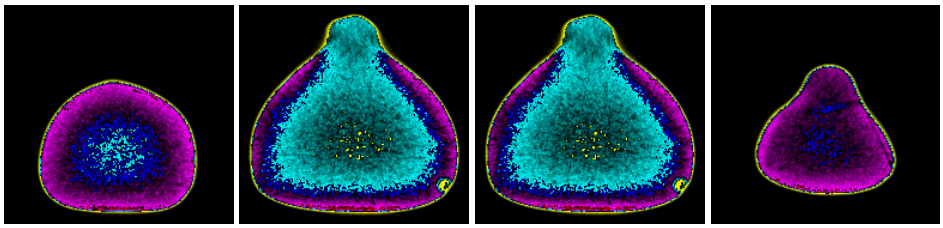

(a) Axial slice 85 (b) Axial slice 155 (c) Axial slice 214 (d) Axial slice 252

Figure B.3: Axial slices of A1932/7.138-A

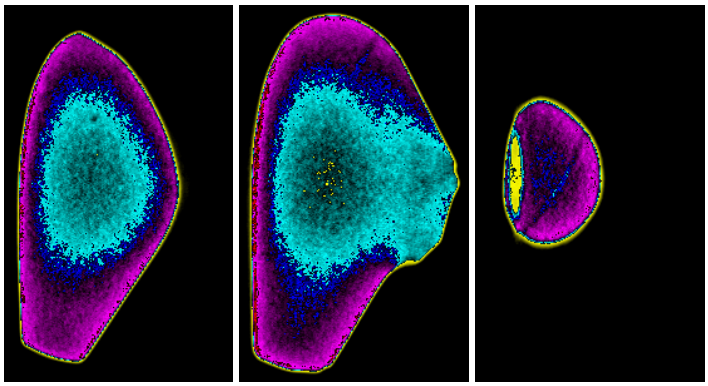

(a) Sagittal slice 62 (b) Axial slice 96 (c) Axial slice 169

Figure B.4: Sagittal slices of A1932/7.138-A

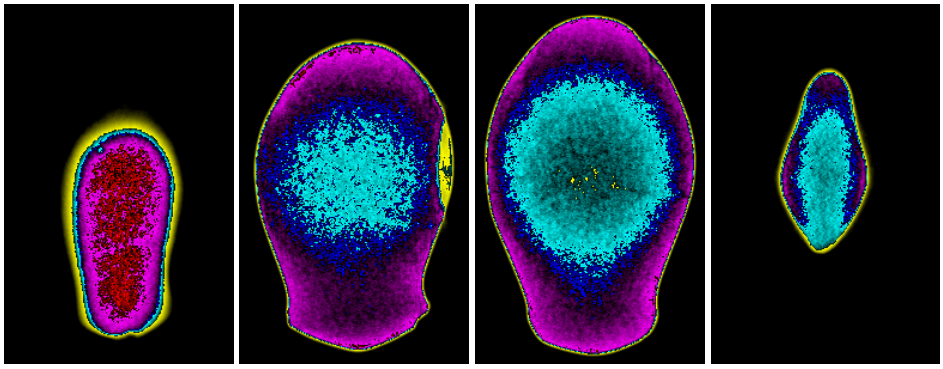

(a) Frontal slice 12 (b) Frontal slice 33 (c) Frontal slice 57 (d) Frontal slice 136

Figure B.5: Frontal slices of A1932/7.138-A

A1932/7.138-B

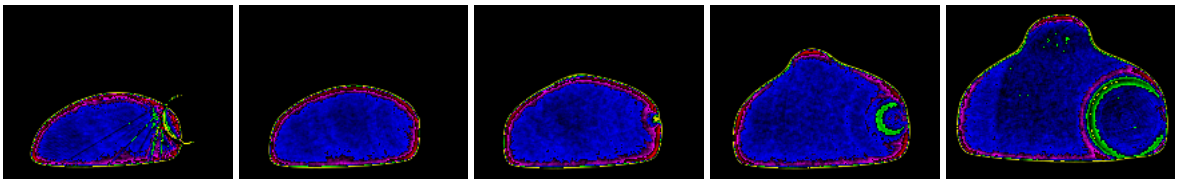

(a) Axial slice 46 (b) Axial slice 57 (c) Axial slice 70 (d) Axial slice 94 (e) Axial slice 176

Figure B.6: Axial slices of A1932/7.138-B

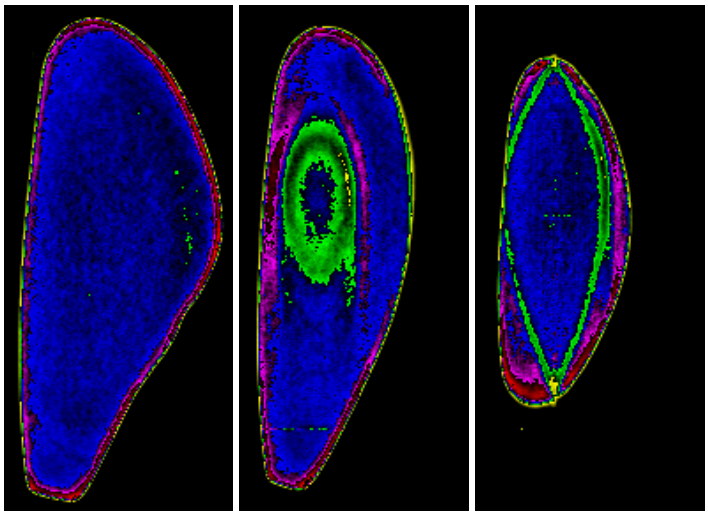

(a) Sagittal slice 86 (b) Sagittal slice 113 (c) Sagittal slice 136

Figure B.7: Sagittal slices of A1932/7.138-B

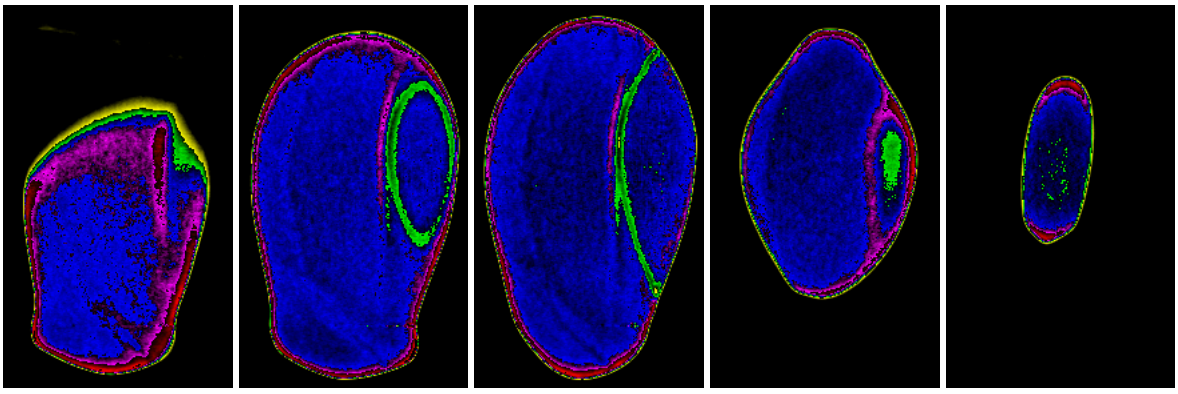

(a) Frontal slice 16 (b) Frontal slice 28 (c) Frontal slice 42 (d) Frontal slice 75 (e) Frontal slice 103

Figure B.8: Frontal slices of A1932/7.138-B

A1932/7.138-C

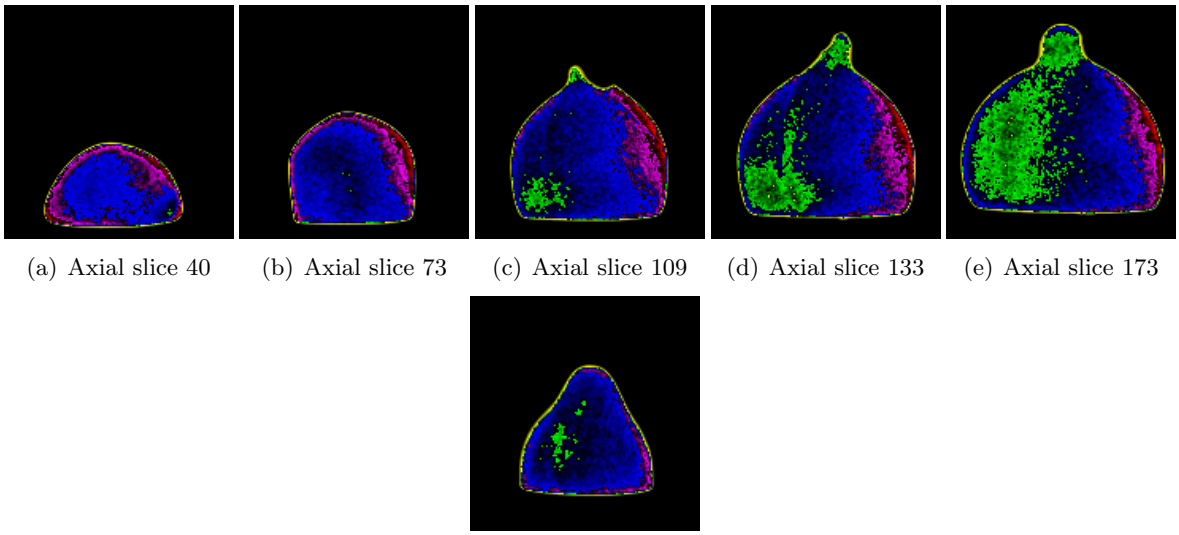

(a) Axial slice 40 (b) Axial slice 73 (c) Axial slice 109 (d) Axial slice 133 (e) Axial slice 173

(f) Axial slice 233

Figure B.9: Axial slices of A1932/7.138-C

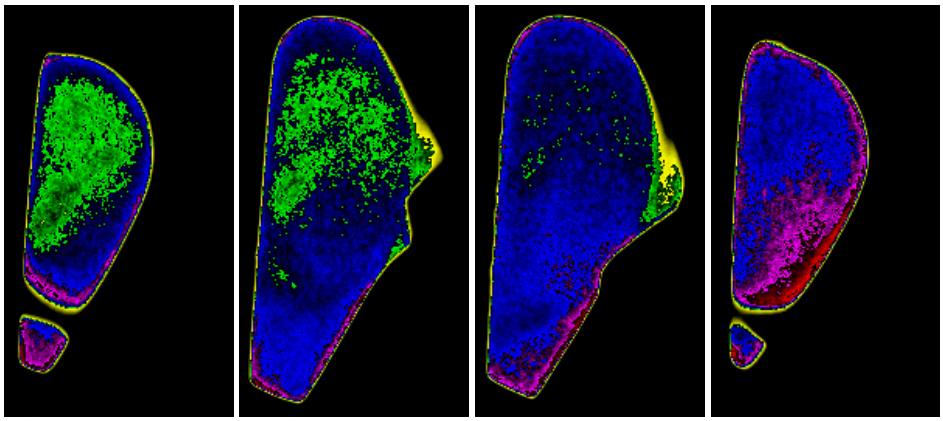

(a) Sagittal slice 32 (b) Sagittal slice 61 (c) Sagittal slice 85 (d) Sagittal slice 109

Figure B.10: Sagittal slices of A1932/7.138-C

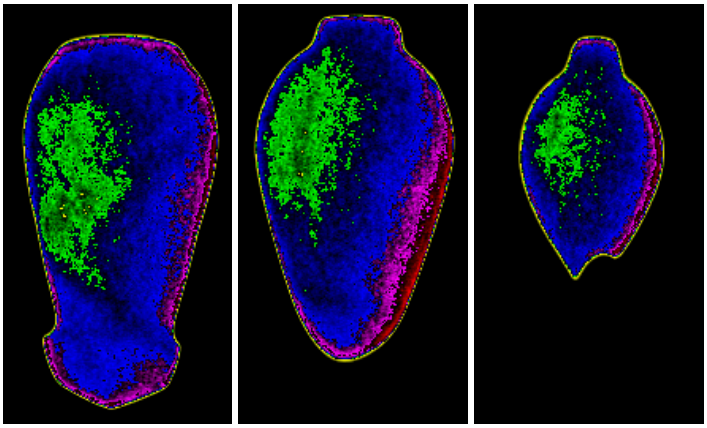

(a) Frontal slice 28 (b) Frontal slice 60 (c) Frontal slice92

Figure B.11: Frontal slices of A1932/7.138-C

A1932/7.138-D

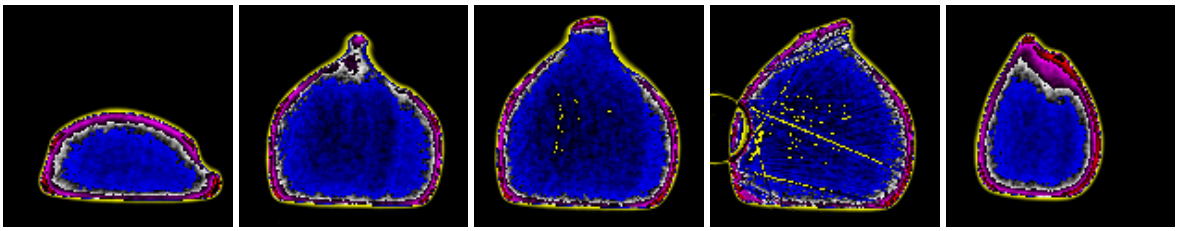

(a) Axial slice 34 (b) Axial slice 72 (c) Axial slice 90 (d) Axial slice 98 (e) Axial slice 203

Figure B.12: Axial slices of A1932/7.138-D

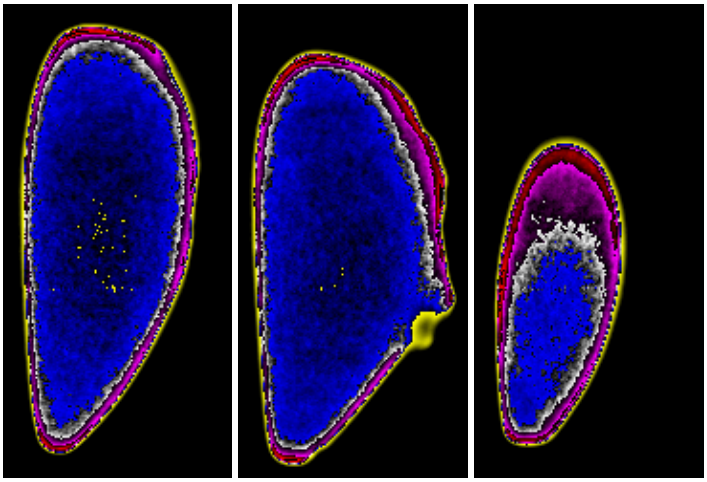

(a) Sagittal slice 35 (b) Sagittal slice 70 (c) Sagittal slice 98

Figure B.13: Sagittal slices of A1932/7.138-D

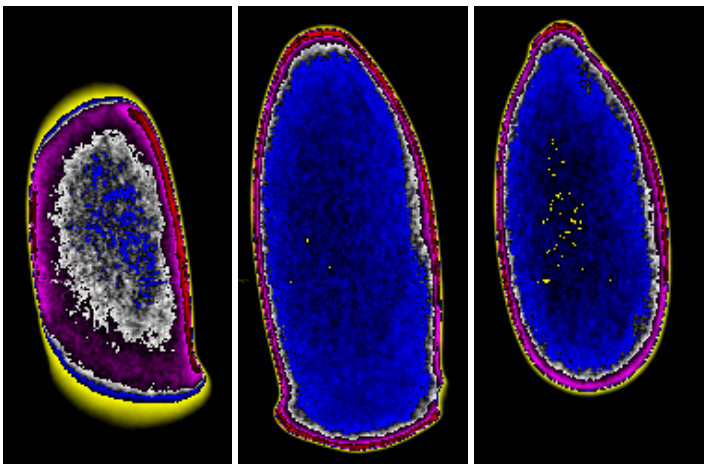

(a) Frontal slice 14 (b) Frontal slice 33 (c) Frontal slice66

Figure B.14: Frontal slices of A1932/7.138-D

A1932/7.138-E without ring filter

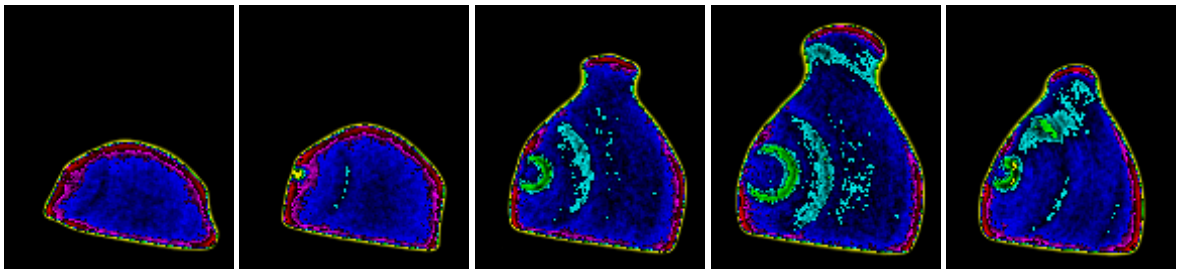

(a) Axial slice 42 (b) Axial slice 54 (c) Axial slice 87 (d) Axial slice 120 (e) Axial slice 170

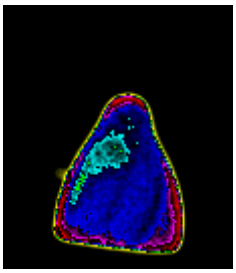

(f) Axial slice 188

Figure B.15: Axial slices of A1932/7.138-E without ring filter

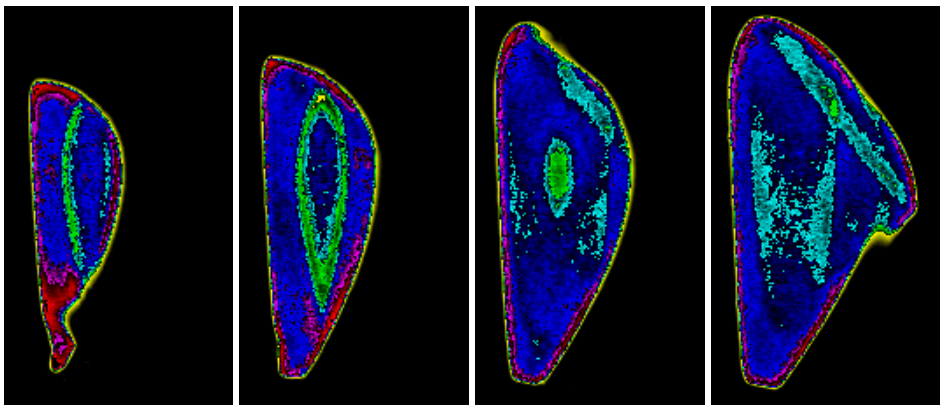

(a) Sagittal slice 23 (b) Sagittal slice 32 (c) Sagittal slice 42 (d) Sagittal slice 50

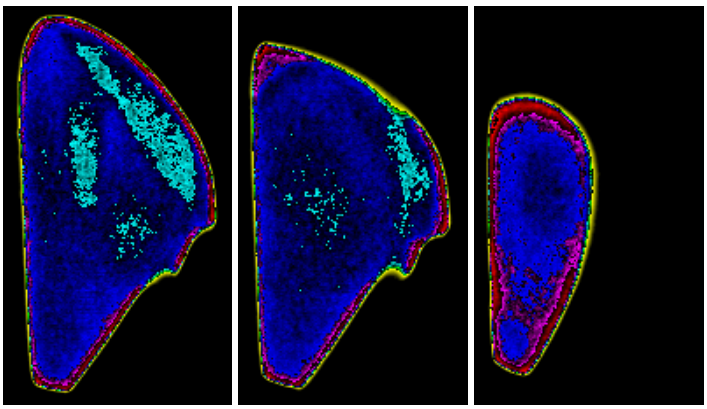

(e) Sagittal slice 60 (f) Sagittal slice 75 (g) Sagittal slice 95

Figure B.16: Sagittal slices of A1932/7.138-E without ring filter

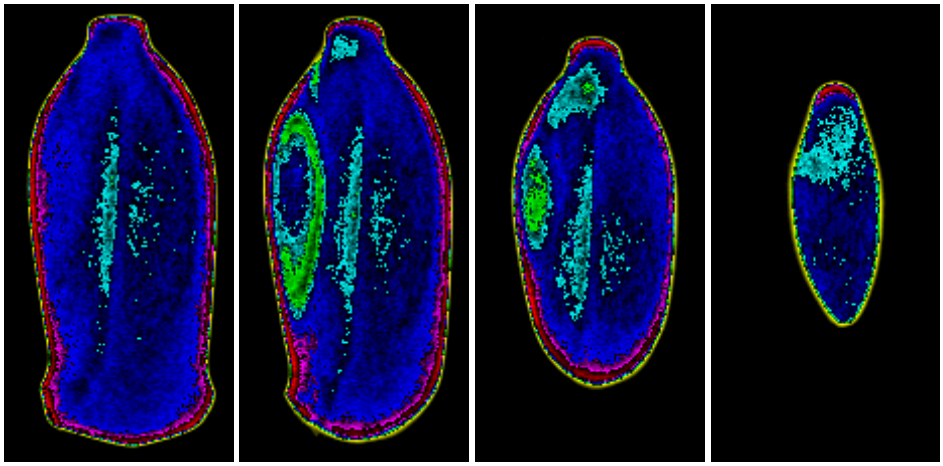

(a) Frontal slice 30 (b) Frontal slice 40 (c) Frontal slice 60 (d) Frontal slice 86

Figure B.17: Frontal slices of A1932/7.138-E without ring filter

A1932/7.138-E with ring filter

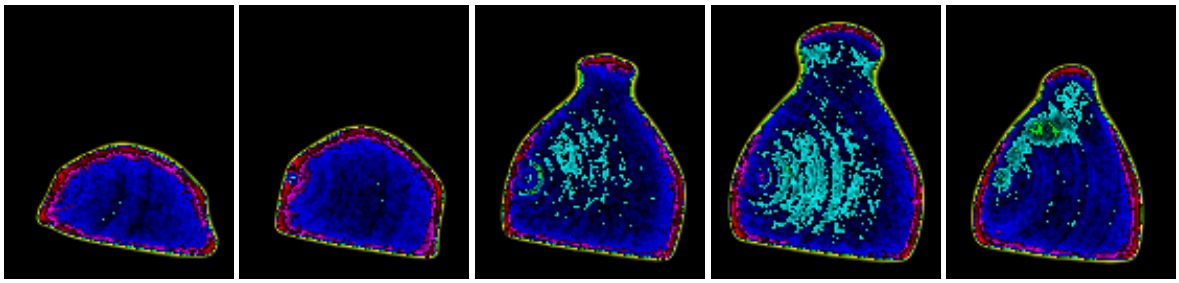

(a) Axial slice 42 (b) Axial slice 54 (c) Axial slice 87 (d) Axial slice 120 (e) Axial slice 170

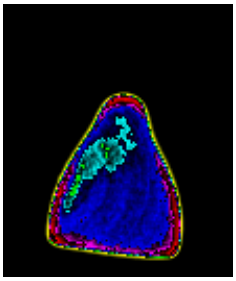

(f) Axial slice 188

Figure B.18: Axial slices of A1932/7.138-E with ring filter

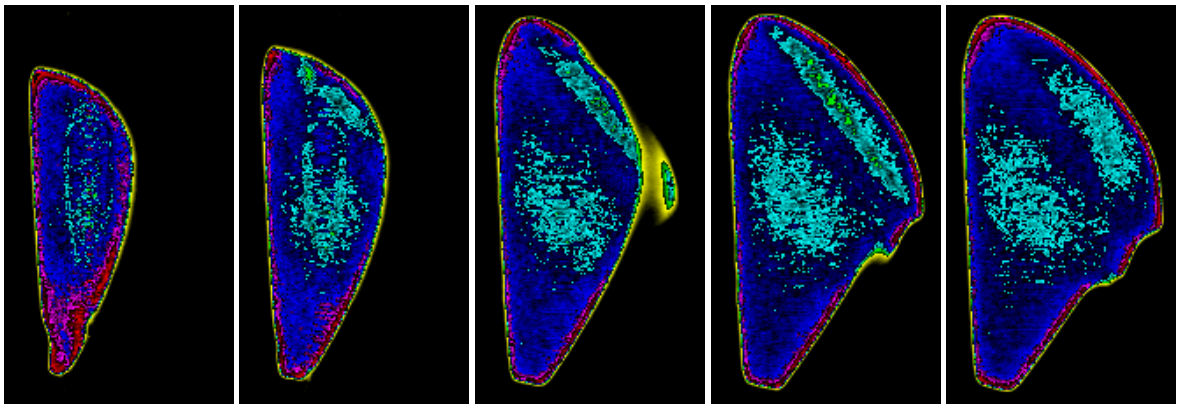

(a) Sagittal slice 23 (b) Sagittal slice 32 (c) Sagittal slice 42 (d) Sagittal slice 50 (e) Sagittal slice 60

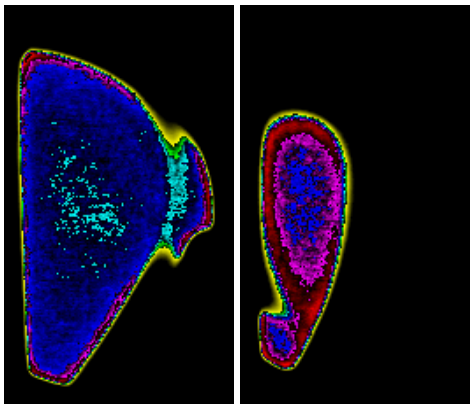

(f) Sagittal slice 75 (g) Sagittal slice 95

Figure B.19: Sagittal slices of A1932/7.138-E with ring filter

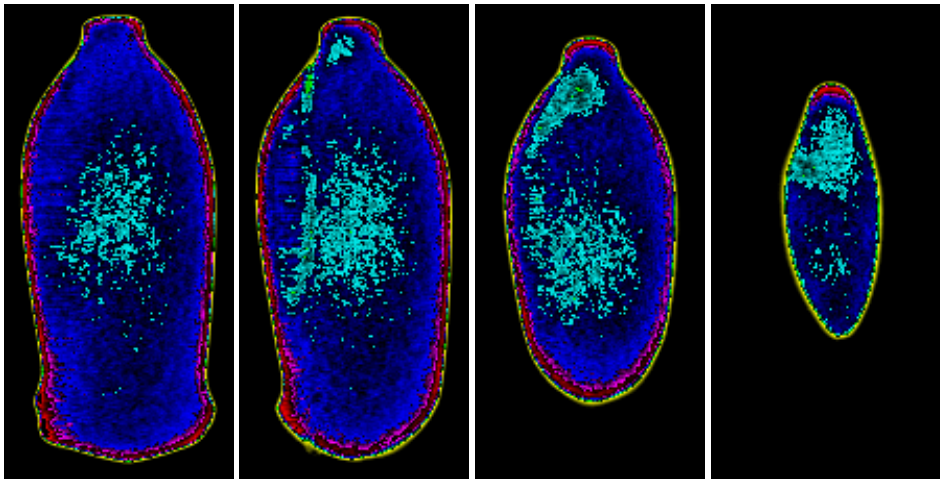

(a) Frontal slice 30 (b) Frontal slice 40 (c) Frontal slice 60 (d) Frontal slice 86

Figure B.20: Frontal slices of A1932/7.138-E with ring filter

A1932/7.138-F

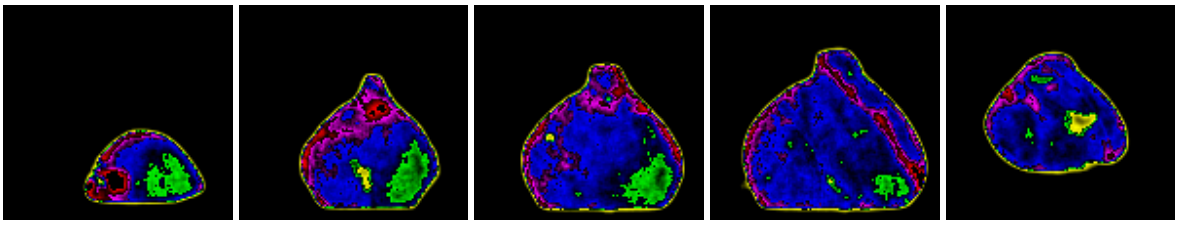

(a) Axial slice 25 (b) Axial slice 49 (c) Axial slice 60 (d) Axial slice 76 (e) Axial slice 146

Figure B.21: Axial slices of A1932/7.138-F

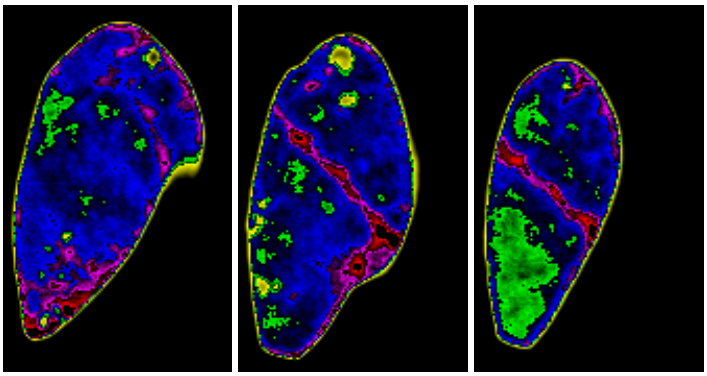

(a) Sagittal slice 49 (b) Sagittal slice 74 (c) Sagittal slice 90

Figure B.22: Sagittal slices of A1932/7.138-F

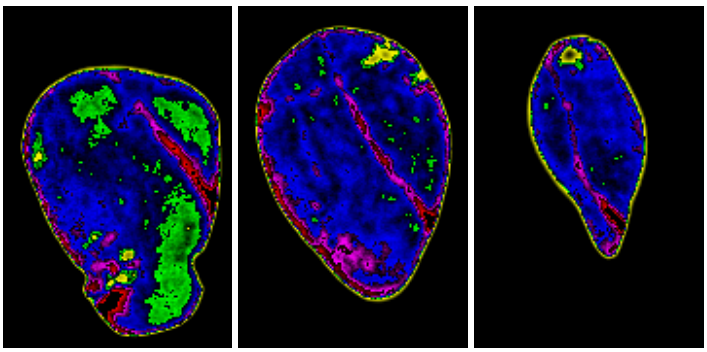

(a) Frontal slice 22 (b) Frontal slice 45 (c) Frontal slice72

Figure B.23: Frontal slices of A1932/7.138-F

A1932/7.138-G without ring filter

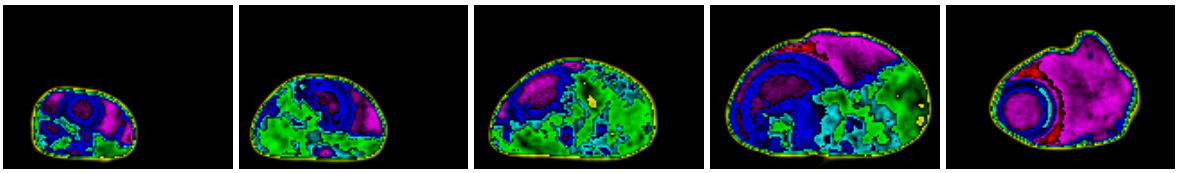

(a) Axial slice 18 (b) Axial slice 31 (c) Axial slice 50 (d) Axial slice 92 (e) Axial slice 138

Figure B.24: Axial slices of A1932/7.138-G without ring filter

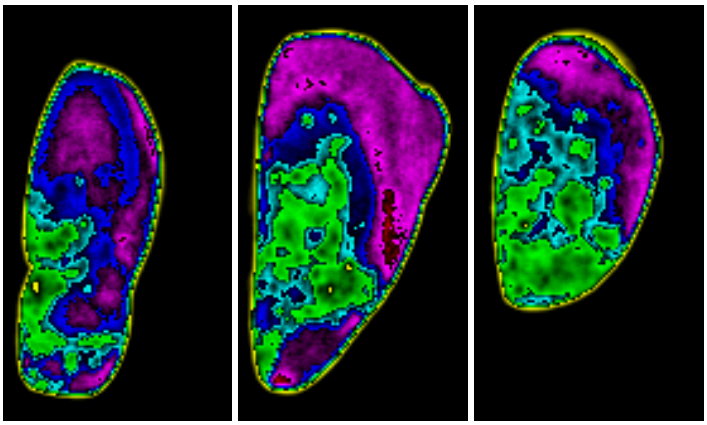

(a) Sagittal slice 28 (b) Sagittal slice 68 (c) Sagittal slice 94

Figure B.25: Sagittal slices of A1932/7.138-G without ring filter

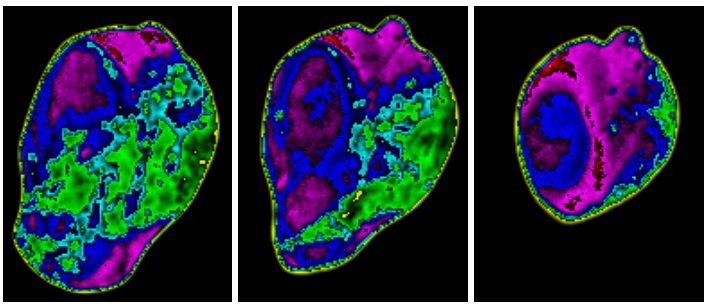

(a) Frontal slice 23 (b) Frontal slice 43 (c) Frontal slice58

Figure B.26: Frontal slices of A1932/7.138-G without ring filter

A1932/7.138-G with ring filter

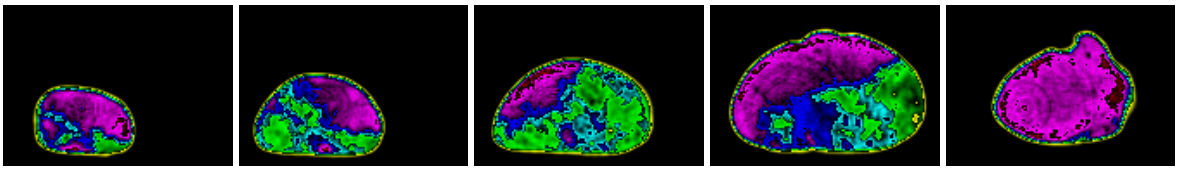

(a) Axial slice 18 (b) Axial slice 31 (c) Axial slice 50 (d) Axial slice 92 (e) Axial slice 138

Figure B.27: Axial slices of A1932/7.138-G with ring filter

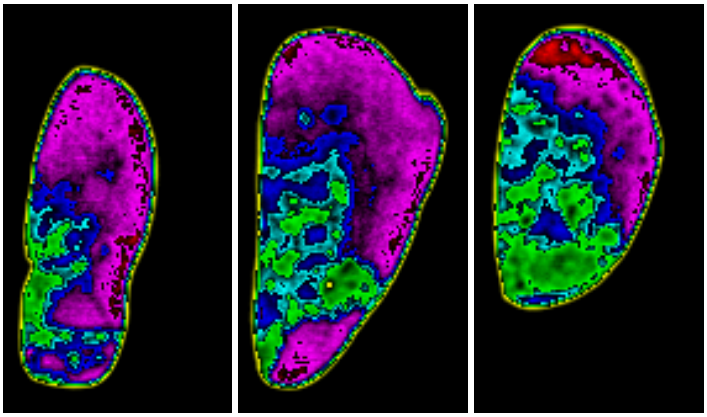

(a) Sagittal slice 28 (b) Sagittal slice 68 (c) Sagittal slice 94

Figure B.28: Sagittal slices of A1932/7.138-G with ring filter

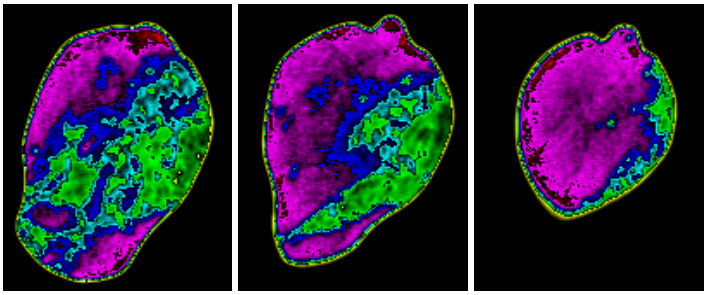

(a) Frontal slice 23 (b) Frontal slice 43 (c) Frontal slice58

Figure B.29: Frontal slices of A1932/7.138-G with ring filter

A1932/7.138-H

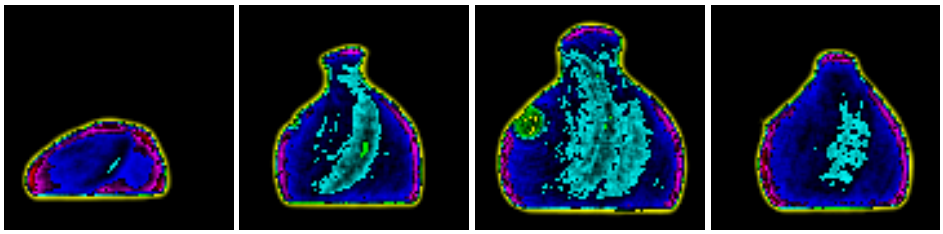

(a) Axial slice 29 (b) Axial slice 65 (c) Axial slice 104 (d) Axial slice 149

Figure B.30: Axial slices of A1932/7.138-H

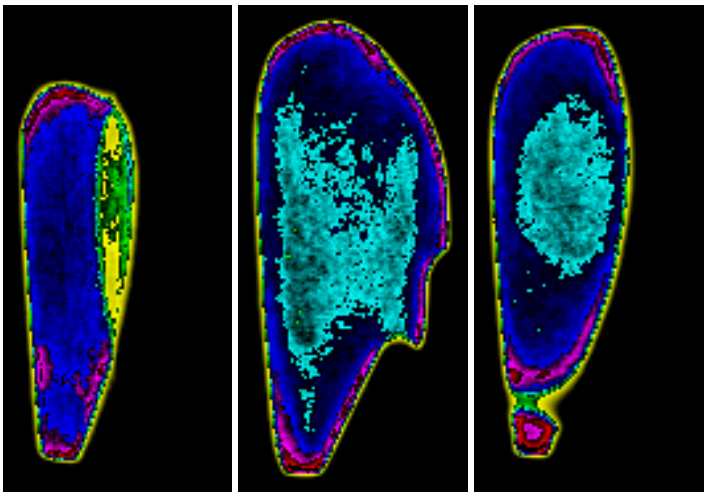

(a) Sagittal slice 21 (b) Sagittal slice 43 (c) Sagittal slice 61

Figure B.31: Sagittal slices of A1932/7.138-H

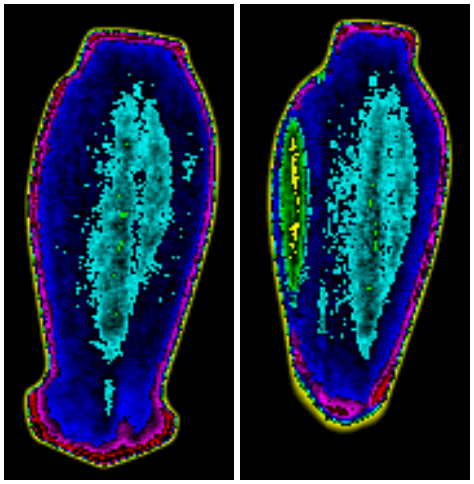

(a) Frontal slice 22 (b) Frontal slice 38

Figure B.32: Frontal slices of A1932/7.138-H

A1932/7.138-I

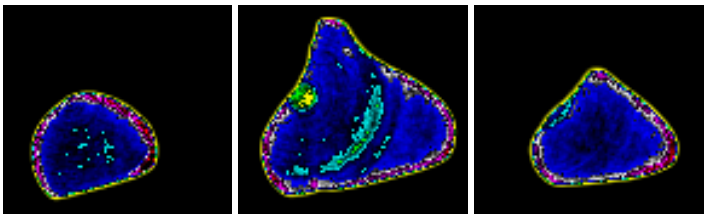

(a) Axial slice 46 (b) Axial slice 101 (c) Axial slice 143

Figure B.33: Axial slices of A1932/7.138-I

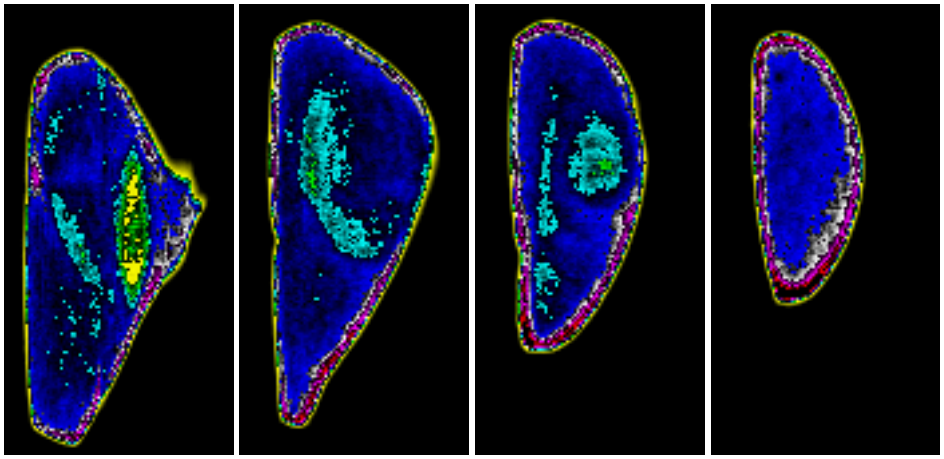

(a) Sagittal slice 30 (b) Sagittal slice 49 (c) Sagittal slice 58 (d) Sagittal slice 70

Figure B.34: Sagittal slices of A1932/7.138-I

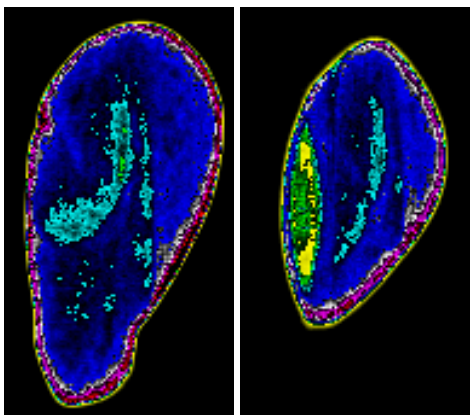

(a) Frontal slice 26 (b) Frontal slice 45

Figure B.35: Frontal slices of A1932/7.138-I

A1952/1.3

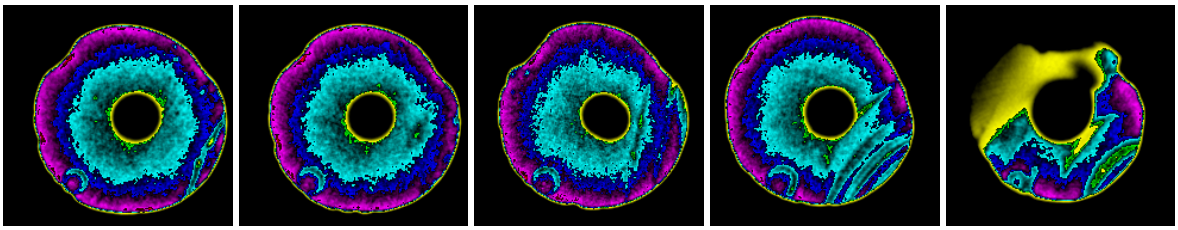

(a) Axial slice 46 (b) Axial slice 60 (c) Axial slice 150 (d) Axial slice 273 (e) Axial slice 317

Figure B.36: Axial slices of A1952/1.3

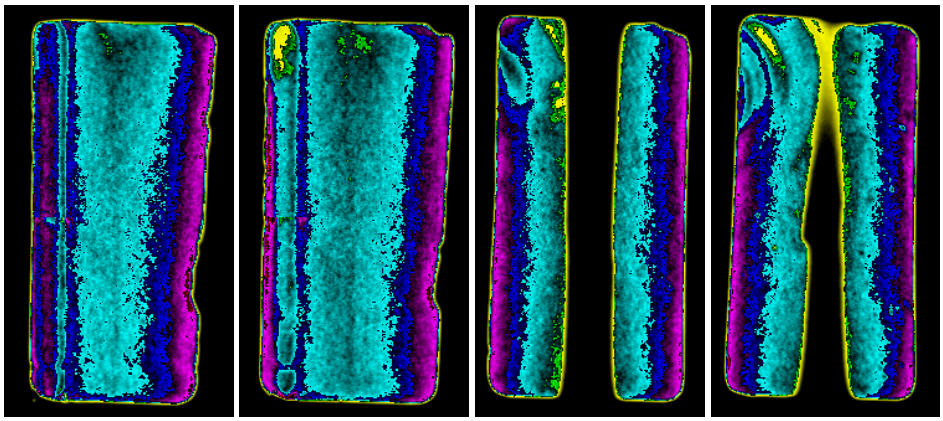

(a) Sagittal slice 62 (b) Sagittal slice69 (c) Sagittal slice 105 (d) Sagittal slice 122

Figure B.37: Sagittal slices of A1952/1.3

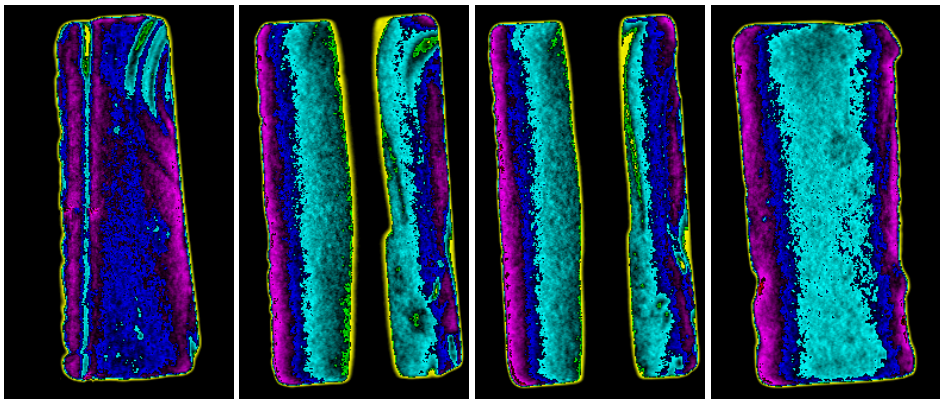

(a) Frontal slice 32 (b) Frontal slice 78 (c) Frontal slice 92 (d) Frontal slice 129

Figure B.38: Frontal slices of A1952/1.3

B1982/5.1324

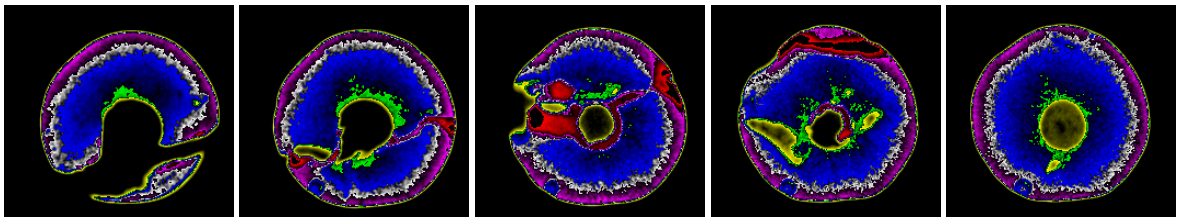

(a) Axial slice 30 (b) Axial slice 50 (c) Axial slice 92 (d) Axial slice 132 (e) Axial slice 166

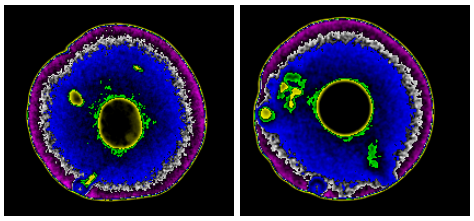

(f) Axial slice 179 (g) Axial slice 299

Figure B.39: Axial slices of B1982/5.1324

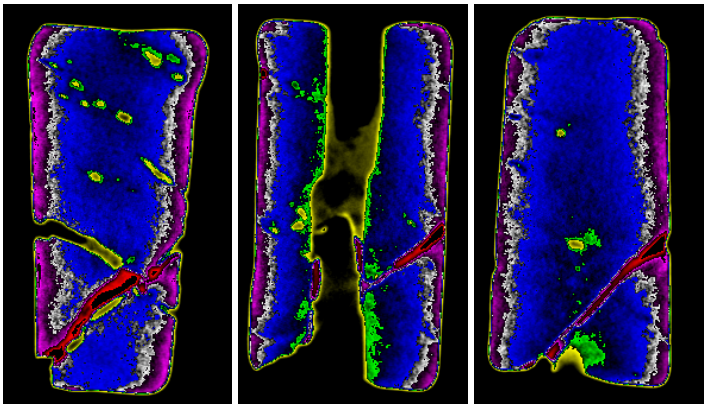

(a) Sagittal slice 58 (b) Sagittal slice106 (c) Sagittal slice 142

Figure B.40: Sagittal slices of B1982/5.1324

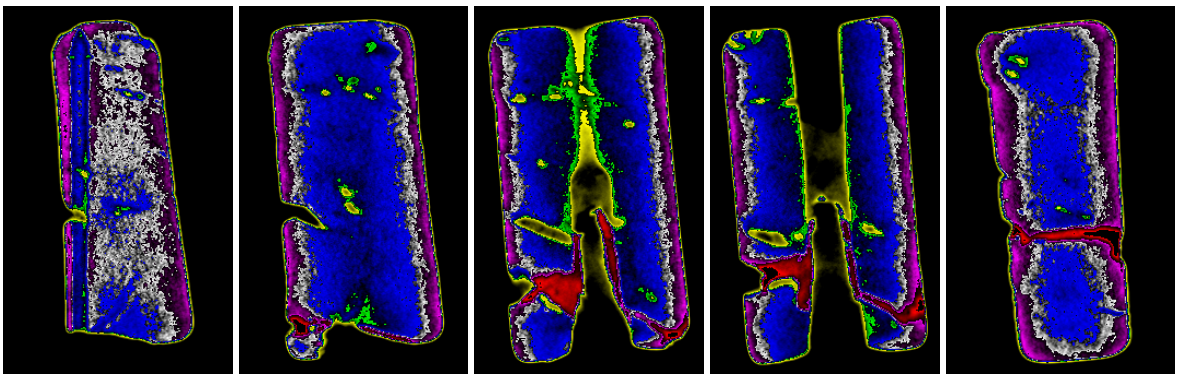

(a) Frontal slice 28 (b) Frontal slice 47 (c) Frontal slice 73 (d) Frontal slice 89 (e) Frontal slice 148

Figure B.41: Frontal slices of B1982/5.1324

B1982/5.1343

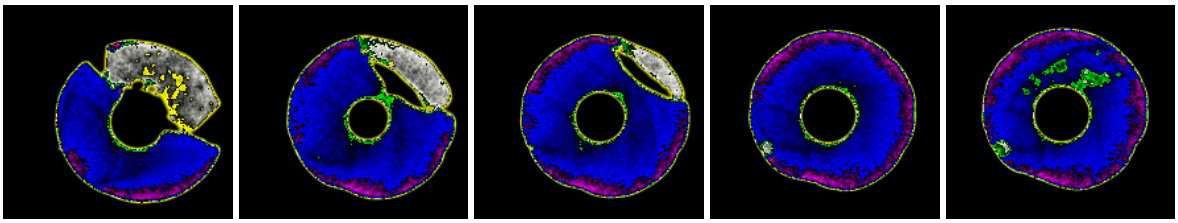

(a) Axial slice 40 (b) Axial slice 79 (c) Axial slice 96 (d) Axial slice 160 (e) Axial slice 181

Figure B.42: Axial slices of B1982/5.1343

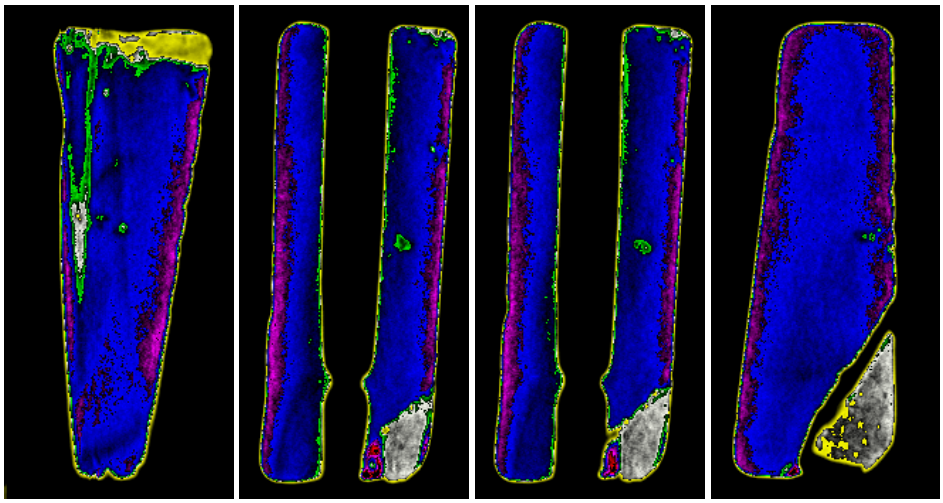

(a) Sagittal slice 46 (b) Sagittal slice 87 (c) Sagittal slice 90 (d) Sagittal slice 128

Figure B.43: Sagittal slices of B1982/5.1343

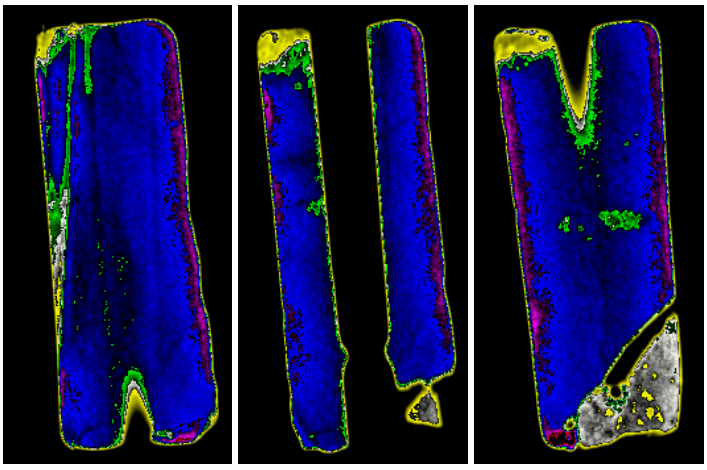

(a) Frontal slice 54 (b) Frontal slice 73 (c) Frontal slice 105

Figure B.44: Frontal slices of B1982/5.1343

LB3502

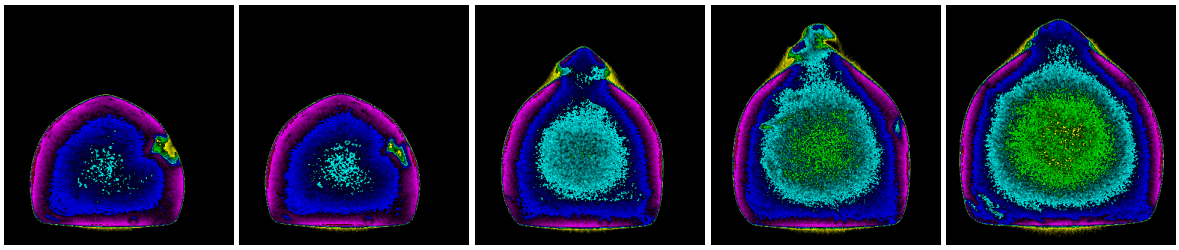

(a) Axial slice 175 (b) Axial slice 179 (c) Axial slice 258 (d) Axial slice 322 (e) Axial slice 400

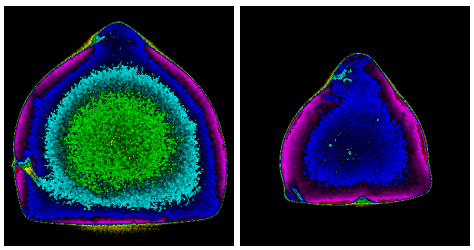

(f) Axial slice 464 (g) Axial slice 593

Figure B.45: Axial slices of LB3502

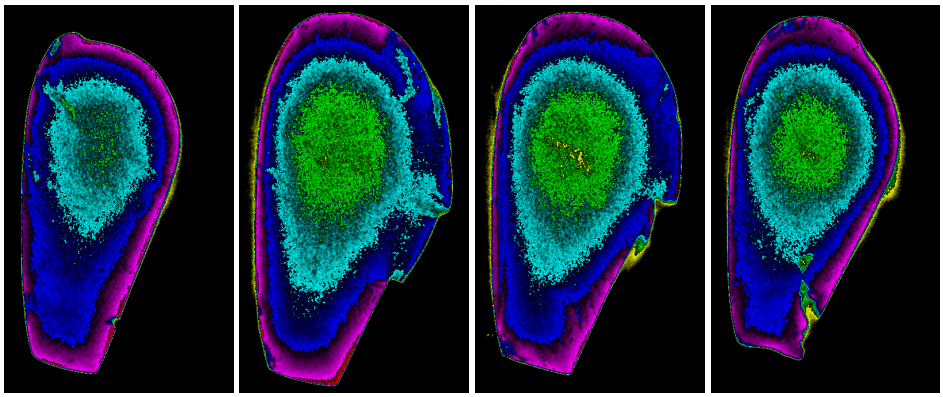

(a) Sagittal slice 98 (b) Sagittal slice 167 (c) Sagittal slice 219 (d) Sagittal slice 249

Figure B.46: Sagittal slices of LB3502

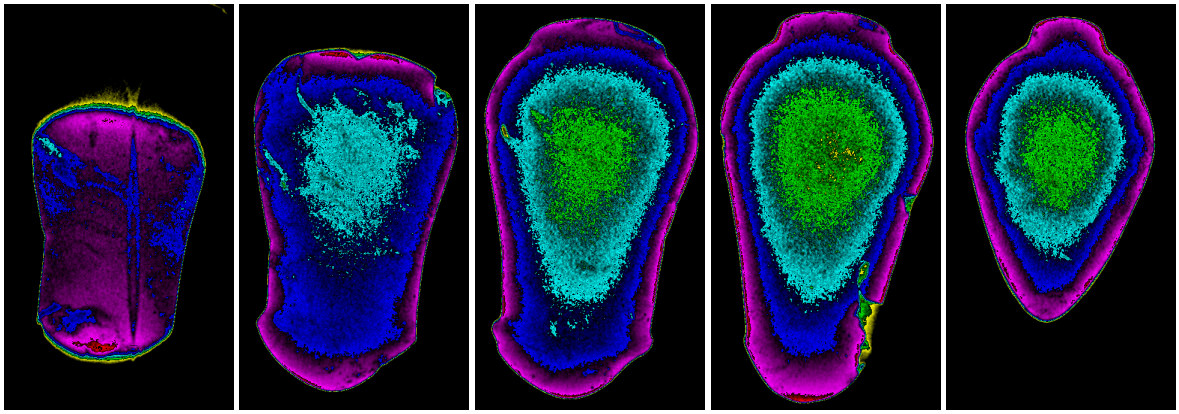

(a) Frontal slice 41 (b) Frontal slice 73 (c) Frontal slice 117 (d) Frontal slice 161 (e) Frontal slice 235

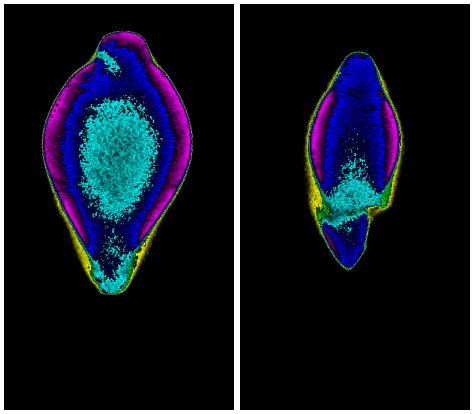

(f) Frontal slice 280 (g) Frontal slice 317

Figure B.47: Frontal slices of LB3502